Equilibrium Phase Separation in Polymer Brushes

K. Geoffrey Soga
Centre for the Physics of Materials
Department of Physics, McGill University
Montréal, Québec

A Thesis submitted to the
Faculty of Graduate Studies and Research
in partial fulfillment of the requirements for the degree of
Doctor of Philosophy

ISBN 0-612-19774-3

Canada

Contents

FIGURES AND TABLES

FIGURES

TABLES

RÉSUMÉ

Les propriétés d'équilibre de polymères greffés par une extrémité à une interface impénétrable (la "brosse polymérique") sont étudiées. Les concepts et les techniques de physique statistique des polymères pertinents à ce probleme sont discutés. En particulier, une technique de simulation très efficace pour étudier les brosses polymériques est introduite. Cette technique est illustrée par des simulations de systèmes de brosses polymériques bien caractérisés. Les résultats des études originales de separation de phase dans les systèmes de brosses polymériques sont aussi présentés. Une instabilité dans la densité latérale des monomères est trouvée dans les conditions de solvant suffisamment mauvais. La valeur du seuil d'instabilité est en accord avec une prédiction précédente. Une instabilité compositionnelle est trouvée dans les densités latérales d'une brosse de deux composantes avec des conditions d'immiscibilité suffisante entre celles-ci. Les effets de conditions diverses du solvant sont considérés. Enfin, la valeur du seuil de l'instabilité compositionnelle est trouvée avec une technique de champ moyen autocohérent, et les résultats sont comparés à des simulations.

ABSTRACT

The equilibrium properties of polymers end-grafted to an impenetrable interface, the "polymer brush", are investigated. Relevant concepts and techniques of statistical polymer physics are discussed; in particular, a simulation technique that is very efficient for studying polymer brushes is introduced. This technique is demonstrated through simulations of a well characterized polymer brush system. The results of original investigations of phase separation in polymer brushes are also presented. An instability in the lateral monomer density of a polymer brush is observed under sufficiently poor solvent conditions. The onset of this instability is found to agree with a previous prediction. A compositional instability is found in the lateral densities of a two-component polymer brush under conditions of sufficient immiscibility between the two components. The effects of varying solvent conditions are considered. Finally, the onset of the compositional instability is determined using the technique of the self consistent mean field, and the results compared to simulation.

ACKNOWLEDGMENTS

I would foremost like to thank Martin Zuckermann and Hong Guo for supervision and guidance during my studies, and for collaboration during my research. I would also like to thank Anna Balazs and Ron Dickman for their generous help, with discussions, notes, and computer code in our impressionable, formative days at the beginning. I would like to acknowledge the financial support of the Natural Sciences and Engineering Research Council and the Fonds pour la Formation de Chercheurs et l'Aide à la Recherche.

As I look back to remember the people I want to thank on a more personal level, I realize how difficult it is, for I see a crowd of people, friends and acquaintances past and present, and they're doing many things. They're sittinng in chairs, standing by blackboards, listening to me and explaining things I never understood. Some are drinking beer, playing guitar, flirting with occasional success and generally reminding me to have a life. Others confide in me, cook for me, invite me to their parties, take their coffees with me. They're sometimes challenging and annoying, but there when I need them. Some believed in me, others put up with me, and some still wait for me. These are the people who have done more for me than I could ever acknowledge. And there are others who have helped more than I realize. And there are some, some whom I owe the most, who can no longer or will never read these words.

I apologize for not mentioning you all by name; trying do so only seems to diminish all the good I remember. But thank you, every one, for your help.

"It's like the information superhighway, without the information"

- David Letterman

1

INTRODUCTION

1.1 *pŏ'lў-mer* n.

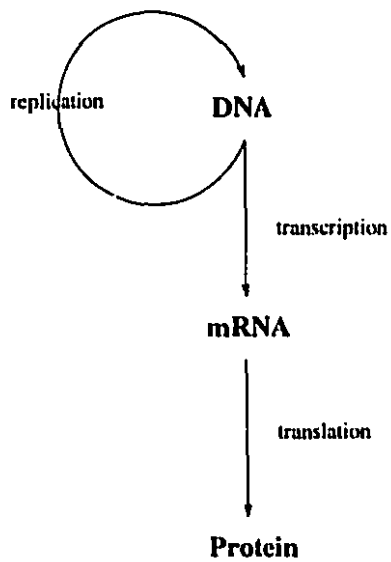

Figure 1.1: The central dogma of molecular genetics.

"Modern biochemical research on gene structure and function has brought to biology an intellectual revolution comparable to that evoked over a hundred years ago by Darwin's theory on the origin of species" [48]. This revolution is the development of the **central dogma of molecular genetics**, illustrated above in fig. (1.1), embodying the principle of genetic continuity through which life and evolution progress. It describes the transcription of the hereditary information of DNA into RNA, a messenger molecule that copies the genetic code of a specific fragment of DNA for translation into proteins, the building blocks and catalysts responsible for building and maintaining the cell, ultimately providing the infrastructure for the replication of DNA. While it is difficult to overemphasize the significance of this process and the

miracle of biology that attends it, this thesis is not about biochemistry, nor about genetics, nor the evolution of species. Rather, it is about polymers. Whatever else it may be, the central dogma of molecular genetics is fundamentally a statement about polymers. Each element, every molecule of DNA and RNA, each protein, structural or catalytic, is a polymer, and molecular genetics is the relationship between them. Life, it would appear, is a creation of polymers, a process of polymers reinventing themselves and producing life along the way.

A **polymer** [1] is a molecule composed of repeating structural units, known generically as monomers. The word polymer itself derives from the Greek roots *polus*, meaning "many", and *meros*, denoting parts, or segments [74]. For example, all the DNA, or deoxyribonucleic acid, in an organism is formed from only four basic structural units, the **nucleotides**, which are the monomers of DNA. Messenger ribonucleic acid, or mRNA, is very similar to DNA, composed also of four nucleotides which vary only slightly from those that constitute DNA. In fact, the mRNA molecule is designed to mirror the information contained in a linear sequence of nucleotides in a section of DNA. A sequence of three nucleotides in the mRNA code uniquely for an **amino acid**, of which there are twenty. The amino acids are the monomers of the proteins.

Another, more operational definition asserts that a polymer is formed when the conditions for adding the $(n+1)$st monomer become independent of n [2]. In other words, there need not be specialized reactions to add subsequent monomers; provided that certain conditions are maintained, an arbitrary number of monomers can be added. In consequence, the **degree of polymerization**, the number of monomers comprising the polymer, can be very large. Consider that in one human cell, there are forty six chromosomes, each composed of one continuous, double stranded length of DNA. The contour length of all this DNA is approximately two metres [48]. This yields a contour length for a single molecule of human DNA on the order of centimetres. That is, each molecule of DNA is of *macroscopic* size. In fact, a molecule of DNA has a degree of polymerization on the order of 10^9, and is the largest known macromolecule [32] [3].

[1] Compound whose molecule is formed from many repeated units of one or more compounds [3].
[2] See the introduction of reference [22].
[3] The base sequence of the human genome has been estimated to require 820,000 pages of fine print, where a base is represented by one letter [48]. This means a single molecule of DNA would require

Polymers can also possess extraordinary physical properties, which has driven an extraordinary interest in the development of synthetic polymers. A simple example of a synthetic polymer is **polyethylene**, illustrated in fig. (1.2). Polyethylene

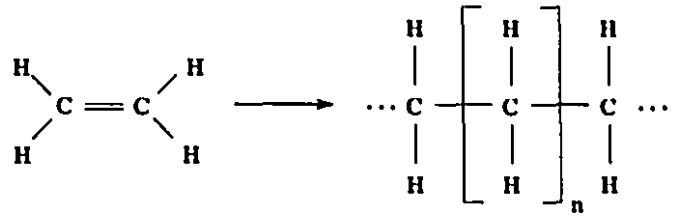

Figure 1.2: The synthetic polymer polyethylene is shown on the right, with the constituent monomer ethylene shown on the left. Polyethylene can have a high degree of polymerization, with n, the number of repeat units, on the order of 10^5.

is the material used, for example, in plastic bags and some plastic squeeze bottles. When one or more of the hydrogen side groups in the ethylene monomer are substituted, polymers with different, useful physical properties result. If all hydrogens are replaced by flourines, the resulting polymer, poly(tetraflouroethylene) or "Teflon", is a well known non-stick coating useful for frying pans and mechanical bearings. With similar substitutions one can produce polyvinyl chloride (pipes, raincoats, ...), polystyrene (packing chips, ...), poly(methyl methacrylate) ("Plexiglas"), among many others [73, 60]. Because of the low density and high strength of some polymers, they have become some of the most advanced synthetic materials. Polymers such

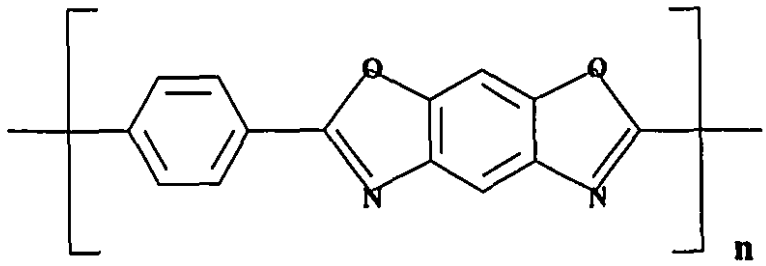

Figure 1.3: Poly(paraphenylene benzobisoxazole). This polymer is highly oriented since the only easy rotation is about the axis. A close variant is Kevlar, poly(paraphenylene terephthalamide).

as poly(paraphenylene benzobisoxazole) (fig. (1.3)) and related materials are highly oriented, closely packed, and consequently form materials with outstanding tensile strengths, despite being very light [53]. Still, it is interesting to compare these most

close to ten thousand pages filled with print much smaller than in this footnote.

advanced synthetic materials to material produced quietly in our back yards by creatures often beneath our notice. "Spiders, aided by several million years of evolution, have succeeded in producing a polymer fiber [major ampullate silk (MAS)] with a strength-to-weight ratio exceeding that of nearly all synthetic materials. Even the exceptions - specialty fibers such as carbon, silica, and some variants of Kevlar - pale in comparison when toughness (energy required to bring about failure) is taken into account" [72]. A single strand of silk can be kilometres in length, giving silk cloth the characteristic smoothness when woven that makes it much valued as a fabric. It is naturally biodegradable, and can be produced under normal conditions in an aqueous environment.

The final example of this introduction is a technology developed five millennia ago in Ancient China and Egypt, where it was discovered that the use of gum arabic [1] allows carbon black to mix uniformly in water [59]. This mixture was the earliest form of ink and was used to write on papyrus, revolutionizing the recording of information. This is an example of **colloidal stabilization**, with the gum arabic stabilizing the dispersion of the carbon particles in solution. A common mechanism of colloidal stabilization is illustrated in fig. (1.4), showing polymers attached through one end onto

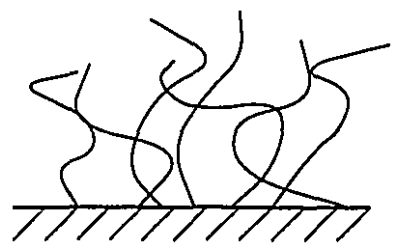

Figure 1.4: The polymer brush.

the surface of a particle. Provided the monomers are able to mix in the surroundings in which they are immersed, the polymers will stretch away from the relatively high monomer concentrations at the interface, forming a **polymer brush**. Since the interpenetration of brushes is entropically unfavourable, brush-carrying particles can be kept sufficiently far removed to avoid coagulation [2]. The polymer brush will be the primary focus of this thesis.

[1] A substance obtained from the *acacia* tree.

[2] A useful example of a failure of stabilization is in milk, where enzymatic removal of natural occurring polymer brushes results in the coagulation of milk proteins, producing cheese.

Polymers, then, come in many forms and serve many functions. Nature has developed extremely sophisticated materials with polymers to solve very demanding materials problems, as polymer scientists are learning to do. A deeper understanding of polymers, their structure and interactions, will lead not only to the creation of new and important materials, but to a better understanding of processes in all living systems. Polymers appear in the simplest forms of life, catalyze the most sophisticated reactions, provide much of the structure of the world around us. And from these polymers arise automobile sidepanels, bulletproof vests, human beings.

1.2 *Polymer physics and universal descriptions*

Statistical physics has been described in an insightful way as the "gestalt of physics" [42]. In other words, this part of physics admits that the whole is sometimes greater than the sum of its parts, that studies the properties emerging from the interactions of things with as much interest as the things themselves. A model, along with the statistical theory that elucidates its properties, can explain properties in diverse systems. It can be of as much interest as a particular material in which it is made manifest.

With this in mind, consider the troubling question of the role of statistical physics in polymer science. The study of polymers at first seems inextricably tied to questions of chemistry; *i.e.*, what are the monomers and how are they connected. Indeed, polymers are named by specifying the chemical monomer and adding the prefix *poly*, as in polyethylene or polystyrene, giving the impression that this describes the relevant aspects of the polymer. However, a polymer has properties that could not be easily predicted from examining one of its monomers. To take one example, the determination of the three dimensional structure of a protein given its linear sequence, or **primary structure**, remains an outstanding challenge [15] [1], even though the protein's tertiary structure is known to be indispensable to its function. Polymer physics, in contrast, searches for general descriptions to study those properties that are hopefully common to many polymers. "Here we try to omit the details of the chain structure as much as possible and to extract simple, universal features which

[1] Furthermore, there are many indications that it is necessary to understand the dynamics of proteins in order to understand their function [27].

will remain true for a large class of polymer chains [1]". For example, a polymer could be considered a long, thin, flexible object that doesn't intersect itself. Another example is a long, thin, flexible object that does intersect itself. Whether or not the object intersects itself has a significant effect on its large scale structure. That is, we seek to describe the properties that arise from the interactions between many monomers. We believe such descriptions are **universal**, applying to a class of polymers and not simply to one in particular. Thus, a polymer is more than so many of its constituent monomers – it is a "gestalt of monomers".

1.3 About this thesis

This thesis consists of both an introduction to relevant aspects of polymer physics as well as results of original research conducted in the course of this degree. It divides naturally into two parts: the next two chapters comprise an overview of general aspects of polymer theory important for topics to be explored later, while the chapters following concentrate on the subject of the present work, the polymer brush, and describe the results of our investigations of these systems.

The important pedagogical task of describing a polymer with the language and concepts of statistical mechanics will be the focus of chapter 2. It will be argued that essential aspects of polymers are captured by a self-avoiding random walk model, which is a conceptually simple and well defined. Unfortunately, its configurational properties cannot be described analytically, and for this reason, it will be useful to analyze the self-avoiding walk as a purely random walk, whose configurational statistics are known, with short range interactions between all segments of the walk to model the self-avoidance. In the absence of these short range interactions, the random walk polymer is described energetically as a connected linear sequence of ideal springs. In this manner, the polymer can be described with a Hamiltonian, known in the polymer literature as the Edwards Hamiltonian.

Given a Hamiltonian appropriate for systems of polymers, one can access the techniques of equilibrium statistical mechanics to determine the systems' equilibrium properties. In chapter 3, the statistical methods used in this thesis will be described

[1] See reference [17], pg. 25

within the framework of the Edwards Hamiltonian. Monte Carlo and Langevin simulation will be discussed in general, as well as the particulars of implementation with systems of polymers. Mean field theory will be introduced, in which the potential of interaction between polymer segments is replaced by a self consistently determined average field which is proportional to the average monomer density. Finally, corrections to the mean field theory will be examined assuming that the fluctuations from the mean field solution are Gaussian.

For the remainder of the thesis, discussion will specialize to polymer brushes. The polymer brush will be re-introduced in chapter 4, along with important results and representative papers selected from the literature. The method of simulation with an Edwards Hamiltonian will be applied to the brush in its canonical form; *i.e.*, a homogeneous brush grafted to a plane interface in good solvent. This will serve both to demonstrate the method and to illustrate many features typical of the brush. The next two chapters will report the results of original investigations of phase separation in polymer brushes. If the solvent in which the brush is immersed is made sufficiently poor, the monomers will phase separate from the solvent. Similarly, not all brushes are homogeneous in composition, leading to the possibility that immiscibility between polymers of different kinds will drive a phase separation where incompatible polymers phase separate. The polymeric connections of the monomers, the presence of a surface, the solvent quality, and the grafting constraint all combine to modify phase separation in both cases. The polymer brush in poor solvent will be examined in in chapter 5, where a predicted density instability will be confirmed with the results of an extensive simulation. The onset of this instability will be seen to compare favourably to predictions from a linear stability analysis. A particularly simple form of heterogeneity, the two component or "binary brush", will be considered in chapter 6. Simulations of a compositional instability, the demixing of the two components, will be combined with a numerical mean field analysis to examine the effects of solvent quality and immiscibility.

2

The Spherical Polymer

In the introduction, a polymer was defined as a connected sequence of monomers, although the precise nature of the monomer was not specified. However, under reasonable conditions, it is possible to have a generic understanding of polymers, to elucidate properties that are independent of the precise chemical composition of the polymer; *i.e.*, there is a level of description in which the exact meaning of "monomer" is irrelevant. A monomer is therefore understood to be *structureless*, without internal features, unlike the chemical monomer from which a real polymer is made. Perhaps the structureless monomer is **coarse-grained**, a representation of many neighbouring chemical monomers. It could be endowed with particular properties (size, charge, hydrophobicity, *etc.*) as a whole, which could be regarded as an average over the coarse grained sequence. Presumably, two polymers that at some degree of coarse graining can be described by the same structureless model should have the same large scale properties. The term "polymer", therefore, will from now on refer to this statistical polymer comprised of structureless monomers, unless otherwise clear in context.

In this chapter, a well defined model of a polymer will be developed and adopted for the balance of the thesis. A natural point of departure is the description of a polymer as a random walk, where a bond of the polymer is represented by a step of the walk. By introducing a particular form of random walk, the Gaussian chain, the random walk can be described by a Hamiltonian which determines the average squared bond length. It will afterwards be seen that under typical conditions, the random walk model is not adequate since self-avoiding interactions between monomers far apart along the sequence have a considerable effect on polymer statistics. This "excluded volume" effect will be accounted for by introducing n-body interactions between monomers of the Gaussian chain. In this way, the self avoiding walk can be

described by a Hamiltonian, the Edwards Hamiltonian, which combines the Gaussian chain and monomer interaction potentials. A polymer will be henceforth conceived of as a self avoiding walk described by an Edwards Hamiltonian.

2.1 Random walk polymers

In the **random walk model**, a linear polymer [1] composed of N identical monomers joined by bonds of length b is considered to be a random walk of N steps, each with step length b. This is illustrated in fig. (2.1) as a walk of N steps on a lattice of lattice constant b. A random walk polymer is thus specified by two parameters: the step size,

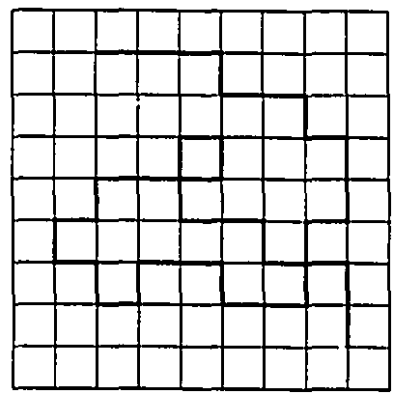

Figure 2.1: A polymer as represented by a random walk on a lattice of lattice constant b.

b, and the **degree of polymerization**, N. This model determines the manner in which monomers are connected, or the **connectivity**, in a simple and useful manner.

With the lattice random walk model, it is straightforward to calculate the possible number of **configurations**, or unique random walks. The number of configurations of a polymer with N monomers is $\Gamma = z^N$, where z is the coordination number of the lattice. Thus, the number of configurations quickly grows as N increases, and is large even for moderate values of N. Most descriptions of the polymer will therefore be statistical; *i.e.*, the result of an average over the ensemble of configurations of the polymer. For example, one important description is some measure of the size of the polymer [2], which could be, for example, the absolute value of the displacement vector

[1] This thesis will deal exclusively with linear polymers in three dimensions. Of course, there are many other interesting polymer architectures, from linear polymers with a few side branches, to polymers attached to themselves in a two dimensional network [38, 61].

[2] All measures of size of a random walk must be simple multiples of each other; thus, any one will

between the two ends of the polymer, the end vector $\mathbf{R}$, averaged over all possible configurations.

A more general configuration of a random walk, not restricted to lie on a regular lattice, is shown in fig. (2.2). The configuration is specified by the set of monomer

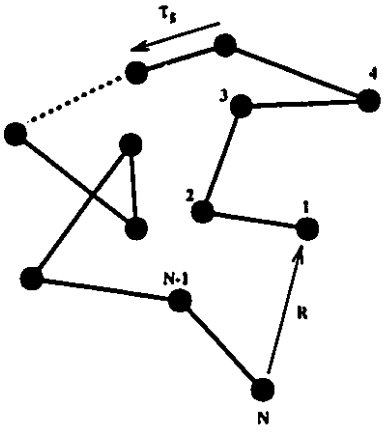

Figure 2.2: A configuration of a random walk polymer, not restricted to a lattice.

coordinates

$$\{\mathbf{R}_n\} \equiv \{\mathbf{R}_1, \mathbf{R}_2, \cdots, \mathbf{R}_N\}, \tag{2.1}$$

where $\mathbf{R}_n$ is the coordinate of nth monomer. A configuration can also be specified by the set of **bond vectors** $\{\tau_n\}$ [1], where

$$\tau_n \equiv \mathbf{R}_{n+1} - \mathbf{R}_n. \tag{2.2}$$

With these definitions, it is straightforward to calculate the "size" of a polymer; for example, some average of the end vector $\mathbf{R}$. If there is no preferred direction in space, symmetry demands that the average value of $\mathbf{R}$ must vanish; therefore, the first non-zero moment is $\langle \mathbf{R} \cdot \mathbf{R} \rangle$. Since $\mathbf{R}$ can be expressed as the vector sum of all bond vectors, $\mathbf{R} = \sum_{n=1}^{N-1} \tau_n$,

$$\langle \mathbf{R} \cdot \mathbf{R} \rangle = \left\langle \left(\sum_{i=1}^{N-1} \tau_i \right) \cdot \left(\sum_{j=1}^{N-1} \tau_j \right) \right\rangle$$

suffice as a characteristic length scale beyond the monomeric length. This will be shown from dimensional analysis.

[1] To completely specify the configuration, one monomer coordinate must be given in addition to $\{\tau_n\}$, although it is usually sufficient to know only the relative monomer positions.

$$= \sum_{i,j=1}^{N-1} \langle \tau_i \cdot \tau_j \rangle$$

$$= \sum_{i \neq j} \langle \tau_i \cdot \tau_j \rangle + \sum_i \langle \tau_i \cdot \tau_i \rangle$$

$$= \sum_i \langle \tau_i \cdot \tau_i \rangle \tag{2.3}$$

where $\sum_{i \neq j} \langle \tau_i \cdot \tau_j \rangle$ is zero since the steps are uncorrelated. If $\langle \tau_n \cdot \tau_n \rangle = b^2$ independent of n, then the size of the polymer

$$R = \left(Nb^2\right)^{\frac{1}{2}}, \tag{2.4}$$

where the scalar $R \equiv \langle |\mathbf{R}|^2 \rangle^{1/2}$, the root mean squared (rms) value of the end vector $\mathbf{R}$. This illustrates an important exponent, $R \sim N^{\nu}$, which specifies how the size of the polymer scales with the degree of polymerization. For the random walk, $\nu = \frac{1}{2}$. Moreover, the bond length b only appears in this calculation through its identification with $(\langle \tau_n \cdot \tau_n \rangle)^{1/2}$, suggesting that the important random walk parameter is the **bond variance**, b^2.

Some important definitions arising from the introduction of the random walk model are summarized in table 2.1.

symbol	
N	degree of polymerization
b^2	bond variance
τ_n	bond vector
$\mathbf{R}$	end vector
R	rms value of the end vector
$\mathbf{R}_n$	position of nth monomer
$\{\mathbf{R}_n\}$	set of monomer coordinates

Table 2.1: Parameters and definitions from the random walk model of a polymer.

2.1.1 *Dimensional analysis of the random walk*

In this section, **dimensional analysis** will be used to establish important scaling properties of a random walk [1].

Suppose a chain of N monomers is transformed by grouping together λ monomers, resulting in a chain with $N' = N/\lambda$ monomers. In particular, the bonds of the transformed chain connect every λth monomer, as illustrated in fig. (2.3). The mean

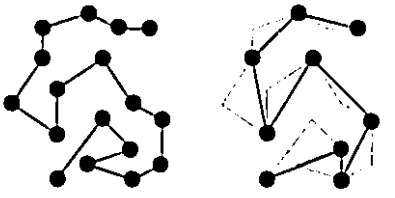

Figure 2.3: A random walk configuration, and its "renormalized" counterpart, after grouping together monomers in groups of $\lambda = 2$.

squared bond length of the transformed chain is the mean squared value of the end vector for the groups of λ monomers. If $1 < \lambda << N$, then each group is individually a random walk; therefore,

$$\begin{aligned} N &\to N/\lambda \\ b^2 &\to \lambda b^2. \end{aligned} \tag{2.5}$$

Eqn. (2.5) summarizes an important transformation property of a random walk. It describes the rescaling of the basic unit of the polymer chain, the coarse-graining of the monomers.

The coarse-graining process should not affect "macroscopic" properties of the random walk, such as the size. This can be explicitly verified for the mean squared value of the end vector, R^2. From eqn. (2.4),

$$\begin{aligned} (R')^2 &= N'(b')^2 \\ &= (N/\lambda)\left(\lambda b^2\right) \\ &= Nb^2, \end{aligned}$$

[1] This discussion follows reference [22], pg 32.

which is the size of the original chain. Therefore, coarse graining a random walk results in another random walk that retains the same macroscopic property.

To this point, the rms value of the end vector has been used to characterize the size of a random walk polymer. This choice is somewhat arbitrary, as many other lengths could have been chosen; for example, the radius of gyration. Nonetheless, dimensional analysis shows that any definition of size can differ from another only by a simple factor, and will have the same dependence on N and b.

Recall that there are only two parameters in the random walk model, the step size b, and the number of steps N. Furthermore, the average size of a polymer, regardless of its definition, must have dimensions of length. Thus, the size of the polymer must be expressed as

$$R(N,b) = F(N)\,b \tag{2.6}$$

where F is a dimensionless function of its arguments. F has no dependence on b because there is no dimensionless combination of parameters involving b. However, we expect the size of a random walk polymer to be invariant under transformation eqn. (2.5); thus,

$$F(N)b = F(N/\lambda)b\lambda^{\frac{1}{2}} \tag{2.7}$$

must be independent of λ. Assuming that $F(x) \sim x^{\alpha}$,

$$F(N/\lambda)b\lambda^{\frac{1}{2}} \sim (N/\lambda)^{\alpha}\, b\lambda^{\frac{1}{2}}. \tag{2.8}$$

This is independent of λ if $\alpha = 1/2$, and so the size R satisfies

$$R(N,b) \sim \left(Nb^2\right)^{\frac{1}{2}}. \tag{2.9}$$

Thus, any scalar quantity with the dimensions of length and which is invariant under coarse graining is simply a multiple of R. In this sense, there is only one characteristic macroscopic lengthscale, and one can limit discussion to R without losing generality.

2.1.2 *Finite correlations along the chain*

Until now, zero correlation between bond vectors has been assumed, although generally, one would expect a large degree of correlation amongst monomers close in

sequence. For example, in the simple polymer polyethylene, there are fixed bond angles between neighbouring monomers, resulting in large correlations amongst near neighbours on the polymer. Similarly, there are many models with this property in the literature: fixed bond angle models, models with specific bond angle potentials, semi-rigid polymer models, amongst others. All these models are characterized by finite correlations along the contour of the chain, and as a result, are not truly random.

Nonetheless, the results derived for a random walk still apply to models with a finite correlation length as long as there is the freedom to coarse grain the polymer into sections much larger than this correlation length [1]. These resulting coarse grained units will be uncorrelated by construction, and according to the basic transformation property of a random walk, eqn. (2.5), this equivalent polymer is an uncorrelated random walk with a renormalized bond length. As a consequence, molecular details that determine the persistence of correlations, though certainly important to physical properties, can be viewed as important only at length scales on the order of the correlation length. The calculation of the correlation length may in general be very difficult, and may depend sensitively on the microscopic specifics of the model being considered. However, if only long wavelength properties are of interest, the effect of molecular details is only to determine the bond length, which can be considered a phenomenological parameter to be determined by comparison to experiment.

2.1.3 *The Gaussian chain*

The random walk has thus far been parameterized by the degree of polymerization, N, and the bond variance, b^2. As the exact nature of the bond only affects the random walk through rescaling the bond variance, we are free to choose a random walk model for its analytical convenience.

In the **Gaussian chain** model, the probability for a bond to take a particular length is assumed to satisfy a Gaussian distribution. Typically, each individual bond distribution is assumed to have the same variance, σ^2. In three dimensions,

$$P(\boldsymbol{r}) = \left(\frac{3}{2\pi\sigma^2}\right)^{\frac{3}{2}} \exp\left(-\frac{3|\boldsymbol{r}|^2}{2\sigma^2}\right). \tag{2.10}$$

[1] This correlation length is also known as the **persistence length** [32].

The probability of a configuration, $\{\tau_i\}$, is therefore

$$P\{\tau_i\} = \prod_{i=1}^{N-1} P(\tau_i)$$

$$= \left(\frac{3}{2\pi\sigma^2}\right)^{\frac{3N}{2}} \exp\left(-\frac{3}{2\sigma^2}\sum|\tau_i|^2\right). \qquad (2.11)$$

The assumption of a random walk is present in eqn. (2.11) in the independence of the individual bond distributions. Eqn. (2.11) can be written

$$P\{\tau_i\} \sim \exp\left(-\frac{1}{k_BT}H_G\{\tau_i\}\right), \qquad (2.12)$$

where

$$H_G\{\tau_i\} = \frac{3k_BT}{2\sigma^2}\sum\tau_i^2$$

$$= \frac{3k_BT}{2\sigma^2}\sum_{i=2}^{N}(\mathbf{R}_i - \mathbf{R}_{i-1})^2. \qquad (2.13)$$

Thus, the Gaussian probability is analogous to a Boltzmann factor, where the "Hamiltonian" of the Gaussian chain is given by eqn. (2.13). For the remainder of the thesis, k_BT will be set to one. The Gaussian chain reproduces our previous fixed bond length model if $\sigma^2 = b^2$. The Gaussian chain is not identical to the previous model, but equivalent in that it has the same number of monomers N, the same mean squared bond length, and preserves the same size R of the previous model.

An alternate description of the Gaussian chain specifies the position along the chain by a continuous index n, rather than discrete indices labelling discrete monomers. This is the **continuous chain**, where the polymer is considered to be a continuous curve. In this description, the contour length is specified along with the chain's "flexibility", which is related to R. This limit is sometimes called the **functional integral limit**, so-called because in this limit, the polymer partition function is a functional integral.

The continuous chain limit is illustrated in fig. (2.4). It is achieved by increasing the number of monomers in the discrete case arbitrarily, decreasing the bond length to zero in such a way that the average size of the polymer is preserved. In the discrete case, the position of the nth monomer is given by $\mathbf{R}_n$, where n is a discrete index. In

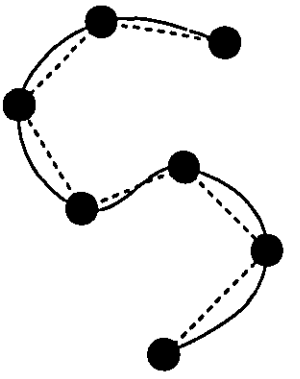

Figure 2.4: Continuous chain limit of the discrete chain.

the functional integral limit, n becomes a continuous variable, and the set of discrete monomer positions $\{\mathbf{R}_n\}$ becomes a function of n, $\mathbf{R}(n)$. If the contour length of the curve is L, the ratio R^2/L is some parameter, b, which is a measure of the flexibility of the chain [1]. Furthermore, any portion of this chain is assumed to be characterized by the same value b. Thus, if τ is the distance along the contour of the curve, then for any portion of curve $\Delta\tau$, $\sigma^2/\Delta\tau = b$, where σ^2 is the mean squared separation of the ends of the portion. If $\Delta\mathbf{r}$ is the end vector for this portion of chain,

$$\begin{aligned} P(\Delta\tau) &\sim \exp\left[-\frac{3}{2\sigma^2}(\Delta\mathbf{r})^2\right] \\ &= \exp\left[-\frac{3}{2b\Delta\tau}(\mathbf{R}(\tau)-\mathbf{R}(\tau-\Delta\tau))^2\right] \\ &= \exp\left[-\frac{3\Delta\tau}{2b}\left(\frac{\mathbf{R}(\tau)-\mathbf{R}(\tau-\Delta\tau)}{\Delta\tau}\right)^2\right], \end{aligned}$$

where $\mathbf{R}(\tau)$ is the spatial coordinate of the point along the chain a distance τ along the contour from a chosen end. The Gaussian chain Hamiltonian thus becomes

$$\begin{aligned} H_G &= \frac{3}{2b}\sum\Delta\tau\left(\frac{\mathbf{R}(\tau)-\mathbf{R}(\tau-\Delta\tau)}{\Delta\tau}\right)^2 \\ &\to \frac{3}{2b}\int_0^L d\tau\left(\frac{\partial\mathbf{R}(\tau)}{\partial\tau}\right)^2, \end{aligned} \tag{2.14}$$

where the integral holds in the limit $\Delta\tau \to 0$. Finally, eqn. (2.14) can be written in

[1] This quantity is usually called the **Kuhn length**, or the **statistical segment length**, and is related to the persistence length (see section 2.1.2).

terms of the dimensionless index n by setting $\tau = nb$, in which case

$$H_G = \frac{3}{2b^2}\int_0^N dn \left(\frac{\partial \mathbf{R}(n)}{\partial n}\right)^2. \tag{2.15}$$

The Gaussian chain Hamiltonians for the discrete and continuous random walk models of a polymer are shown here in summary:

$$H_G\{\mathbf{R}_i\} = \frac{3}{2b^2}\sum_i (\mathbf{R}_i - \mathbf{R}_{i-1})^2$$

$$H_G[\mathbf{R}(n)] = \frac{3}{2b^2}\int_0^N dn \left(\frac{\partial \mathbf{R}(n)}{\partial n}\right)^2. \tag{2.16}$$

Some definitions relating the discrete case and its functional limit counterpart are summarized in table 2.2.

discrete	continuous	
$\{\mathbf{R}_n\}$	$\mathbf{R}(n)$	polymer configuration
$f\{\mathbf{R}_n\}$	$f[\mathbf{R}(n)]$	configuration functional
$d\{\mathbf{R}_n\}$	$D[\mathbf{R}(n)]$	functional measure
$\sum_n^N$	$\int_0^N dn$	integral along polymer contour
$\mathbf{R}_n - \mathbf{R}_{n-1}$	$\partial \mathbf{R}(n)/\partial n$	derivative along contour

Table 2.2: Continuous limit equivalents to the discrete chain.

The Gaussian chain is often called the **ideal chain**, reflecting the analytical facility of this model. Unfortunately, the random walk description is very limited in its ability to describe polymer properties. What has yet to be discussed is the vital contribution of "non-local interactions".

2.2 *Non-local interactions*

Two monomers that are far apart along the contour of the polymer may still be close enough in space to interact directly. This type of interaction is often called a **long-range interaction** in the polymer literature, illustrated in fig. (2.5). In this context, "long range" refers to the separation of monomers in sequence; however,

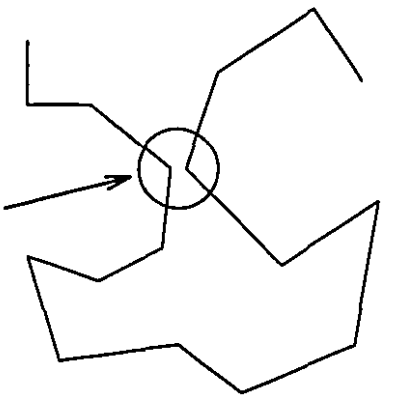

Figure 2.5: An example of a non-local interaction between segments far apart on the sequence of the polymer.

the interaction itself is typically very short ranged. The unfortunate nature of this nomenclature has been previously noted [15], and for this reason, the term **non-local** will be used in this thesis to refer to this type of interaction, reserving long-ranged for long-ranged in space. In discussions of random walks, it has been tacitly assumed that there are no non-local interactions. A walk with finite correlations along the contour of the polymer can only be renormalized into a random walk if correlations between monomers disappear as the polymer is coarse-grained. In the presence of non-local interactions, this is not true, even for a very flexible molecule.

One inescapable non-local interaction, rooted deeply in the language of polymer physics, is **hard-core repulsion**, the fact that two monomers may not occupy the same volume. In fact, non-local interactions are often categorized under the general rubric of **excluded volume** interactions, even though non-local interactions are rarely plain hard core interactions. The inclusion of non-local interactions has a dramatic effect on configurational properties.

> The great difficulty in the statistical mechanics of polymer chains with excluded volume is that the position of a link depends on the positions of all the other links instead of on the position of just the previous one; this difficulty is reflected by the extensive literature on the subject ... [23]

The excluded volume interaction introduces non-trivial correlations between monomers; the effect of monomer A upon monomer B depends very much on the state of the rest of the polymer, on whether or not the configuration brings the two monomers

close enough to interact. A simple model incorporating excluded volume interactions is the **self-avoiding walk**, a random walk that at no point intersects itself. It is generated on a lattice as a random walk where sites are excluded that were previously occupied by the walk.

Nonetheless, one can infer broad consequences of an excluded volume interaction. For example, a dense random walk configuration will more likely violate an excluded volume constraint (no monomer overlap) than an extended random walk configuration. Thus, extended configurations are favoured in the presence of excluded volume interactions, and the polymer will be swollen with respect to the ideal polymer. Furthermore, since the probability of excluded volume interactions increases with N, long polymers are more susceptible than short polymers. Therefore, one would expect excluded volume effects to change the exponent ν, introduced in section 2.1, that describes how the size of the polymer scales with the degree of polymerization. A rough estimate of this exponent can be made as follows. The probability distribution for the size R of a Gaussian chain with N monomers is Gaussian with variance Nb^2; *i.e.*,

$$P_G \sim \exp\left(-\frac{R^2}{N}\right), \tag{2.17}$$

where only the dependence on R and N is made explicit. For a polymer of size R, the excluded volume energy E roughly follows

$$\begin{aligned} E &\sim \phi^2 V \\ &\sim \left(\frac{N}{R^3}\right)^2 R^3 \end{aligned}$$

where ϕ is the monomer density, assumed uniform throughout the volume $V \sim R^3$ of the polymer. Consequently, the probability due to the excluded volume energy is

$$P_E \sim \exp(-E), \tag{2.18}$$

giving the total probability of a random walk with excluded volume interaction as

$$\begin{aligned} P &\sim P_G P_E \\ &\sim \exp\left(-\frac{R^2}{N} - \frac{N^2}{R^3}\right). \end{aligned}$$

The value of R is determined by maximizing P with respect to R, or equivalently, minimizing the quantity

$$\frac{R^2}{N} + \frac{N^2}{R^3}, \tag{2.19}$$

with respect to R. This yields

$$R \sim N^{\frac{3}{5}}, \tag{2.20}$$

giving the exponent $\nu = 3/5$ for the polymer with non-local interactions. As advertised, the exponent is modified from the random walk value of 1/2. Considering the simplicity of this argument, the value for the exponent turns out to be surprisingly accurate. Computer simulations [75] with self-avoiding walks give $2\nu = 1.18$, which is consistent with a renormalization group calculation for the n-vector model [33], giving $\nu = 0.5880 \pm 0.0015$. Experiments [16] with polymers in solution give the value $\nu = 0.586 \pm 0.004$. For these reasons, the self-avoiding walk has been called the **minimal model** of the polymers in solution [1]. In fact, it is a large part of the truth to say that polymer physics is the physics of self-avoiding walks.

Since any two monomers must minimally interact via a hard core interaction, it may seem that the concept of an ideal polymer is unrealizable, and therefore of limited value. In actual fact, the Gaussian chain remains central to developing polymer models for a number of reasons. In some instances, circumstances conspire to produce a polymer that is indeed close to being ideal. For example, if polymers are immersed in solvent, under certain conditions the interaction between solvent and polymer can mitigate the excluded volume effect. Under this condition, called the **Θ condition**, the polymer is well described as a random walk [2]. Another situation where the excluded volume effect is screened is, counter-intuitively, under conditions of high polymer concentration, such as in a **polymer melt** [3].

There is another more subtle, and arguably more important reason to understand the Gaussian chain. That is, in many polymer models, including ones to be introduced shortly, there is a rarely stressed, implicit assumption that there is a valid description of the polymer configuration in terms of a random walk, independent of the excluded

[1] A minimal model is one that "most economically caricatures the essential physics" [29] of a class of related phenomena.

[2] See, for example, the results of reference [76].

[3] See reference [17], chapter 2.

volume effect. An example of this is seen in the scaling argument immediately preceding, where there were assumed to be two independent probabilities contributing to the total probability, one from a probability of a certain random walk (of size R), and one due to excluded volume effects [1]. For these reasons, the Gaussian chain remains an important concept and a major influence on the language of polymer physics.

2.2.1 *Computer methods*

The excluded volume problem outlined in the previous section can be understood as a problem of characterizing polymer configurations; *i.e.*, finding the average of some measurable quantity over only those configurations that do not violate the excluded volume condition. Not surprisingly, computers are powerful tools in answering such question, especially since a self avoiding walk is naturally represented on a lattice, which is easily represented in the computer milieu.

For small polymers, it is possible to generate every random walk configuration and explicitly check for self avoiding configurations. This technique, known as **exact enumeration**, was one of the early computer methods, and is still used currently due to recent interest in random copolymers as models of biopolymers [14, 37]. The problem with this method is that the number of configurations grows as $\Gamma = z^N$, where z is the coordination number of the lattice. Exact enumeration is feasible only for very short polymers.

Since exact enumeration is impractical for most polymer problems, another possible approach is to sample randomly the configuration space of self avoiding walks. A brute force method for generating self avoiding configurations is to grow random walks on a lattice and eliminate any walk that violates the excluded volume condition. This has the advantage of being straightforward, and of generating uncorrelated self avoiding configurations. Unfortunately, it has become accepted, largely through computer work of the type described so far, that the ratio of the number of self avoiding configurations to random walk configurations decreases exponentially with N [75]. In other words, the **acceptance ratio**, the number of configurations accepted per num-

[1] This assumption is the basis of **two parameter theory**, which assumes, not surprisingly, two independent parameters: one that describes that random walk configuration, and one that describes non-local interactions.

ber of configurations generated, quickly falls to zero, making this a very inefficient scheme for large N. This problem can be mitigated to some extent by decorations to the basic algorithms, but the underlying problem remains.

A significant improvement is realized by introducing local moves to update polymer configurations. With this method, a new configuration is generated through a small change from the previous one. This small change is called a local move if it changes the polymer only locally, perhaps moving one or a small number of connected monomers. The great advantage of this method is that small changes from a valid self-avoiding configuration are very likely to generate another valid configuration, improving the acceptance ratio enormously. The drawback of this method is that the new configuration generated is highly correlated with the previous one. However, two configurations will be uncorrelated from one another when enough configurations have been generated in between. This method of sampling configurations is the one of choice for long polymers, and is almost always implemented with the Monte Carlo method. In fact, a variant of this method will be introduced later in this thesis.

Another approach to generating polymer configurations is **molecular dynamics**, where the equations of motion for a model polymer are solved numerically, generating a dynamic evolution for the polymer. Molecular dynamics and local move Monte Carlo simulation are the dominant simulation schemes in use currently.

2.2.2 *Expansion in density*

In order to develop analytical theories, it is convenient to have an expression for the energy due to excluded volume interactions, H_I.

In principle, H_I is a function of configuration of the polymer,

$$H_I = H_I\{\mathbf{R}_n\}, \tag{2.21}$$

where $\{\mathbf{R}_n\}$ is the set of all monomer coordinates. If the potential does not distinguish between monomers, it is natural to frame H_I in terms of the local monomer concentration. This transformation between a configuration and density is made formally explicit with the definition of the microscopic density

$$\phi(\mathbf{r}) = \sum_n \delta(\mathbf{r} - \mathbf{R}_n), \tag{2.22}$$

where the sum over n is a sum over all monomers, and for all polymers in a many polymer system. Hence, H_I can be written as a functional of the density

$$H_I = \int d\mathbf{r}\, U\left(\phi(\mathbf{r})\right). \tag{2.23}$$

If there are no long-range interactions and the monomer density is everywhere small, U can be expanded in powers of the local monomer concentration,

$$H_I = \int d\mathbf{r} \sum_k \left(a_k \phi^k(\mathbf{r})\right). \tag{2.24}$$

This expansion is typically truncated at the lowest nontrivial order,

$$H_I = \frac{w_2}{2} \int d\mathbf{r}\, \phi^2(\mathbf{r}). \tag{2.25}$$

The coefficient of the quadratic term, w_2, is called the **excluded volume parameter.**

At this level of approximation, H_I is equivalent to summing over all pairwise interactions between monomers [1]. In order to see this, recall that all interactions are short ranged. Thus, the pairwise potential between monomers i and j can be approximated

$$U(\mathbf{R}_i, \mathbf{R}_j) = w_2 \delta(\mathbf{R}_i - \mathbf{R}_j), \tag{2.26}$$

and H_I becomes

$$\begin{aligned} H_I &= \frac{1}{2} \sum_{i,j} U(\mathbf{R}_i, \mathbf{R}_j) \\ &= \frac{w_2}{2} \sum_{i,j} \delta(\mathbf{R}_i - \mathbf{R}_j), \end{aligned}$$

where the factor of two is to correct for double counting. The delta function can be written

$$\delta(\mathbf{R}_i - \mathbf{R}_j) = \int d\mathbf{r}\, \delta(\mathbf{r} - \mathbf{R}_i)\, \delta(\mathbf{r} - \mathbf{R}_j). \tag{2.27}$$

Thus, H_I becomes

$$H_I = \frac{w_2}{2} \sum_{i,j} \int d\mathbf{r}\, \delta(\mathbf{r} - \mathbf{R}_i)\, \delta(\mathbf{r} - \mathbf{R}_j). \tag{2.28}$$

Using the expression for the microscopic density, eqn. (2.22), we see that in fact the above equation is exactly eqn. (2.25). With this interpretation, w_2 parameterizes

[1] In this context, pairwise monomer interactions are assumed to be mediated by the solvent in which the monomers are immersed. This point will be discussed in the next section.

pairwise interactions amongst monomers. If $w_2 < 0$, the interaction lowers the system energy, corresponding to an attractive interaction. Conversely, $w_2 > 0$ models an effective repulsion, giving rise to an excluded volume effect.

2.2.3 *Potential of the mean force*

It is important to note that the potential of interaction between monomers implicitly includes the effect of the solvent. That is, it is the potential between monomers averaged over all possible positions of solvent molecules. Specifically, if $\{\mathbf{R}_i\}$ and $\{\mathbf{s}_j\}$ are the sets of all monomer coordinates and solvent coordinates respectively, then the partition function of the whole system, monomers plus solvent particles, is

$$Z = \sum_{\{\mathbf{R}_i\}} \sum_{\{\mathbf{s}_j\}} \exp\left(H_G\left\{\mathbf{R}_i\right\} + H_{rs}\left\{\mathbf{R}_i, \mathbf{s}_j\right\},\right) \tag{2.29}$$

where the interaction potential H_{rs} appears explicitly as a function of the monomer coordinates as well as the solvent coordinates. If we perform the sum over all the solvent coordinates, eqn. (2.29) formally becomes

$$Z = \sum_{\{\mathbf{R}_i\}} \exp\left(H_G\left\{\mathbf{R}_i\right\} + H_I\left\{\mathbf{R}_i\right\},\right) \tag{2.30}$$

where the interaction potential now only depends on the monomers positions. It is sometimes called the **potential of the mean force** [15], since it is like a potential averaged over all the non-monomer degrees of freedom. Although it will not be explicitly stated from now on, monomer interaction potentials are in fact potentials of the mean force.

2.3 *The Edwards Hamiltonian*

The probability of a configuration is assumed to be a combination of two effects already discussed: the bond probability modelled by the Gaussian chain, and the interaction probability that depends on the interaction potential, H_I. The Gaussian chain probability distribution has been derived earlier (eqn. (2.16));

$$P \sim \exp\left(-\frac{3}{2b^2}\int dn \left(\frac{\partial \mathbf{R}(n)}{\partial n}\right)^2\right). \tag{2.31}$$

The probability due to non-local interactions is proportional to e^{-H_I}, where an expression for the interaction energy H_I has been given above, in eqn. (2.25). Thus, the total configuration probability becomes

$$P[\mathbf{R}(n)] \sim \exp\left(-\frac{3}{2b^2}\int dn \left(\frac{\partial \mathbf{R}(n)}{\partial n}\right)^2 - \frac{w_2}{2}\int d\mathbf{r}\,\phi^2(\mathbf{r})\right), \tag{2.32}$$

where the concentration $\phi(\mathbf{r})$ is also a functional of the configuration $\mathbf{R}(n)$. The probability can be rewritten $\exp(-H[\mathbf{R}(n)])$, where

$$H[\mathbf{R}(n)] = \frac{3}{2b^2}\int dn \left(\frac{\partial \mathbf{R}(n)}{\partial n}\right)^2 + \frac{w_2}{2}\int d\mathbf{r}\,\phi^2(\mathbf{r}). \tag{2.33}$$

This expression is clearly analogous to a Hamiltonian in a Boltzmann factor. For this reason, expression eqn. (2.33) will be referred to as an **Edwards Hamiltonian**, and is an energetic representation of a polymer chain. The connectivity is described through a Gaussian energy, H_G, instead of, for example, a fixed bond length random walk. Non-local interactions are described energetically, in terms of a coarse grained monomer concentration $\phi(\mathbf{r})$, instead of as geometrical constraints, as in a self-avoiding walk on a lattice. The form of an Edwards Hamiltonian may vary, as indeed it will in this thesis, but it retains these basic characteristics. The Edwards Hamiltonian is the central result of this chapter. The polymer partition function, Z, is defined

$$Z = \int D[\mathbf{R}(n)]\exp(-H[\mathbf{R}(n)]). \tag{2.34}$$

This gives a formal expression for the probability of a configuration

$$P[\mathbf{R}(n)] = \frac{1}{Z}\exp(-H[\mathbf{R}(n)]). \tag{2.35}$$

Although the Edwards Hamiltonian has been written for one polymer, the generalization to a system of K polymers of the same type is straightforward;

$$H\{\mathbf{R}_k(n)\} = \frac{3}{2b^2}\sum_k \int dn \left(\frac{\partial \mathbf{R}_k(n)}{\partial n}\right)^2 + \frac{w_2}{2}\int d\mathbf{r}\,\phi^2(\mathbf{r}) \tag{2.36}$$

where

$$\phi(\mathbf{r}) = \sum_k \int dn\,\delta(\mathbf{r} - \mathbf{R}_k(n)). \tag{2.37}$$

The density has been written in terms of the continuous chain, $\mathbf{R}(n)$, where the sum over k is over all different polymers ($k = 1, \cdots, K$).

3

The Hamiltonian Way

In the previous chapter, the Edwards Hamiltonian was arrived at as a model of polymer systems,

$$H = \frac{3}{2b^2} \sum_k \int dn \left(\frac{\partial \mathbf{R}_k(n)}{\partial n} \right)^2 + \frac{w_2}{2} \int d\mathbf{r}\, \phi^2(\mathbf{r}), \tag{3.1}$$

an expression that completely specifies the equilibrium properties of the polymer system. The task outstanding is to elicit those properties, a task that will involve a variety of methods familiar in statistical physics.

The objective of this chapter is to develop these techniques in order to determine the equilibrium properties of a polymer described by an Edwards Hamiltonian, focussing on the methods to be applied in this thesis. Monte Carlo simulation will figure prominently in the original investigations described in chapter 5 and chapter 6; therefore, this method will be introduced in some detail, concentrating on its implementation for polymer systems described by an Edwards Hamiltonian. The linear dynamic response of these polymer systems will then be described with a stochastic differential equation known as a Langevin equation. This equation, together with a fluctuation-dissipation relation, can also be used to determine equilibrium properties, as illustrated in the next chapter. Mean field methods are very powerful when applied to polymers in the semi-dilute regime. They describe a Gaussian polymer in a self-consistent mean field potential, determined using Green function methods. Corrections to mean field theory will be introduced through the random phase approximation, described at the end of this chapter. Under this approximation, the limits of stability of the mean field solution can be found, which will be used in chapter 6 to determine the onset of a density instability in a heterogeneous brush.

3.1 Monte Carlo simulation

As was argued in section 2.2.1, the number of configurations of a polymer quickly increases with N beyond the possibility of rigorously enumerating them all, making it necessary to sample the configuration space of the polymer in an efficient manner. The **Monte Carlo method** is a highly successful sampling technique that has found wide application in statistical physics [8]. The Monte Carlo method will be introduced in general terms in the next section, followed by the details of its implementation with an Edwards Hamiltonian.

3.1.1 A Monte Carlo primer

Suppose a system can exist in one of a discrete number of states, σ_i. Suppose also there is some observable, A, which can be expressed as a function of the state. The objective of the Monte Carlo method is to estimate the average of A

$$\langle A \rangle = \sum_i A(\sigma_i)\,\rho(\sigma_i), \tag{3.2}$$

where the states are distributed according to some probability distribution $\rho(\sigma_i)$, and the sum is over all possible states. If the number of states is too large to permit direct evaluation of eqn. (3.2), it can be approximated by a Monte Carlo average over N samples,

$$\langle A \rangle_{MC} = \frac{1}{N}\sum_{i=1}^{N} A(\sigma_i), \tag{3.3}$$

where the sequence of configurations $\{\sigma_1, ..., \sigma_N\}$ is distributed according to $\rho(\sigma_i)$. This technique, whereby states are sampled according to their probability, is known as **importance sampling.**

Consider, therefore, the question of how to generate a sequence of states with a given probability distribution. Let $p_n(i)$ be the probability of the state σ_i after the nth step of the sequence, and suppose

$$p_n(i) = \sum_j w_{ij} p_{n-1}(j), \tag{3.4}$$

where w_{ij} is the conditional probability of transition per step from state σ_i to σ_j. That is, the probability distribution of states at the nth step depends only on the probability distribution at the $(n-1)$st step. Eqn. (3.4) is characteristic of a **Markov**

process [1]. The Markov process is said to be **ergodic** if transitions between any state σ_i to any other state σ_j is possible in a finite number of steps.

The distribution $p(i)$ is the **stationary distribution** of w_{ij} if and only if

$$p(i) = \sum_j w_{ij} p(j) \tag{3.5}$$

for all i. That is, $p(i)$ is an eigenvector of w_{ij} with eigenvalue one. It is remarkable fact that for any ergodic Markov operator, convergence to a *unique* stationary distribution is guaranteed in the limit of many steps [42].

A sequence of states can therefore be generated with a given probability distribution by appropriately constructing the Markov operator w_{ij} so that the stationary distribution is the required distribution of states, $\rho(\sigma_i)$. The stationary distribution must satisfy

$$\sum_i (w_{ij} p(j) - w_{ji} p(i)) = 0, \tag{3.6}$$

which is equivalent to eqn. (3.5), as $\sum_i w_{ij} = 1$. Eqn. (3.6) will certainly be satisfied if balance is achieved for every i and j, so that

$$w_{ij} p(j) - w_{ji} p(i) = 0, \tag{3.7}$$

a condition known as **detailed balance.** Thus, if the Markov operator w_{ij} satisfies

$$\frac{w_{ij}}{w_{ji}} = \frac{\rho(\sigma_i)}{\rho(\sigma_j)}, \tag{3.8}$$

the stationary distribution will be $\rho(\sigma_i)$.

For a system in the canonical ensemble with the Hamiltonian H,

$$\frac{\rho(\sigma_i)}{\rho(\sigma_j)} = \exp(-\beta(H_i - H_j)). \tag{3.9}$$

One standard choice for w_{ij} that satisfies eqn. (3.7) is the **Metropolis algorithm,**

$$w_{ij} = \begin{cases} \min\{1, \exp(-\beta(H_i - H_j))\} & i \neq j \\ 1 - \sum_{i \neq j} w_{ij} & i = j. \end{cases} \tag{3.10}$$

The implementation of the Monte Carlo method with the Metropolis algorithm is outlined as follows:

[1] Eqn. (3.4) can be interpreted as a matrix equation; thus, the matrix w_{ij} is sometime called a **Markov operator.**

- Randomly choose a trial configuration. This is usually accomplished by making a small change from a previous configuration; *e.g.*, flipping one spin on an Ising lattice, or moving one monomer on a polymer.
- Calculate the energy difference between the trial configuration and the initial configuration, $\Delta H = H_{trial} - H_{initial}$.
- If $\Delta H < 0$, accept the trial configuration and repeat from step one.
  - Otherwise, choose a random number r from a uniform distribution so that $0 \leq r < 1$.
  - If $r < \exp(-\beta \Delta H)$, accept the trial configuration and repeat from step one.
  - Otherwise, reject the trial configuration and repeat from step one.

Monte Carlo averages are then calculated by applying eqn. (3.3) to N configurations chosen from this sequence.

3.1.2 *Monte Carlo with an Edwards Hamiltonian*

The Monte Carlo method can be applied to simulate polymer systems by employing the Edwards Hamiltonian, eqn. (3.1), in the procedure described in section 3.1.1.

In order to represent the polymer on a computer, it is natural to use the discrete Gaussian chain model. Recall from section 2.1 that a configuration of the discrete Gaussian chain can be specified by a set of coordinates $\{\mathbf{R}_n\}$, where n is a discrete index identifying the monomer, and $\mathbf{R}_n$ is a vector specifying the position of the nth monomer. Additional indices may be introduced if there is need to further distinguish monomers; for example, an index k could be introduced for a many polymer system so that $\mathbf{R}_{k,n}$ identifies the nth monomer on the kth polymer.

The "energy" contribution of the discrete Gaussian chain was discussed in section 2.1.3. The Hamiltonian was given by eqn. (2.13),

$$H_G = \frac{3}{2b^2} \sum_{n=2}^{N} (\mathbf{R}_n - \mathbf{R}_{n-1})^2 . \tag{3.11}$$

The discrete Gaussian chain is analogous to mechanical system of N sizeless beads connected by identical springs, each with spring constant $3/b^2$. The calculation of

H_G, the **connected energy contribution**, is straightforward from eqn. (3.11) given a configuration $\{\mathbf{R}_n\}$.

technical

Care must taken with boundary conditions if periodic boundary conditions are used. Monomer separations could be artificially stretched if a monomer is wrapped to the opposite side of the simulation volume. One solution is to store a separate set of monomer coordinates to which periodic boundary conditions do not apply. This does not affect the value of H_G calculated with eqn. (3.11), since the exact location of the monomer in the volume is not needed, only the relative monomer separations.

The non-local energy contribution, H_I, was introduced in section 2.2.2 as an expansion in terms of the local monomer density, where to the first non-trivial order

$$H_I = \frac{w_2}{2} \int d\mathbf{r}\, \phi^2(\mathbf{r}), \tag{3.12}$$

where ϕ is given by

$$\phi(\mathbf{r}) = \sum_n \delta(\mathbf{r} - \mathbf{R}_n). \tag{3.13}$$

The expression for the microscopic density eqn. (3.13) is inappropriate for simulation, since it contains the delta function. However, one can substitute the analytical representation

$$\phi(\mathbf{r}) = \sum_n \left(\frac{3}{2\pi\sigma^2}\right)^{3/2} \exp\left(-\frac{3}{2\sigma^2}(\mathbf{r} - \mathbf{R}_n)^2\right). \tag{3.14}$$

That is, the delta function is approximated by a Gaussian with a finite variance σ^2. This expression is equivalent to eqn. (2.22) in the limit of $\sigma^2 \to 0$. Using eqn. (3.14) for the density,

$$\begin{aligned}\phi^2(\mathbf{r}) &= \left(\frac{3}{2\pi\sigma^2}\right)^3 \sum_{m,n} \exp\left\{-\frac{3}{2\sigma^2}\left((\mathbf{r} - \mathbf{R}_n)^2 + (\mathbf{r} - \mathbf{R}_m)^2\right)\right\} \\ &= \left(\frac{3}{2\pi\sigma^2}\right)^3 \sum_{m,n} \exp\left(-\frac{3}{4\sigma^2}(\mathbf{R}_n - \mathbf{R}_m)^2\right) \exp\left(-\frac{3}{\sigma^2}\left(\mathbf{r} - \frac{\mathbf{R}_n + \mathbf{R}_m}{2}\right)^2\right).\end{aligned}$$

Substituting this expression into eqn. (3.12), the interaction energy H_I becomes

$$H_I = \frac{w_2}{2} \int d\mathbf{r}\, \phi^2(\mathbf{r})$$

$$= \frac{w_2}{2}\left(\frac{3}{2\pi\sigma^2}\right)^3 \sum_{m,n} \exp\left(-\frac{3}{4\sigma^2}(\mathbf{R}_n - \mathbf{R}_m)^2\right)$$

$$\times \int d\mathbf{r} \exp\left(-\frac{3}{\sigma^2}\left(\mathbf{r} - \frac{\mathbf{R}_n + \mathbf{R}_m}{2}\right)^2\right)$$

$$= \frac{w_2}{2}\left(\frac{3}{4\pi\sigma^2}\right)^{3/2} \sum_{m,n} \exp\left(-\frac{3}{4\sigma^2}(\mathbf{R}_n - \mathbf{R}_m)^2\right).$$

That is, the interaction energy can be written in the form

$$H_I = \frac{w_2}{2} \sum_{m,n} U(\mathbf{R}_m - \mathbf{R}_n) \tag{3.15}$$

in terms of a pair potential U,

$$U(\mathbf{R}_m - \mathbf{R}_n) = \left(\frac{3}{4\pi\sigma^2}\right)^{3/2} \exp\left(-\frac{3}{4\sigma^2}(\mathbf{R}_n - \mathbf{R}_m)^2\right), \tag{3.16}$$

which is a function only of the separation of the pair of monomers.

Thus, to second order in the local density expansion, H_I can be expressed as the sum of all pair interactions between monomers. In the bead-spring model described above, this corresponds to a pair interaction between beads. For this discrete model, this formulation is very convenient, because instead of evaluating the integral, eqn. (3.12), over all space, calculating the interaction energy reduces to calculating all pairwise interactions between beads. Therefore, calculating H_I in this manner will be called the **pair interaction method.**

technical

The fact that the pair potential is only a function of the monomer separation leads to a great enhancement in program efficiency. Instead of calculating eqn. (3.16) for all pairs of monomers at each step, the potential U can be calculated once and tabularized in a lookup table indexed by monomer separation. Evaluating eqn. (3.16) is time consuming, since it involves calculating an exponential, and would be very costly since it occurs in the innermost loop of the simulation.

The variance σ^2 is an arbitrary parameter, and so should not influence meaningful results. The variance should be small, however, since it models a short range interaction. This provides another practical advantage, for if the range of interaction is

limited, one can introduce a cutoff to the interaction with no significant penalty. The primary gain in introducing a cutoff is that one can limit the number of pairwise interactions considered by keeping track of monomers within the certain interaction radius. Consider a particular monomer, indicated with a cross in fig. (3.1). The circle

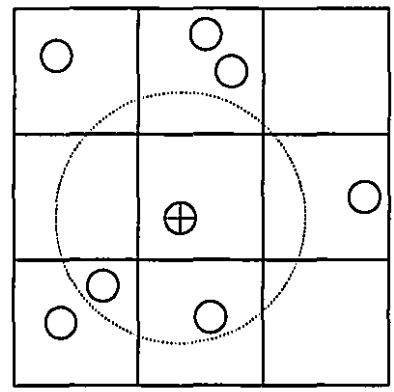

Figure 3.1: Cutoff radius of pair interaction between monomers. The interaction radius is equal to the lattice constant.

indicates the cutoff radius, beyond which the interaction is effectively zero; therefore, one needs only to calculate interactions with monomers that fall within the circle. One practical way of implementing this restricted pairing is also illustrated. The simulation volume can be divided into cells with a linear dimension equal to the radius of the interaction range. If a monomer is found within, say, the central cell, then it can interact with monomers in nearest neighbour or next nearest neighbour cells, depending on its position within the central cell, but no others. Therefore, a list can be kept of the monomers residing in each box. When interactions with the indicated monomer are calculated, only monomers within nearest and next nearest neighbour cells are considered.

technical

One way of keeping these lists is to create a lattice of these cells, and associate with each cell an array with enough elements to identify all monomers in the cell. This is the simplest, most straightforward implementation. However, it suffers from the drawback of being very memory intensive, since each array (there could be many for a large simulation volume) must be large enough to accommodate a possibly large number of monomers in the cell. However,

since most cells will be empty at a given time, this is extremely wasteful of memory; unfortunately, it is difficult to know a priori which cells will be empty. A better way, though more complicated to program, is to associate a **linked list** of monomer identifiers with each cell. If a monomer is in a particular cell, the identifier for that monomer is "linked" to the list associated with the cell. If the monomer changes cells, the identifier is unlinked from the previous list and linked to the new list. With linked lists, only one identifier is allocated for each monomer, drastically reducing the memory requirement. A significant disadvantage is the greater program complexity entailed [1].

In situations of high monomer densities, it is often advantageous to use a different method to calculate H_I, a **coarse grained local density method.** With this method, one explicitly measures the local monomer density, then numerically calculates the integral, eqn. (3.12), over the simulation volume. That is,

$$H_I = \int d\mathbf{r}\, f(\phi(\mathbf{r})), \tag{3.17}$$

where f is some function of the local concentration. Numerically evaluating the integral requires the Riemann sum for eqn. (3.17),

$$H_I \approx \sum_{\mathbf{r}_i} v f(\phi_{\mathbf{r}_i}). \tag{3.18}$$

In eqn. (3.18), the integration volume is divided into cells, each of volume v, with centres at the lattice points $\{\mathbf{r}_i\}$. The density at each point $\mathbf{r}_i$ is calculated from

$$\phi_{\mathbf{r}_i} = \frac{1}{v} \sum_j \delta_{\mathbf{R}_j, \mathbf{r}_i} \tag{3.19}$$

where $\mathbf{R}_j$ is the coordinate of the jth monomer, and takes the value of the nearest of the set of points $\{\mathbf{r}_i\}$. The delta function is replaced by the Kronecker delta. Eqn. (3.19) is equivalent to the definition $\phi_{\mathbf{r}_i} = N_{\mathbf{r}_i}/v$, where $N_{\mathbf{r}_i}$ is the number of monomers in the sample volume at point $\mathbf{r}_i$.

Certain considerations will help determine the choice of method to calculate the non-local energy contribution. The pair interaction model is attractive because the only approximation is analytical, replacing the delta function with a Gaussian, and

[1] Phenomenologically, it seems that any modest increase in program sophistication leads to a dramatic increase in time needed to implement the algorithm.

therefore seems better controlled. However, it is an order N^2 algorithm when implemented to study a system described by eqn. (3.1). Moreover, in situations at or below the Θ point, the monomer density becomes sufficiently large that the third order term in the density expansion of the interaction Hamiltonian must be retained. In this case, three-monomer interactions must be also be calculated, increasing the order of the algorithm to N^3, which is prohibitive except for very small systems or very short interaction range. Furthermore, the method of calculating n-monomer interactions requires that the potential be expressible as a power series in the local concentration. There are potentials of interest that are not of this form. In contrast, calculations using the coarse grained local density method are fast and efficient, especially in problems involving relatively high monomer densities. It is not demanding on memory, since there is no need to distinguish the monomers within the cells; only the numbers of monomers within the cells are important. Furthermore, any interaction which can be expressed as a function of the local monomer density can be easily implemented without a significant increase in computing time or complexity. However, the space must be coarse-grained to implement this method, and details finer than the coarse graining are necessarily not accessible.

The Monte Carlo procedure now follows in a straightforward fashion. A configuration of a polymer, or number of polymers, is chosen. A Markov chain of polymer configurations is generated by selecting one monomer at random and moving it a trial, random distance. The magnitude of this trial distance can be chosen to optimize the acceptance ratio, another factor which improves the efficiency of this algorithm. The connected energy difference between the trial configuration and the new configuration is calculated according to eqn. (3.11), the non-local contribution H_I being calculated with one of the discussed methods. The move is accepted or rejected according to the Metropolis criterion, discussed in the previous section.

3.1.3 *Comparison to previous Monte Carlo algorithms*

In the current literature, standard polymer Monte Carlo simulations are lattice models; that is, random walks are generated on a lattice with self avoidance imposed as a geometrical constraint. A microscopic Hamiltonian is sometimes incorporated, typically as a nearest neighbour interaction. In order to generate a trial configuration, a

small group of connected monomers are moved and tested for self avoidance. This is sometimes called a **local move** algorithm.

technical

It can be shown that algorithms of this sort are "non-ergodic", which in practical terms means that pathological configurations can be generated according to valid rules that cannot be escaped from by the same rules. Also, for any N step self avoiding walk, there exist many others that can never be realized with local moves. There are algorithms involving "non-local moves"; *i.e.*, moves that involve the simultaneous motion of monomers distant in sequence and space, and are consequently non-physical. With the incorporation of some of these moves, it is possible to construct algorithms that are ergodic [49]. Be that as it may, non-ergodic lattice models of the type described above remain in use. Whether or not the pathological configurations constitute a sufficiently large fraction of the total number of configurations to warrant concern is another matter, that to my knowledge has not been addressed.

Fig. (3.2) illustrates some typical local lattice moves. A powerful, state of the art

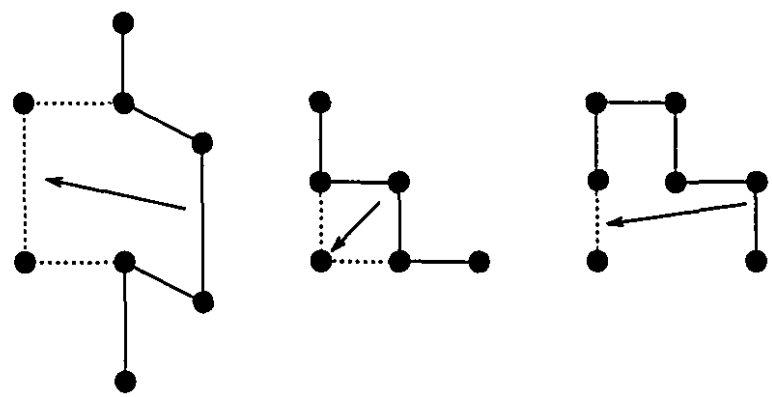

Figure 3.2: Some common lattice local update moves. From left to right: a "crankshaft", a "twist-jump", and a "reptation" move.

algorithm which is common in the current literature is the "bond-fluctuation" algorithm [13]. It is variant of the lattice self avoiding walk algorithm. In this model, the bonds are not constrained to join monomers at adjacent lattice vertices, allowing the bond lengths to "fluctuate". The algorithm is constructed so that the only moves allowed automatically ensure that the polymer does not intersect itself, although self

avoidance must be checked for at each move. This algorithm has the virtue of being easily vectorized, and reaches the asymptotic limit of long chains for smaller N than previous algorithm, perhaps due to the greater internal freedom of the polymer.

Simulation based on the Edwards Hamiltonian has some distinct advantages over these methods. Excluded volume interactions are accounted for energetically by calculating, for example, eqn. (3.18), resulting in a much more efficient simulation. Standard lattice models at high densities are very inefficient because a high percentage of updates are rejected, simply due to a lack of open sites on the lattice. Since there is no hard-core self avoidance in the Edwards approach, the acceptance ratio is much better. Another advantage is that results can be compared directly to most theories, since the Edwards simulation is formulated using the same model as most polymer field theories. This obviates the need for the fitting of parameters, since the parameters of the simulation are in direct correspondence with the theory. For a standard lattice calculation, to take an example, the relation between the excluded volume parameter and some lattice equivalent is not clear. On the other hand, the Edwards simulation allows unrealistic moves, insofar as there is nothing restricting bonds from crossing. Therefore, it is not valid for studies of polymer dynamics. Furthermore, it requires an Edwards Hamiltonian, and will therefore inherit all the approximations of that Hamiltonian.

3.2 *The Langevin equation*

[1] Consider an energy functional H that is a functional of a spatially varying order parameter field $\phi(\mathbf{r})$. If Z denotes the partition functional, then

$$Z = \int D\left[\phi(\mathbf{r})\right] \exp\left(-H\left[\phi(\mathbf{r})\right]\right). \tag{3.20}$$

If $\exp\left(-H\left[\phi(\mathbf{r})\right]\right)$ is strongly peaked about the function $\phi_m(\mathbf{r})$, then a simple approximation to the functional integral, eqn. (3.20), is to replace the integral by the value of the integrand at its maximum value,

$$Z \approx \exp\left(-H\left[\phi_m(\mathbf{r})\right]\right), \tag{3.21}$$

[1] This section follows reference [29], section 8.3.

where ϕ_m satisfies

$$\frac{\delta H}{\delta \phi_m} = 0, \tag{3.22}$$

which gives the spatial distribution of the order parameter in equilibrium.

Sufficiently close to equilibrium, it is reasonable to assume linear response; *i.e.*, the time dependence of the order parameter is proportional to the deviation from equilibrium $\frac{\delta H}{\delta \phi}$. Thus,

$$\frac{\partial \phi}{\partial t} = -\Gamma \frac{\delta H}{\delta \phi}. \tag{3.23}$$

The relaxational dynamics of eqn. (3.23) describes the deterministic evolution of the order parameter. However, there are fluctuations from this deterministic path due to the influence of microscopic variables. These fluctuations are accounted for with a noise term, $\eta(\mathbf{r}, t)$, which is assumed to be a **Gaussian random function.** That is, it is a random function chosen from an ensemble of functions satisfying the distribution

$$P\{\eta(\mathbf{r}, t)\} \sim \exp\left(-\frac{1}{2D}\int dt\, d\mathbf{r}\, \eta^2(\mathbf{r}, t)\right). \tag{3.24}$$

and satisfies

$$\begin{aligned} \langle \eta(\mathbf{r}, t)\rangle &= 0 \\ \langle \eta(\mathbf{r}, t)\eta(\mathbf{r}', t')\rangle &= D\delta(\mathbf{r}-\mathbf{r}')\delta(t-t'). \end{aligned}$$

Therefore, we describe the time evolution of the order parameter as

$$\frac{\partial \phi}{\partial t} = -\Gamma \frac{\delta H}{\delta \phi} + \eta(\mathbf{r}, t), \tag{3.25}$$

which is a stochastic differential equation usually called the **Langevin equation.**

With the Langevin equation, one can show that the time dependence for the probability distribution of the order parameter is given by

$$\frac{\partial P_\phi}{\partial t} = \int d\mathbf{r}' \frac{\delta}{\delta \phi(\mathbf{r}')}\left[\Gamma \frac{\delta H}{\delta \phi(\mathbf{r}')} P_\phi + \frac{D}{2}\frac{\delta P_\phi}{\delta \phi(\mathbf{r}')}\right]. \tag{3.26}$$

This result is the **Fokker-Planck** equation [1]. In the limit of $t \to \infty$, $\partial P_\phi/\partial t \to 0$, the probability distribution approaches the equilibrium distribution

$$P_\phi^{eq} \equiv \exp\left(-\frac{2\Gamma H[\phi(\mathbf{r})]}{D}\right). \tag{3.27}$$

[1] The details of this derivation can be found in reference [29] in the appendix to Chapt. 8.

That this must also be the Boltzmann distribution determines D,

$$D = 2\Gamma k_B T. \tag{3.28}$$

In other words, the strength of the noise must be related to the temperature in order for the solution of the Langevin equation to approach the canonical equilibrium result.

3.2.1 *Langevin equation for polymer systems*

For a system of polymers, the energy functional of the previous section is taken to be the Edwards Hamiltonian. In the discrete case, the Edwards Hamiltonian is a function of the N monomer coordinates $\{\mathbf{R}_n\}$. Therefore, the Langevin equation, eqn. (3.25), has the form

$$\frac{\partial \mathbf{R}_n}{\partial t} = -\Gamma \frac{\delta H}{\delta \mathbf{R}_n} + \eta(n,t), \tag{3.29}$$

which describes the time evolution of $\mathbf{R}_n(t)$. Eqn. (3.29) is actually three equations for each monomer,

$$\frac{\partial x_\beta^k}{\partial t} = -\Gamma \frac{\delta H}{\delta x_\beta^k} + \eta, \tag{3.30}$$

where x_β^k is the βth component of the coordinate of the kth monomer. The various terms of $\partial H/\partial x_\beta^k$ will be derived in the appendix A.1. Anticipating these results,

$$\begin{aligned}\frac{\partial x_\beta^k}{\partial t} &= -\Gamma\left(\frac{\delta H_G}{\delta x_\beta^k} + \frac{\delta H_I}{\delta x_\beta^k}\right) + \eta \\ &= -\frac{3\Gamma}{b^2}\left(x_\beta^{k+1} - 2x_\beta^k + x_\beta^{k-1}\right) + \frac{3\Gamma w_2}{2\sigma^2}\left(\frac{3}{4\pi\sigma^2}\right)^{\frac{3}{2}} \times \\ &\quad \sum_m \left(x_\beta^k - x_\beta^m\right) \exp\left(-\frac{3}{4\sigma^2}\left(\mathbf{R}_n - \mathbf{R}_m\right)^2\right) + \eta(n,t).\end{aligned} \tag{3.31}$$

This formula is straightforward to implement numerically using the finite difference approximation for the time derivative

$$\frac{\partial x_\beta^k}{\partial t} \approx \frac{\Delta x_\beta^k}{\Delta t}. \tag{3.32}$$

3.3 *Mean field theory*

In this section, the **mean field approximation** will be introduced for systems described by an Edwards Hamiltonian. In this approximation, an interacting system

of polymers is considered to be a system of independent polymers experiencing an averaged interaction through the mean field of all monomers. The independent chain problem can be solved using Green function methods assuming the mean field is known. Moreover, the solution to the independent chain problem itself determines the average monomer density. This added "constraint" is used to determine the mean field [1].

3.3.1 *The mean field Hamiltonian*

Once again, for the sake of explicitness, consider the expansion of the interaction Hamiltonian in powers of the local density to second order,

$$H_I = \frac{w_2}{2} \int d\mathbf{r}\, \phi^2(\mathbf{r}). \tag{3.33}$$

Formally, the concentration can be written

$$\phi(\mathbf{r}) = \langle \phi(\mathbf{r}) \rangle + \delta\phi(\mathbf{r}) \tag{3.34}$$

where $\langle \phi(\mathbf{r}) \rangle$ is the **mean field**, and $\delta\phi(\mathbf{r})$ is the fluctuation from the mean field. The average $\langle\rangle$ is the equilibrium average; if $A[\mathbf{R}(n)]$ is some functional of the polymer configuration $\mathbf{R}(n)$,

$$\langle A \rangle = \frac{1}{Z} \int D[\mathbf{R}(n)]\; A[\mathbf{R}(n)] \exp(-H[\mathbf{R}(n)]), \tag{3.35}$$

where

$$Z = \int D[\mathbf{R}(n)] \exp(-H[\mathbf{R}(n)]) \tag{3.36}$$

is the partition functional. The concentration $\phi(\mathbf{r})$ is written explicitly as a function of $\mathbf{r}$, though it is also a functional of the configuration $\mathbf{R}(n)$. The equilibrium average mean field, however, is not a functional of the configuration. With these definitions, H_I can be rewritten

$$H_I = \frac{w_2}{2} \int d\mathbf{r} \left(\langle \phi(\mathbf{r}) \rangle^2 + 2 \langle \phi(\mathbf{r}) \rangle \delta\phi(\mathbf{r}) + (\delta\phi(\mathbf{r}))^2 \right).$$

[1] The method of the self consistent mean field was introduced into the polymer literature by Sir Sam Edwards [26]. It is briefly discussed in the text of Doi and Edwards [22]. Some aspects are considered in more detail in the text of Freed [28].

Noting that $\langle\phi(\mathbf{r})\rangle$ is a constant with respect to functional integration, the mean field interaction becomes

$$w_2 \int d\mathbf{r}\ \langle\phi(\mathbf{r})\rangle\,\phi(\mathbf{r}), \tag{3.37}$$

ignoring constants and terms of order $(\delta\phi)^2$. Including the connected energy contribution with the mean field interaction, the Edwards Hamiltonian for a single polymer in the mean field approximation becomes

$$H_o = \int dn \left(\frac{3}{2b^2}\left(\frac{\partial \mathbf{R}(n)}{\partial n}\right)^2 + w_2\langle\phi(\mathbf{R}(n))\rangle\right), \tag{3.38}$$

using the definition of the microscopic density, eqn. (3.13). For a system of many polymers, eqn. (3.38) is easily generalized, yielding

$$H_o = \sum_k \left[\int dn \left(\frac{3}{2b^2}\left(\frac{\partial \mathbf{R}_k(n)}{\partial n}\right)^2 + w_2\langle\phi(\mathbf{R}_k(n))\rangle\right)\right]. \tag{3.39}$$

The mean field Hamiltonian describes a system of *independent* Gaussian chains under the influence of an external field, which is proportional to the average monomer density. For this reason, the mean field approximation is sometimes called the **independent chain approximation**, since the chains do not interact explicitly. They interact only implicitly through the mean field $w_2\langle\phi\rangle$.

Note that the canonical probability of a configuration $\mathbf{R}(n)$ is proportional to $e^{-H_o[\mathbf{R}(n)]}$ in the mean field approximation, which in turn depends on the mean field concentration of monomers. However, the mean field concentration could in principle be calculated through eqn. (3.35); this is a **self consistency** requirement that the mean field must satisfy. In fact, this additional constraint allows the mean field to be determined. A procedure analogous to this, though somewhat different in detail, is described in the next section.

3.3.2 *Green function methods*

If a polymer is described by an Edwards Hamiltonian H, all equilibrium properties are specified by the quantity

$$G(\mathbf{r},\mathbf{r}';N) = \int_{\mathbf{R}(0)=\mathbf{r}'}^{\mathbf{R}(N)=\mathbf{r}} \mathcal{D}[\mathbf{R}(n)]\,\exp\left(-H[\mathbf{R}(n)]\right), \tag{3.40}$$

where the ends of the polymer are fixed at $\mathbf{r}$ and $\mathbf{r}'$. The functional integral is over all curves $\mathbf{R}(n)$ of contour length N with $\mathbf{R}(0)$ fixed at $\mathbf{r}'$ and $\mathbf{R}(N)$ fixed at $\mathbf{r}$. The measure $\mathcal{D}[\mathbf{R}(n)]$ is defined such that

$$\int_{\mathbf{R}(0)=\mathbf{r}'}^{\mathbf{R}(N)=\mathbf{r}} \mathcal{D}[\mathbf{R}(n)] \exp\left(-\frac{3}{2b^2}\int dn \left(\frac{\partial \mathbf{R}(n)}{\partial n}\right)^2\right) = 1. \tag{3.41}$$

Consider again the mean field Hamiltonian of section 3.3.1,

$$H_o[\mathbf{R}(n)] = \int dn \left(\frac{3}{2b^2}\left(\frac{\partial \mathbf{R}(n)}{\partial n}\right)^2 + V(\mathbf{R}(n))\right), \tag{3.42}$$

where $V(\mathbf{r}) = w_2\langle\phi(\mathbf{r})\rangle$ and can be interpreted as a potential energy per unit monomer at the point $\mathbf{r}$. In the same way that $H[\mathbf{R}(n)]$ was defined as the functional integral limit of the discrete Hamiltonian $H\{\mathbf{R}_i\}$ in section 2.1.3, the distribution $G(\mathbf{r},\mathbf{r}';N)$, eqn. (3.40), can be defined as the functional integral limit of the discrete expression

$$\begin{aligned} G(\mathbf{r},\mathbf{r}';N) = & \\ & \left(\frac{3}{2\pi b^2}\right)^{\frac{3N}{2}} \int d\mathbf{R}_1 d\mathbf{R}_2 \ldots d\mathbf{R}_N\, \delta(\mathbf{r}'-\mathbf{R}_1)\,\delta(\mathbf{r}-\mathbf{R}_N) \times \\ & \exp\left\{-\frac{3}{2b^2}\sum_{i=2}^{N}(\mathbf{R}_i-\mathbf{R}_{i-1})^2 - \sum_{i=1}^{N} V(\mathbf{R}_i)\right\}. \end{aligned} \tag{3.43}$$

An important property of $G(\mathbf{r},\mathbf{r}';N)$ follows from the definition eqn. (3.43),

$$G(\mathbf{r},\mathbf{r}';N+\epsilon) = \int d\mathbf{r}''\, G(\mathbf{r},\mathbf{r}'';\epsilon)\, G(\mathbf{r}'',\mathbf{r}';N). \tag{3.44}$$

Loosely interpreted, eqn. (3.44) states that the unnormalized probability of a curve of length $N+\epsilon$ starting at $\mathbf{r}'$ and ending at $\mathbf{r}$ is equal to the product of the independent probabilities of two curves: a curve of length N starting at $\mathbf{r}'$ and ending at $\mathbf{r}''$, and another of length ϵ starting at $\mathbf{r}''$ and ending at $\mathbf{r}'$, "summed" over all intermediate positions $\mathbf{r}''$. Eqn. (3.44) is characteristic of a Markov process, since the probabilities of the two curves are independent.

If both the curve $\mathbf{R}(n)$ and the potential V are well behaved, then for sufficiently small sections of curve $\Delta N = \epsilon$, the curve will not vary greatly and the potential will

be approximately constant across this interval [1]. Thus,

$$H_o = \int dn \left(\frac{3}{2b^2} \left(\frac{\partial \mathbf{R}(n)}{\partial n} \right)^2 + V(\mathbf{R}(n)) \right)$$

$$\approx \epsilon \left\{ \frac{3}{2b^2} \left(\frac{\Delta \mathbf{R}}{\epsilon} \right)^2 + V(\mathbf{r}) \right\},$$

and from the definition, eqn. (3.40),

$$G(\mathbf{r}, \mathbf{r}''; \epsilon) \approx \left(\frac{3}{2\pi\epsilon b^2} \right)^{3/2} \exp\left(-\frac{3(\mathbf{r} - \mathbf{r}'')^2}{2\epsilon b^2} - \epsilon V(\mathbf{r}) \right)$$

$$\approx (1 - \epsilon V(\mathbf{r})) \left(\frac{3}{2\pi\epsilon b^2} \right)^{3/2} \exp\left(-\frac{3(\mathbf{r} - \mathbf{r}'')^2}{2\epsilon b^2} \right). \tag{3.45}$$

Substituting eqn. (3.45) into eqn. (3.44) and changing variables $\mathbf{r}'' = \mathbf{r} + \eta$,

$$G(\mathbf{r}, \mathbf{r}'; N + \epsilon) = \int d\eta \, (1 - \epsilon V(\mathbf{r})) \left(\frac{3}{2\pi\epsilon b^2} \right)^{3/2} \exp\left[-\frac{3\eta^2}{2\epsilon b^2} \right] G(\mathbf{r} + \eta, \mathbf{r}'; N). \tag{3.46}$$

The advantage of rewriting eqn. (3.46) in terms of η is that for small values of ϵ, the factor $\exp(-3\eta^2/(2\epsilon b^2))$ is small except for small values of η. Therefore, one can expand $G(\mathbf{r} + \eta)$ to find [2]

$$G(\mathbf{r} + \eta) \approx G(\mathbf{r}) + \eta \cdot \nabla G(\mathbf{r}) + \frac{1}{2} \left(\sum_{i,j} \eta_i \eta_j \frac{\partial^2}{\partial x_i \partial x_j} \right) G(\mathbf{r}) + \cdots \tag{3.47}$$

If the expansion of $G(\mathbf{r} + \eta)$ is kept only to second order in η, the right hand side of eqn. (3.46) becomes, after integration,

$$(1 - \epsilon V(\mathbf{r})) \left(G(\mathbf{r}) + \frac{\epsilon b^2}{6} \right) \nabla^2 G(\mathbf{r}). \tag{3.48}$$

Similarly, the left hand side of eqn. (3.46) can be expanded in powers of ϵ,

$$G(N + \epsilon) \approx G(N) + \epsilon \frac{\partial G(N)}{\partial N} + \cdots \tag{3.49}$$

Finally, the left hand side, eqn. (3.49), when combined with the right hand side, eqn. (3.48), yields a partial differential equation for $G(\mathbf{r}, \mathbf{r}'; N)$

$$\left[\frac{\partial}{\partial N} - \frac{b^2}{6} \nabla^2 + V(\mathbf{r}) \right] G(\mathbf{r}, \mathbf{r}'; N) = 0, \tag{3.50}$$

[1] There are some subtle details involved in making these assumptions. There is discussion on this point in Freed [28].

[2] For the sake of clarity, only the relevant argument will be written explicitly. The meaning should be clear in context.

for $N > 0$ with the boundary condition

$$\lim_{N\to 0} G(\mathbf{r},\mathbf{r}';N) = \delta(\mathbf{r}-\mathbf{r}'). \tag{3.51}$$

The boundary condition can be seen, for example, from the expression for G for small N, eqn. (3.45). Thus, $G(\mathbf{r},\mathbf{r}';N)$ satisfies the diffusion equation for a particle in an external potential V. It is a **Green function** for a Gaussian chain polymer in an external field. And if occasions when eqn. (3.50) can be solved analytically are rare, a numerical solution can always be attempted.

technical

Eqn. (3.50) can be solved numerically using standard finite difference methods. One finite difference representation of the Laplacian operator in one dimension is

$$\nabla^2 f(x) \approx \frac{f(x_{i-1}) - 2f(x_i) + f(x_{i+1})}{(\Delta x)^2}. \tag{3.52}$$

Similarly, the derivative with respect to N is

$$\frac{\partial f(N)}{\partial N} \approx (f(N+\Delta N) - f(N))\,\Delta N. \tag{3.53}$$

Therefore, the Green function $G(x_i,N)$ can be calculated using

$$G(x_i;N+\Delta N) = G(x_i;N) + \Delta N D_n(\{x_i\},N) \tag{3.54}$$

where

$$D_n(\{x_i\},N) = \frac{b^2}{6(\Delta x)^2}\Big(G(x_{i-1};N) - 2G(x_i;N) + G(x_{i+1};N)\Big) - V(x_i)\,G(x_i;N). \tag{3.55}$$

Thus, $G(x_i;N)$ is completely specified given the initial condition

$$G(x_i',0) = 1/\Delta x. \tag{3.56}$$

This method works well provided $\Delta N/(\Delta x)^2$ is small.

In the polymer case, the Green function is of direct interest; as can be seen from its definition eqn. (3.40), it is proportional to the probability that a polymer of contour length N starts at the point $\mathbf{r}$ and ends at the point $\mathbf{r}'$. For example,

$$\langle A\rangle_o = \frac{1}{G(\mathbf{r},\mathbf{r}';N)}\int d\mathbf{r}''\,G(\mathbf{r},\mathbf{r}'';N-n)\,A(\mathbf{r}'')\,G(\mathbf{r}'',\mathbf{r}';n). \tag{3.57}$$

is the mean field average of some quantity $A(\mathbf{r})$. Recall, however, that the external potential V has the form

$$V(\mathbf{R}(n)) = w_2\langle\phi(\mathbf{R}(n))\rangle_o. \tag{3.58}$$

Therefore, given the solution to eqn. (3.50) with $V = w_2\langle\phi\rangle_o$, the resulting Green function $G(\mathbf{r},\mathbf{r}';N)$ can be used to calculate the mean field

$$\langle\phi(\mathbf{r})\rangle_o = \int dn\,\langle\delta(\mathbf{r}-\mathbf{R}(n))\rangle_o, \tag{3.59}$$

which in terms of the Green function becomes

$$\langle\phi(\mathbf{r}'')\rangle = \frac{1}{G(\mathbf{r},\mathbf{r}';N)}\int dn\,G(\mathbf{r},\mathbf{r}'';N-n)\,G(\mathbf{r}'',\mathbf{r}';n)\,. \tag{3.60}$$

Therefore, the external potential V can be determined self-consistently; *i.e.*, the two equations, eqn. (3.50) and eqn. (3.60), are iterated until $\langle\phi\rangle_o$ converges.

technical

If eqn. (3.50) is solved numerically, $G(x_i;N)$ can be used to numerically evaluate the integral, eqn. (3.60), to determine V. Eqn. (3.50) is now solved again using this V. This iteration proceeds until convergence is reached; for example, convergence could be operationally defined by

$$\left(\sum_i |\langle\phi'(x_i)\rangle|\right) / \left(\sum_i |\langle\phi(x_i)\rangle|\right) \leq \epsilon, \tag{3.61}$$

where ϵ is some small number, say 10^{-6}, and where $\langle\phi'\rangle$ refers to the value after the next iteration.

In practice, convergence is more robust using a linear combination of the new potential with the potential from the previous iteration [24],

$$V' \to \alpha V' + (1-\alpha)\,V,\ 0 < \alpha \leq 1. \tag{3.62}$$

This appears to damp the iteration process; otherwise, the iterative process is more likely to be unstable.

To conclude this section, it is interesting to note that mean field methods have been very successful in predicting detailed properties of polymer systems in a wide

variety of situations. The success of mean field theory is probably due, in a large part, to the nature of the polymer molecule itself. It is a very large molecule that pervades a large amount of space, allowing a single polymer to interact with a large number of others. Thus, for polymers, it is often physically reasonable to speak of a mean field.

3.4 *The random phase approximation*

Having described the mean field theory in section 3.3, the effect of second order fluctuations will be discussed in this section. Fluctuations will be included in a particularly simple fashion; *i.e.*, they are assumed to be independent Gaussians. Unfortunately, the mean field contribution is not described naturally in this representation. Therefore, a Gaussian approximation is made for the mean field Hamiltonian. Consequently, the first correction to the correlation function will be rendered transparent. The correlation function can then be used to determine the stability of the mean field solution. In the polymer literature, this approximation is typically referred to as the **random phase approximation** [1].

As suggested in section 3.3.1, the Edwards Hamiltonian can be written in terms of a mean field Hamiltonian plus a contribution from the fluctuations from the mean field,

$$H = H_o + H_\delta, \tag{3.63}$$

where H_o is given by eqn. (3.38), and by comparison to to eqn. (3.37), H_δ is written as

$$H_\delta = \frac{w_2}{2} \int d\mathbf{r}\, \delta\phi^2(\mathbf{r}). \tag{3.64}$$

In this representation, H_δ has a particularly simple quadratic form [2]; however, it is difficult to cast H_o in terms of concentration fluctuations. Therefore, one assumes

[1] Much of this section follows the work of Yeung *et.al.*; for example, see reference [80].

[2] This form is due to the model we are using, eqn. (3.1). If not, H_δ could be approximated by

$$H_\delta \approx \frac{1}{2} \int d\mathbf{r} \left(\frac{\partial^2 H_I[\phi]}{\partial \phi^2} \right)_{\phi=\langle\phi\rangle} \delta\phi^2(\mathbf{r}). \tag{3.65}$$

that H_o can be approximated by the quadratic form

$$H_o \approx \frac{1}{2}\int dr dr'\, \delta\phi(\mathrm{r})\, \mathbf{A}_o^{-1}(\mathrm{r},\mathrm{r}')\, \delta\phi(\mathrm{r}'). \tag{3.66}$$

If the assumption is valid and H_o can be approximated by eqn. (3.66), the approximation reduces to choosing the correct $\mathbf{A}_o$. Since the mean field probability is proportional to e^{-H_o}, eqn. (3.66) gives rise to a Gaussian probability distribution, allowing us to identify $\mathbf{A}_o(\mathrm{r},\mathrm{r}')$ with the mean field correlation function

$$\mathbf{A}_o = \langle \delta\phi(\mathrm{r})\, \delta\phi(\mathrm{r}')\rangle_o \tag{3.67}$$

where $\langle\rangle_o$ is the average with respect to the mean field Hamiltonian. Even if this average cannot be performed analytically, it may be possible to obtain it numerically using the methods developed in the previous section. The specifics of calculating the correlation function given the mean field Green function will be discussed in the next section.

Combining eqn. (3.67) with eqn. (3.66) and eqn. (3.64), the Hamiltonian in the random phase approximation, H_δ, becomes

$$H_\delta = \frac{1}{2}\int dr dr'\, \delta\phi(\mathrm{r})\left(\mathbf{A}_o^{-1}(\mathrm{r},\mathrm{r}') + w_2\delta(\mathrm{r}-\mathrm{r}')\right)\delta\phi(\mathrm{r}'). \tag{3.68}$$

Since eqn. (3.68) is quadratic, it gives rise to Gaussian probability distributions for the concentration fluctuations. Furthermore, one can directly read off the correlation function in the random phase approximation

$$\mathbf{A}^{-1}(\mathrm{r},\mathrm{r}') = \mathbf{A}_o^{-1}(\mathrm{r},\mathrm{r}') + w_2\delta(\mathrm{r}-\mathrm{r}'). \tag{3.69}$$

In many instances, it is of direct interest to calculate the correlation function; for example, to calculate the structure factor of a polymer solution. Moreover, the correlation function also contains information regarding the stability of the mean field solution. If $\{\psi_\alpha(\mathrm{r})\}$ is a complete, orthonormal set of basis functions, then

$$\delta\phi(\mathrm{r}) = \sum_\alpha \delta\phi_\alpha \psi_\alpha(\mathrm{r}) \tag{3.70}$$

where

$$\delta\phi_\alpha = \int dr\, \psi_\alpha^*(\mathrm{r})\, \delta\phi(\mathrm{r}). \tag{3.71}$$

If $\{\psi_\alpha(\mathbf{r})\}$ is chosen to be the set that diagonalizes $\mathbf{A}_o$; *i.e.*,

$$\int dr\, dr'\, \psi_\alpha^*(\mathbf{r})\, \mathbf{A}_o(\mathbf{r},\mathbf{r}')\, \psi_\beta(\mathbf{r}') = (\mathbf{A}_o)_{\alpha,\alpha}\, \delta_{\alpha,\beta}, \tag{3.72}$$

then

$$H_\delta = \frac{1}{2}\sum_\alpha \delta\phi_\alpha^* \left((\mathbf{A}_o)_{\alpha,\alpha}^{-1} + w_2\right) \delta\phi_\alpha. \tag{3.73}$$

Thus, the probability distribution function in the random phase approximation has the form

$$\exp\left[-\frac{1}{2}\sum_\alpha \delta\phi_\alpha^* \left((\mathbf{A}_o)_{\alpha,\alpha}^{-1} + w_2\right) \delta\phi_\alpha.\right] \tag{3.74}$$

From eqn. (3.74), it can be seen that the mean field solution becomes unstable if $\left((\mathbf{A}_o)_{\alpha,\alpha}^{-1} + w_2\right)$ is negative. This can also be seen from the dynamic response of fluctuations from the mean field, calculated using the analysis in section 3.2; *i.e.*, the linear response of the modes of fluctuation are governed by the Langevin equation, eqn. (3.25), using the Hamiltonian, eqn. (3.73),

$$\begin{aligned}\frac{\partial\delta\phi_\alpha}{\partial t} &= -\Gamma\frac{\delta H_\delta}{\delta(\delta\phi_\alpha)} + \eta(\mathbf{r},t) \\ &= -\Gamma\left((\mathbf{A}_o)_{\alpha,\alpha}^{-1} + w_2\right)\delta\phi_\alpha + \eta(\mathbf{r},t).\end{aligned} \tag{3.75}$$

If $\mathbf{A}_{\alpha,\alpha}^{-1} > 0$, then according to the deterministic part of eqn. (3.75), small fluctuations away from the mean field equilibrium will decay back to the mean field solution in time. The system is **linearly stable** to small fluctuations. On the other hand, if $\mathbf{A}_{\alpha,\alpha}^{-1} < 0$, then small fluctuations will grow, and the system is **linearly unstable.** Thus, the values of parameters where $\left((\mathbf{A}_o)_{\alpha,\alpha}^{-1} + w_2\right) = 0$ signals the limit of stability of the mean field solution within the random phase approximation. This type of analysis is common in studying instability in polymer brushes [50, 65, 80, 71].

3.4.1 The mean field correlation function

As can be seen from eqn. (3.69), the correlation function in the random phase approximation requires the mean field correlation function. If the mean field Green function is known, then mean field averages can be calculated according to the techniques of section 3.3.2. In this section, the calculation of the mean field correlation function in terms of the Green function will be presented [1].

[1] A similar calculation is summarized in reference [80].

The correlation function, **A**, measures the correlation of fluctuations in the density,

$$\begin{aligned}\mathbf{A}(\mathbf{r},\mathbf{r}') &= \langle \delta\phi(\mathbf{r})\,\delta\phi(\mathbf{r}')\rangle \\ &= \langle \phi(\mathbf{r})\,\phi(\mathbf{r}')\rangle - \langle \phi(\mathbf{r})\rangle\,\langle \phi(\mathbf{r}')\rangle\,, \end{aligned} \tag{3.76}$$

where $\delta\phi = \phi - \langle\phi\rangle$. The mean field correlation function can be obtained by calculating the averages in eqn. (3.76) with respect to the mean field Hamiltonian, eqn. (3.38), using the Green function as in section 3.3.2. The mean field $\langle\phi(\mathbf{r})\rangle_o$ was calculated in the previous section, eqn. (3.60). Thus, there remains only the calculation of the first term, $\langle\phi(\mathbf{r})\,\phi(\mathbf{r}')\rangle_o$.

Using the microscopic definition of the density, eqn. (3.13),

$$\langle \phi(\mathbf{r})\,\phi(\mathbf{r}')\rangle_o = \int dn\,dn'\,\langle \delta(\mathbf{r}-\mathbf{R}(n))\,\delta(\mathbf{r}'-\mathbf{R}(n'))\rangle_o. \tag{3.77}$$

For a polymer of contour length N with ends fixed at $\mathbf{r}$ and $\mathbf{r}'$, the equilibrium average with respect to the mean field Hamiltonian H_o is

$$\langle \delta(\mathbf{r}-\mathbf{R}(n))\,\delta(\mathbf{r}'-\mathbf{R}(n'))\rangle_o = \frac{1}{G(\mathbf{r}_0,\mathbf{r}_N;N)}\int_{\mathbf{R}(0)=\mathbf{r}_0}^{\mathbf{R}(N)=\mathbf{r}_N}\mathcal{D}[\mathbf{R}(n)]\;\delta(\mathbf{r}-\mathbf{R}(n))\,\delta(\mathbf{r}'-\mathbf{R}(n'))\exp\left(-H_o[\mathbf{R}(n)]\right).$$

According to the definition of the Green function, eqn. (3.40), and integrating over the delta functions,

$$\langle \delta(\mathbf{r}-\mathbf{R}(n))\,\delta(\mathbf{r}'-\mathbf{R}(n'))\rangle_o = \begin{cases} \frac{1}{G(\mathbf{r}_N,\mathbf{r}_0;N)}\left(G(\mathbf{r}_N,\mathbf{r};N-n)\,G(\mathbf{r},\mathbf{r}';n-n')\,G(\mathbf{r}',\mathbf{r}_0;n')\right) & n>n' \\ \frac{1}{G(\mathbf{r}_N,\mathbf{r}_0;N)}\left(G(\mathbf{r}_N,\mathbf{r}';N-n')\,G(\mathbf{r}',\mathbf{r};n'-n)\,G(\mathbf{r},\mathbf{r}_0;n)\right) & n'>n. \end{cases}$$

Since $G(\mathbf{r}_N,\mathbf{r}';n-n')\equiv 0$ for $n<n'$, the average of the two delta functions is

$$\begin{aligned}&\langle \delta(\mathbf{r}-\mathbf{R}(n))\,\delta(\mathbf{r}'-\mathbf{R}(n'))\rangle_o = \\ &\quad\frac{1}{G(\mathbf{r}_N,\mathbf{r}_0;N)}\Big\{\,G(\mathbf{r}_N,\mathbf{r};N-n)\,G(\mathbf{r},\mathbf{r}';n-n')\,G(\mathbf{r}',\mathbf{r}_0;n') + \\ &\quad G(\mathbf{r}_N,\mathbf{r}';N-n')\,G(\mathbf{r}',\mathbf{r};n'-n)\,G(\mathbf{r},\mathbf{r}_0;n)\,\Big\}.\end{aligned}$$

Substituting the above result into eqn. (3.77),

$$\langle \phi(\mathbf{r})\,\phi(\mathbf{r}')\rangle_o =$$

$$\frac{1}{G(\mathbf{r}_N,\mathbf{r}_0;N)}\int_0^N dn \int_0^n dn'\, G(\mathbf{r}_N,\mathbf{r};N-n)\,G(\mathbf{r},\mathbf{r}';n-n')\,G(\mathbf{r}',\mathbf{r}_0;n') +$$

$$\frac{1}{G(\mathbf{r}_N,\mathbf{r}_0;N)}\int_0^N dn \int_n^N dn'\, G(\mathbf{r}_N,\mathbf{r}';N-n')\,G(\mathbf{r}',\mathbf{r};n'-n)\,G(\mathbf{r},\mathbf{r}_0;n)$$

Interchanging the order of the integration in the second integral yields

$$\langle \phi(\mathbf{r})\,\phi(\mathbf{r}')\rangle_o =$$

$$\frac{1}{G(\mathbf{r}_N,\mathbf{r}_0;N)}\int_0^N dn \int_0^n dn' \Big\{ G(\mathbf{r}_N,\mathbf{r};N-n)\,G(\mathbf{r},\mathbf{r}';n-n')\,G(\mathbf{r}',\mathbf{r}_0;n') +$$

$$G(\mathbf{r}_N,\mathbf{r}';N-n)\,G(\mathbf{r}',\mathbf{r};n-n')\,G(\mathbf{r},\mathbf{r}_0;n') \Big\}.$$

Thus, eqn. (3.78), together with eqn. (3.60) for the mean field gives the mean field correlation function

$$\mathbf{A}_o(\mathbf{r},\mathbf{r}') = \langle \phi(\mathbf{r})\,\phi(\mathbf{r}')\rangle_o - \langle \phi(\mathbf{r})\rangle_o \langle \phi(\mathbf{r}')\rangle_o \tag{3.78}$$

in terms of the polymer Green function [1].

[1] A similar result was given in reference [80], although it differs from the result obtained here. It is probably a small typographic error in reference [80].

"The interaction of adsorbed macromolecules is arguably the most important process in modern colloid science."

- attributed to Jacob Israelachvili

4

Polymers Grafted at Interfaces

To this point, important concepts and techniques of polymer physics have been introduced in a general way, requiring at most that the polymers be described by an Edwards Hamiltonian. For the remainder of the thesis, discussion will focus on a particular system, the end-grafted polymer layer, or polymer brush. In this chapter, the polymer brush is introduced in its simplest form; the homogeneous polymer brush grafted to a plane interface in good solvent. Some important results from the literature are reviewed. Also, the Langevin simulation technique discussed in section 3.2.1 is applied to this simple brush, both to demonstrate simulating with an Edwards Hamiltonian, and to gain an understanding of some equilibrium brush properties.

4.1 The polymer brush

Consider a situation where polymer molecules are attached, or grafted, through one end to an interface at a sufficiently high grafting density so that the polymers overlap significantly. In the presence of good solvent, where monomer-monomer contacts are unfavourable, the polymers will stretch away from the relatively high monomer concentration at the surface, forming a polymer brush, as seen in fig. (1.4). The primary application of polymer brushes is **colloidal stabilization**, where the steric repulsion between brushes on nearby particles helps maintain a sufficient distance between all particles to prevent coagulation due to attractive long range van der Waals forces. Apart from direct application, the polymer brush model can be applied in some abstraction in many situations. Diblock copolymer melts form "brushes" at domain interfaces under strong segregation conditions, or when localized at high densities at domain boundaries between incompatible polymer phases. Polymers localized at an air-liquid interface can be studied conveniently with a Langmuir trough, where

interesting conformations have been observed [82, 83]. Brushes at solid-solid interfaces act as adhesives if the chains are grafted in one phase and extend into the other.

4.2 *Brushes in retrospective*

An early attempt to model the stabilization, due to Dolan and Edwards, was to consider a brush of random walk polymers grafted through one end to an interface, and confined between two plane surfaces [23]. The plane surfaces were assumed to be attracted through van der Waals forces. Two types of association between the planes were found depending on the size of the polymers: a close association for short polymers, and a loose association if the length exceeded a certain critical length. Before this critical value of the chain length, the van der Waals attraction dominates at all separations, and the polymers do not stabilize the suspension. For chains greater than this value, there is an energy minimum at a larger particle separation. Finally, for even longer chains, the energy minimum becomes negligible compared to k_BT, and thus association would not be expected to be observed. This study, however, did not include excluded volume effects.

In a subsequent work [24], the authors included the excluded volume effect through the method of a self consistent field, described in section 3.3. They found, not surprisingly, that the excluded volume effect greatly enhances the repulsion between the two surfaces and is the dominant effect at large plane separations. For small separations, the decrease in the number of configurations was expected to be the dominant effect. Since the particles are expected to form a loose association at large distances, the excluded volume effect was concluded to be an important part of colloidal stabilization.

Some years later, Alexander [1, 2] and de Gennes [18] introduced a new approach to the brush problem, seeking only power law dependences of rough measures upon system parameters. For example, one can write the energy contribution, per polymer, of the Gaussian chains in a brush of height h as

$$H_G \sim \left(\frac{h}{N}\right)^2 \tag{4.1}$$

ignoring constants and keeping only the dependences of interest. At the same level

of description, the excluded volume contribution per polymer can be written

$$\begin{aligned}\frac{H_I}{K} &= \frac{w_2}{2K}\int d\mathbf{r}\,\phi^2(\mathbf{r}) \\ &\sim \frac{w_2}{K}V\left(\frac{KN}{V}\right)^2 \\ &\sim \frac{w_2 N^2\sigma}{h}\end{aligned}$$

where $V = hA$ is the volume of a system with area A and a grafting density $\sigma = K/A$, and K is the number of polymers. If the total energy per polymer is minimized with respect to h, one finds

$$h \sim N(\sigma w_2)^{1/3}. \tag{4.2}$$

Therefore, h, the typical extent of a polymer in the direction perpendicular to the surface, varies linearly with the degree of polymerization N. This is qualitatively different from, say, isolated grafted polymers, which would have an extent that varies as $N^{3/5}$. Furthermore, since the lateral extent of a polymer in a brush [1] is expected to vary as $N^{1/2}$, the polymers in a brush are stretched in the direction perpendicular to the surface for large N. Alexander came to this conclusion based on an energy balance argument of the type detailed above, while de Gennes found the same strong stretching regime using a scaling picture of densely packed "blobs" filled with self-avoiding walk polymers.

A drawback of scaling arguments is that they are unable to predict detailed features of brush structure. The re-introduction of the self-consistent mean field approach of Edwards allowed for a more detailed description of brush structure. The mean field theory of the strongly stretched polymer brush in good solvent was developed by Milner *et.al.* [55, 54], and independently by Zhulina *et.al.* [86]. The argument, following Milner, can be briefly outlined as follows [54]. The configuration of a Gaussian chain in a self consistent potential can be considered analogous to the trajectory of a particle in an external field, where the position of the particle at time n is equivalent to the position of the nth monomer. The most likely configuration of the polymer, the one that minimizes the configurational free energy, is the one for which the analogous

[1] In the direction lateral to the surface, the grafting produces monomer concentrations high enough to expect that excluded volume interactions are screened.

particle follows the classical trajectory. Now consider the polymer brush problem, where many polymers, each of contour length N, start with the free end at some value of z perpendicular to the grafting plane and end at the wall at $z = 0$. Thus, the potential must have the property that all trajectories, regardless of where they start, end at $z = 0$ in the same amount of "time", N. This potential is the potential of the harmonic oscillator,

$$U(z) = \text{constant} - \frac{\pi^2}{8N^2} z^2. \tag{4.3}$$

Translational invariance in the (x, y) plane is assumed when writing the potential as a function of z only. The prefactor comes from the fact that the "period" of the analogous oscillator is four times the contour length of the polymers. In this approximation, the average monomer density is proportional to the potential U. Thus, the density profile of a polymer brush in good solvent is also parabolic. In the work of Zhulina *et.al.*, on the other hand, the free energy was expressed as a functional of both the local stretching, $E(x, x')$, at x of a chain with free end at x', and the distribution of free ends $g(x')$. The free energy was explicitly minimized and expressions for E and g were obtained. The resulting expression for the density profile in the same limit was equivalent to the result discussed above.

Ever since the mean field theory was developed for the good solvent brush, there have been many numerical confirmations of the basic predictions. The mean field equations were solved directly using numerical methods [56] and the results compared to analytical theory [55]. Good agreement was found for the density profile and the distribution of free chain ends for moderate N. Corrections were calculated and again found to be in agreement with the numerical results. A parabolic profile was found by simulation in a molecular dynamics study that also calculated the force between two brush covered parallel surfaces [57]. Using a lattice Monte Carlo simulation [12] of a self-avoiding walk polymer, density profiles and the free chain end distribution were fit to the predictions of Milner [55] with the excluded volume parameter as an adjustable parameter. Good agreement was found, and the fitted values of the excluded volume parameter were consistent for several simulations. In a similar vein, a polymer brush simulated with the bond-fluctuation algorithm [44] found agreement with the scaling of the profiles with the grafting density and the degree of polymerization predicted

from the mean field theory. The same bond-fluctuation results were compared in more detail in a following publication [46]. Recently, a simulation based on a polymer system described by the Edwards Hamiltonian again found agreement with mean field theory [47].

The first direct experimental evidence of a brush regime was obtained from small angle neutron scattering experiments of polymers end-grafted to the surfaces of porous silica [4]. By varying the grafting density σ and the molecular weight of the grafted polymer, they were able to confirm the scaling relations

$$h \sim \begin{cases} N\sigma^{\frac{1}{3}} & \text{good solvent} \\ N\sigma & \text{poor solvent,} \end{cases} \tag{4.4}$$

where h is some measure of the brush height and N is the degree of polymerization. This was the first clear experimental evidence of anisotropic stretching normal to the grafting surface.

The subject of polymer brushes has been the focus of much research, and has generated a large literature in recent years. A good overview of polymer brushes, especially in context of the mean field theories of Milner [55] and Zhulina [86], can be found in the review of Milner [54]. Scaling arguments as applied to polymer brushes are reviewed by de Gennes [19]. Results of computer simulations on polymer brushes can be found in a recent review by Grest [31].

4.3 *The "parabolic" brush: an illustration*

As the parabolic brush has become a central result in the study of polymer brushes, a few important results from the self consistent field (SCF) theory of polymer brushes in good solvent will be discussed in this section. Although the SCF mean field results have been tested against simulation on many occasions, to the best of my knowledge the Langevin formalism has not been used to simulate polymer systems. Therefore, this opportunity will be taken to compare the mean field theory with results from a Langevin simulation, which will serve to illustrate both the Langevin method and the mean field theory. The polymer brush in good solvent was previously studied using Monte Carlo methods and the Edwards Hamiltonian [47], with results similar to these Langevin results.

In this Langevin demonstration, K polymers with N monomers each are randomly grafted onto the (x, y) plane at $z = 0$. The grafting plane of area $L \times L$ is considered impenetrable. The top of the simulation volume is placed far enough away from the grafting plane to be effectively at infinity. After specifying the initial positions of all the monomers, the monomer coordinates are updated according to the Langevin method, detailed in chapter 3. Since the grafting plane is impenetrable, it is necessary to restrict the monomers to lie in the half space $z > 0$. After an initial period of equilibration, the time averages of quantities of interest can be measured. For this example, $L = 10$, $K = 10$, and $N = 40$, unless otherwise stated. Units of length [1] are chosen such that $b^2 = 3$.

The scaling of the height of the brush with the degree of polymerization, N, is quite distinct from the case of non-grafted polymers. In a brush, the height $h \sim N$, whereas in the free case the average polymer extent $R \sim N^{3/5}$. This characteristic linear scaling is a clear signature of the brush regime; *i.e.*, when polymers are grafted at sufficiently high density to cause considerable overlap [4]. Furthermore, this scaling is a robust result. It is predicted from Flory type energy balance argument, from the scaling arguments of Alexander, and also from the more detailed SCF mean field calculations. Results for the brush height are shown in fig. (4.1), where the brush height has been measured in two separate ways. In one case, the average z value is used, and in the other, the z component of the radius of gyration. With either definition, the brush height appears [2] to scale linearly with N.

A central result of the SCF mean field theory is a prediction for the density profile; *i.e.*, the monomer concentration as a function of z, the perpendicular distance away from the wall, defined by the expression

$$\phi(z) = \frac{1}{L_x L_y} \int_0^{L_y} dy \int_0^{L_x} dx \, \phi(x, y, z), \tag{4.5}$$

where L_x and L_y are the dimensions of the grafting surface in the x and y directions, respectively. According to SCF theory [55], the density profile is expected to be

[1] Units have been chosen in this way in order to conform with previous literature. For the remainder of the thesis, any quantity with dimensions of length is expressed in units of $(b^2/3)^{1/2}$, though this is not stated explicitly for notational convenience.

[2] The possibility that the dependence on N is weaker than linear cannot be discounted with this data, which may not reach the scaling regime [41, 7].

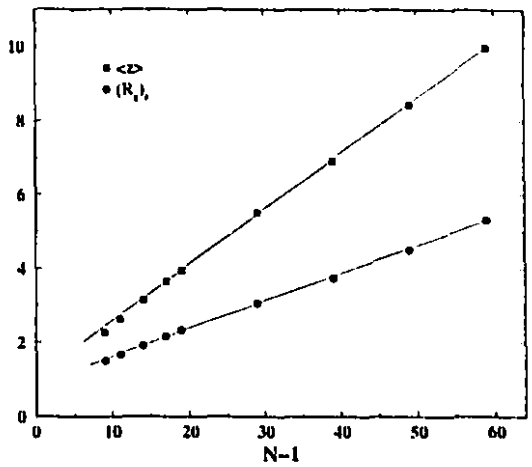

Figure 4.1: The brush height as a function of the number of bonds, $N-1$. The height has been measured in two ways: (squares) the average value of z, and (circles) the z component of the radius of gyration averaged over all monomers. The height is linear with both definitions. The lines are guides to the eye only.

parabolic,

$$\phi(z) = \frac{\pi^2}{8w_2N^2}\left[h^2 - z^2\right], \tag{4.6}$$

where the brush height h is

$$N\left(\frac{12\sigma w_2}{\pi^2}\right)^{1/3}. \tag{4.7}$$

An example of the SCF density profile and the associated density profile obtained from a Langevin simulation with the same parameters is shown in fig. (4.2). This figure demonstrates some important features. The density profile from simulation is dramatically lower than the mean field result near the wall, which has a maximum at the wall. This region is known as the **depletion zone**. Also, the simulation has a smooth tail at the top edge of the brush, unlike the SCF result, which becomes strictly zero at the brush height. Both these effects are well established features of more realistic brushes, and have been observed in many simulations that followed the parabolic brush prediction. Besides these two regions, the simulation is consistent with the SCF prediction.

This "classical path" SCF results relies on the **strong stretching approximation**, that the brush height greatly exceeds the typical lateral dimensions of the polymers. Detailed SCF predictions, such as the density profile, should only be valid

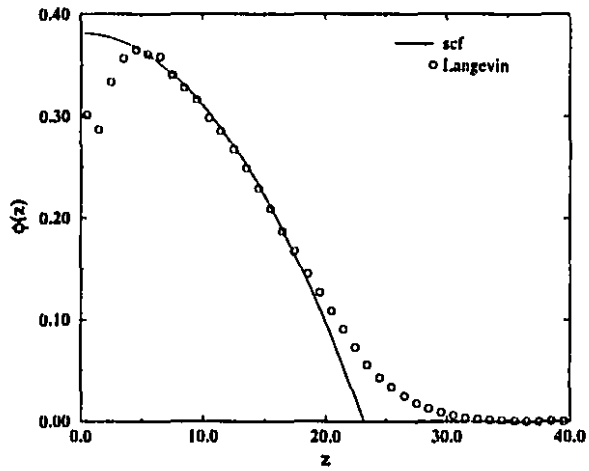

Figure 4.2: Monomer density profiles as a function of the distance perpendicular from the grafting plane. The line is the prediction from mean field theory. The figure clearly shows a "depletion zone" near the wall, and a smooth tail at the top of the brush. Away from these two areas, the agreement is consistent. The simulation parameters are $L = 10$, $K = 10$, $N = 40$, and $w_2 = 0.5$.

to the degree to which the strong stretching approximation is satisfied. According to SCF theory, energy balance arguments and scaling arguments, the brush height h should scale as $N(\sigma w_2)^{1/3}$; thus, one should be able to achieve "not-so-strong stretching" by varying these parameters appropriately. If the two variables, ϕ and z are rescaled according to

$$\phi \to \phi \left(\frac{w_2}{\sigma^2}\right)^{1/3}$$

$$z \to \frac{z}{N(\sigma w_2)^{1/3}},$$

then eqn. (4.6) becomes independent of the parameters N, σ, w_2. That is, the rescaled ϕ should be a universal function of the rescaled z. In fig. (4.3), the scaled density profiles are shown as a function of the perpendicular distance away from the grafting plane. The concentration ϕ' is plotted in units of $(w_2/\sigma^2)^{-1/3}$, and z' in units of $N(\sigma w_2)^{1/3}$. The density profiles are shown for different values of $h = (12/\pi^2)^{1/3} N(\sigma w_2)^{1/3}$. There is the general trend that for smaller h, there is greater deviation from the expected SCF profile. For large h, however, both the depletion zone and the smooth tail become much less pronounced, and the SCF result fits the simulation results over a wider range. This accords well with the notion that the

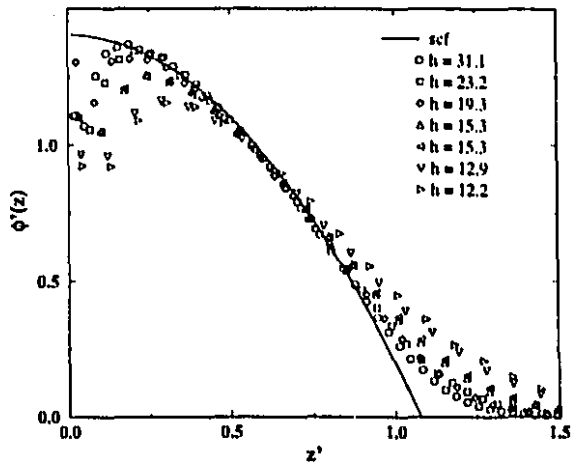

Figure 4.3: Monomer density profiles as a function of the distance perpendicular from the grafting plane. The density is plotted in units of $(w_2/\sigma^2)^{-1/3}$, and z in units of $N(\sigma w_2)^{1/3}$. In these units, the data should collapse onto a universal curve. The curve predicted by self-consistent field theory is shown as a line on the same graph.

mean field theory is valid in the strong stretching limit.

This comparison highlights one of the advantages of simulations based on the Edwards Hamiltonian. Comparisons can be made between the results of the simulation and the field theory results without the fitting of parameters. This is not possible with lattice Monte Carlo simulations, nor with molecular dynamics simulations. In these cases, there is no direct correspondence between parameters, making it necessary to fit one or more parameters.

5

Polymer Brush in Poor Solvent

The equilibrium structure of a homogeneous polymer brush is investigated in poor solvent conditions. Using the Monte Carlo technique developed in section 3.1.2, much larger systems are simulated than previously possible. When solvent quality becomes sufficiently poor, lateral inhomogeneities develop in the monomer density in the direction parallel to the grafting plane. A micro-phase separated conformation is observed at long times. The length scale characteristic of the micro-phase structure is consistent with a two dimensional random walk. The use of an Edwards Hamiltonian allows for control of solvent quality, facilitating direct comparison with previous numerical work which predicted the limits of stability of the laterally homogeneous layer [80]. Our simulation results are consistent with these findings.

5.1 Introduction

The structure of grafted polymer layers depends strongly on the interaction of the polymers with the solvent in which they are immersed. In the previous chapter, the homogeneous brush under good solvent conditions was considered. It was seen that for polymers grafted onto a plane surface, often assumed for convenience, translational invariance in the plane parallel to the grafting plane can be invoked to reduce the study of the brush to a one dimensional problem in the direction perpendicular to the grafting surface. In this instance, the properties of polymer layers are well characterized by one dimensional self-consistent mean field theories, as seen, for example, from the results of chapter 4.

The study of polymer brushes under poor solvent conditions is also important, from an applications point of view as well as that of pure theoretical interest. For example, the application potential of self-assembled monolayers is well known [77]; if

such a monolayer is formed from a polymer brush, then variations in layer thickness of order ten are possible by adjusting solvent quality [40]. If the brush is used for colloidal stabilization, it is potentially useful to be able to induce coagulation by changing the solvent quality [35]. Moreover, under poor solvent conditions, one must account for the possibility that the polymers will phase separate from the solvent. In this case, it is no longer obvious that the assumption of translational invariance is still valid. Nevertheless, the simplification resulting from this assumption remains very compelling, and indeed early studies of polymer brushes in poor solvent assume structureless layers in the plane parallel to the grafting surface [35, 66, 85].

In an early attempt to describe the polymer brush in poor solvent without assuming translational invariance, Ross and Pincus [65] applied the random phase approximation to include density fluctuations about a self consistent mean field solution for a brush with a step function profile. They found no instability in the poor solvent regime, and therefore concluded that the standard assumption of uniform and continuous collapse was indeed correct.

Perhaps the earliest indication that lateral inhomogeneities may in fact be present under poor solvent conditions was from Monte Carlo simulations of Lai and Binder using the bond-fluctuation algorithm [45], designed to study the influence of varying solvent quality. Poor solvent conditions were introduced through an effective attraction between monomers, modelled by an energy reduction if two monomers were neighbours on the lattice. Strong lateral fluctuations in the monomer density were indeed found, as the authors observed one region of relatively high monomer density. However, the results in poor solvent conditions were preliminary, by the author's own admission, as they were unable to simulate a large enough system to characterize the structure formed in the poor solvent regime. In a similar study, Grest and Murat [30] investigated the structure of polymer brushes in various solvent conditions with molecular dynamics in which poor solvent conditions were introduced through an attractive pair potential. Similar results were obtained in this study; the authors observed evidence of laterally inhomogeneous phase separation, although with a limited system size resulting in only one domain of high polymer density, and thus strongly constrained by finite size effects.

In a numerical study, Yeung, Balazs, and Jasnow [80] used the random phase approximation to describe fluctuations in the poor solvent brush, calculating a self-consistent mean field solution numerically instead of making the step function ansatz, as had Ross and Pincus. They found that in sufficiently poor solvent conditions, a laterally homogeneous layer becomes linearly unstable to fluctuations. In the unstable regime, they found that the polymer layer undergoes a **micro-phase separation** [1] into small domains, or "dimples", of predictable size and spacing. They also calculated a stability diagram, showing the limits of stability separating stable, laterally uniform conformations from inhomogeneous micro-phase separated configurations.

Since the work of Yeung *et.al.*, more analytical work has supported their conclusion of micro-phase separation in sufficiently poor solvent conditions. Huang and Balazs [36] performed a two dimensional self consistent field calculation, thus obviating the need for assuming translational invariance. They also found dimples, in qualitative agreement with the Yeung picture. More recently, Tang and Szleifer [71] performed a scaling analysis for the poor solvent brush and found a similar "phase-diagram" including a laterally homogeneous regime, the micro-phase separated regime, and a regime where individual grafted polymers form mushroom-like structures. Scaling analyses have been peformed for the "micelles", or individual polymer aggregates, formed in sufficiently poor solvent [79, 84]. Very recently, a classical limit self-consistent field analysis determined the equilibrium height profile and its stability for a melt brush, which is a special case of a brush in a poor solvent [70].

Lateral instabilities were observed experimentally using atomic force microscopy. Homogeneous polymer layers and islands were observed when the brush was exposed to air [81]. A polymer brush was studied using neutron reflectivity in which the density profile in the direction perpendicular to the surface was determined in various solvent conditions [39]. There was no attempt to determine structure in the lateral plane, so microphase separation could not be observed. However, it was clear that there was no step function like discontinuity in the density profile, even below the Θ point, contrary to the assumption of Ross and Pincus. More recently, an atomic force

[1] The term micro-phase separation refers to equilibrium separation that occurs only "locally", as opposed to when individual phases separate completely into single domains separated by a single interface. This latter separation is referred to as **macro-phase separation** in this context.

microscopy study of the same system was published, in which the lateral structure was directly observed [40]. A polymer brush was synthesized by adsorption of polymer end groups to a surface from poor solvent, the grafting density being determined by the time allowed for adsorption. Laterally inhomogeneous structures were indeed found for low grafting density. However, it seems likely that the effective attractive interaction between polymers in poor solvent would affect the pattern of grafting. It is not clear to what extent this factor affected their results. Very recently, phase separated structure were again observed directly with atomic force microscopy [67]. The polymers were adsorbed from good solvent, and would be expected to have a random grafting pattern. Regimes with isolated mushrooms, phase separated dimples, and homogeneous layers were reported.

In this chapter, results are presented from an extensive Monte Carlo simulation of grafted polymer layers under poor solvent conditions, with particular emphasis on determining the influence of phase separation on the structure of these layers. Simulation is performed within the Edwards model as described in section 3.1.2, enabling the investigation of much larger systems than previously possible. We are thus able to provide detailed structural information, well into the region of micro-phase separation. We are also able to confirm theoretical predictions based on scaling analysis and numerical self-consistent field theory. Moreover, since the same Hamiltonian used in analytical treatments is employed here, results can be compared directly without the use of fitting parameters. This study is the first demonstration of the utility of this method in dense polymer conditions. This chapter is adapted from our previously published work [68].

5.2 Method

We describe a system of K polymers, each having N monomers, with the Edwards Hamiltonian

$$H\left\{\mathbf{R}_k(n)\right\} = \frac{3}{2b^2}\sum_{k=1}^{K}\int_0^N dn\left(\frac{\partial \mathbf{R}_k(n)}{\partial n}\right)^2 + H_I\left\{\mathbf{R}_k(n)\right\}, \tag{5.1}$$

where $\mathbf{R}_k(n)$ is the configuration of the kth polymer. As discussed in chapter 3, the first term represents a Gaussian chain with mean squared bond lengths b^2. The second

term is an interaction potential that depends on the set of polymer configurations $\{\mathbf{R}_k(n)\}$. Following eqn. (2.24), H_I can be expanded in powers of the local monomer concentration,

$$H_I\{\mathbf{R}_i(n)\} = \frac{w_2}{2}\int d\mathbf{r}\,\phi^2(\mathbf{r}) + \frac{w_3}{3}\int d\mathbf{r}\,\phi^3(\mathbf{r}), \tag{5.2}$$

to third order in the expansion. As discussed in section 2.2.2, unfavourable monomer-solvent interactions are modelled with a negative value of w_2. Increasingly negative values of w_2 are associated with decreasing solvent quality. The third order term is retained in this instance since negative values of w_2 can lead to situations of higher monomer density. The value of w_3 is always positive. This form for the potential for poor solvent in near Θ conditions is customary in the literature [65, 80], and is the basis of our simulations. The integrals are over all space, with the local monomer density, $\phi(\mathbf{r})$, given by eqn. (2.22).

In this study, the Monte Carlo method developed in section 3.1.2 is implemented with the Hamiltonian of eqn. (5.1) and eqn. (5.2). The Hamiltonian is approximated using the coarse grained local density method [1] [2]. One end of every polymer is grafted at a random position onto a surface of area A, fixing the grafting density to be $\sigma = K/A$. The surface is considered to lie in the (x,y) plane, restricting the polymers to move in the half space given by $z \geq 0$. Periodic boundary conditions are imposed in the (x,y) directions, and the top of the simulation box is set far enough away to be effectively at infinity. In particular, the polymer brush consists of $K = 655$ polymers with $N = 64$ monomers each, grafted on a plane of area 128×128. The polymers are initially given random walk configurations with step size b. Units of length are such that $b^2 = 3$. We checked that for all results presented below, different initial conditions produced qualitatively similar results.

5.3 *Results*

A typical extended configuration of a grafted layer is shown in fig. (5.1) with the excluded volume parameter, w_2, set to zero, corresponding to a situation with no

[1] The pair interaction method described in section 3.1.2 has been applied to polymer brushes in good solvent conditions [47]; however, even in good solvent conditions, the coarse grained local density method is several times faster, an advantage that is certainly amplified in higher density poor solvent conditions.

[2] The cells of eqn. (3.18) are cubic and of linear size $l = 2$.

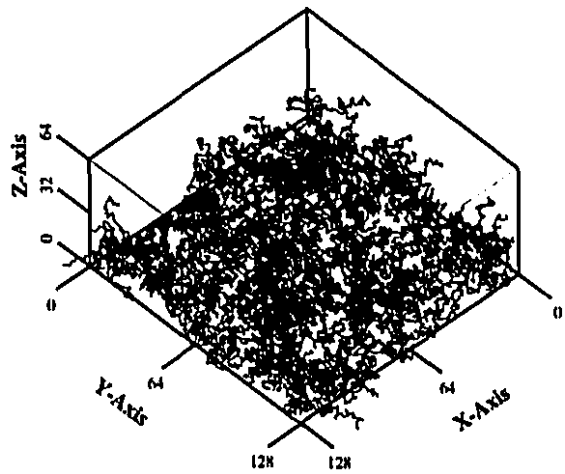

Figure 5.1: The polymer brush in an extended configuration, with $w_2 = 0.0$ and $w_3 = 0.5$. Other system parameters are $L = 128, K = 655, N = 64$. For purposes of presentation, only $K = 400$ randomly selected polymers are drawn.

effective attraction between the monomers. There is little lateral structure evident in the monomer density; *i.e.*, the monomers are uniformly distributed in the plane parallel to the grafting surface.

Under poor solvent conditions, the resulting effective attractive force between the monomers can lead to micro-phase separation. Fig. (5.2) shows a configuration of a polymer brush where a sufficiently negative value of w_2 causes the extended configuration of fig. (5.1) to become unstable, resulting in micro-phase separation into polymer rich regions and solvent rich regions. The phase separated regions are quite structured, forming almost regularly spaced clusters. Evidence for such inhomogeneity was observed in previous lattice Monte Carlo [45] and molecular dynamics [30] simulations, but not on a scale large enough to show the structure clearly evident here. Since the grafting points of the polymers are irreversibly fixed onto the surface, complete macro-phase separation into a single polymer phase is not possible due to the energy cost involved in stretching a bond. Polymers therefore collapse into clusters locally, giving rise to a length scale that characterizes the structure formed in the phase separated regime.

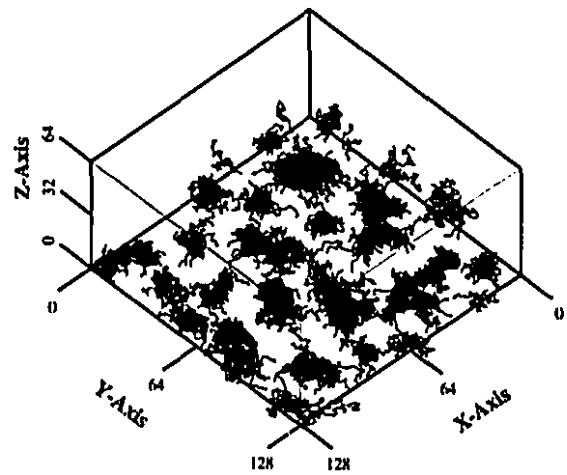

Figure 5.2: The polymer brush in a micro-phase separated configuration, with $w_2 = -1.0, w_3 = 0.5$. The polymer droplets form a near-regular structure in the lateral plane. Other system parameters are $L = 128, K = 655, N = 64$. For consistency, the same 400 selected polymers as in fig. (5.1) are shown.

The onset of inhomogeneity in the lateral density which accompanys micro-phase separation is conveniently observed via the structure factor. The structure factor for a system of $N_o = NK$ monomers can be defined [1]

$$S(\mathbf{q}) \equiv \frac{1}{N_o} \sum_{m,n}^{N_o} \langle \exp[i\mathbf{q} \cdot (\mathbf{r_m} - \mathbf{r_n})] \rangle \tag{5.3}$$

where a monomer n is considered a scattering unit at position $\mathbf{r}_n$. We define the Fourier transform of a function $f(\mathbf{r})$

$$\hat{f}(\mathbf{q}) \equiv \int d\mathbf{r}\, f(\mathbf{r}) \exp(-i\mathbf{q} \cdot \mathbf{r}). \tag{5.4}$$

Using the microscopic definition, eqn. (3.13), of the concentration $\phi(\mathbf{r})$ and the definition of the Fourier transform, eqn. (5.4), the Fourier transform of the concentration becomes

$$\hat{\phi}(\mathbf{q}) = \sum_{n}^{N_o} \exp(-i\mathbf{q} \cdot \mathbf{r_n}). \tag{5.5}$$

[1] See reference [22], section 2.4.

With these definitions, the structure factor can be alternately written

$$S(\mathbf{q}) \equiv \frac{1}{N_o}\left\langle |\hat{\phi}(\mathbf{q})|^2 \right\rangle . \tag{5.6}$$

In this and the next chapter, we shall use the form eqn. (5.6) to define the structure factor of a function.

Since the density inhomogeneities of interest are in the (x, y) plane, we restrict our attention to the two dimensional structure factor

$$S(q_x, q_y) = \frac{1}{N_o}\left\langle |\hat{\phi}_{pp}(q_x, q_y)|^2 \right\rangle , \tag{5.7}$$

where $\hat{\phi}_{pp}(q_x, q_y)$ is the Fourier transform of the plane projected monomer density,

$$\hat{\phi}_{pp}(q_x, q_y) = \int dx dy\, \phi_{pp}(x, y)\, e^{-i(q_x x + q_y y)}, \tag{5.8}$$

and

$$\phi_{pp}(x, y) = \int dz\, \phi(x, y, z). \tag{5.9}$$

Examples of plane projected monomer densities are seen in fig. (5.3), corresponding to the configurations shown in fig. (5.1) and fig. (5.2). The micro-phase structure is

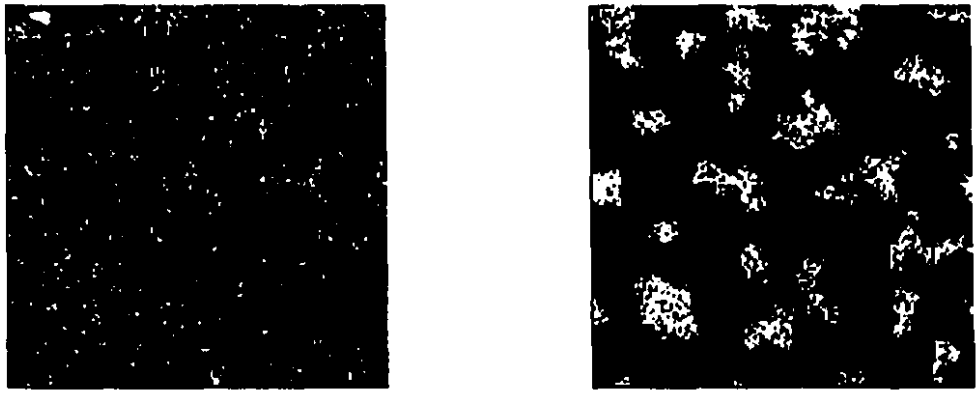

Figure 5.3: The plane projected monomer density ϕ_{pp}, corresponding to the previously shown configurations. Both views are perpendicularly down onto the (x, y) plane, with monomer density shown in gray-scale: black corresponds to low monomer density, white to high monomer density. The figure on the left corresponds to the extended configuration of fig. (5.1), with $w_2 = 0$ and $w_3 = 0.5$. The figure on the right corresponds to the micro-phase separated configuration of fig. (5.2), with $w_2 = -1.0$ and $w_3 = 0.5$. In both cases, $L = 128$, $K = 655$, and $N = 64$.

clearly visible, with high concentrations of monomer showing up as white. We also define $S(q)$ as the circular average of the two dimensional structure factor, a function

a) $w_2 = 0.0$

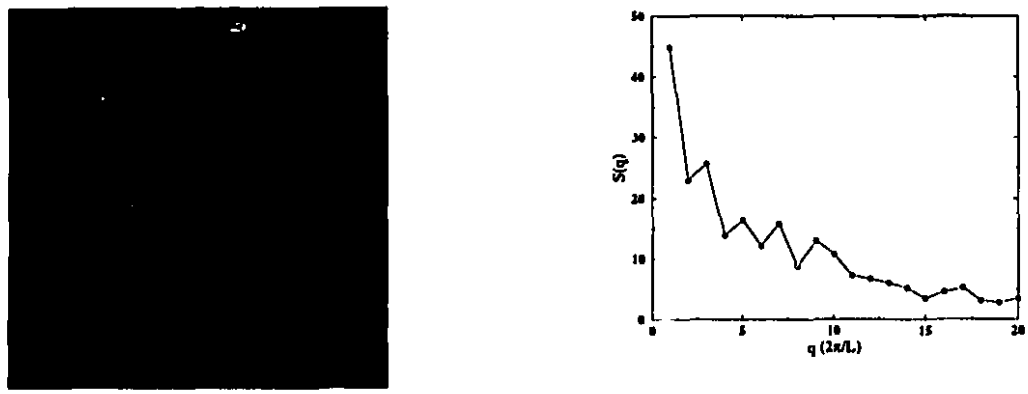

b) $w_2 = -1.0$

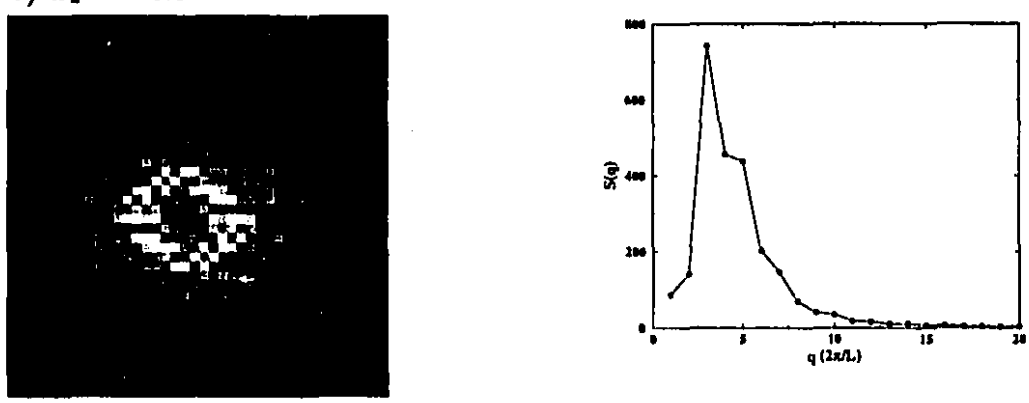

Figure 5.4: Two dimensional structure factors of the plane project monomer density ϕ_{pp}, corresponding to the example configurations of fig. (5.1) and fig. (5.2). Figure a) on top corresponds to fig. (5.1), with $w_2 = 0$ and $w_3 = 0.5$. Figure b) on the bottom corresponds to fig. (5.2), with $w_2 = -1.0$ and $w_3 = 0.5$. The circularly averaged counterparts are shown to the right in each case. In both cases, $L = 128$, $K = 655$, and $N = 64$.

only of the magnitude of the wave vector q. Examples of two dimensional structure factors and corresponding circular averages are shown in fig. (5.4). Circularly averaged structure factors are shown in fig. (5.5) for several values of w_2 at fixed w_3.

The emergence of structure associated with micro-phase separation is marked by the appearance of a peak at a non-zero value of q in the circularly average structure factor. The peak position, q_{peak}, corresponds to a new length scale which by comparison with the real space configuration of fig. (5.2) is found to be consistent with the average distance between micro-phase separated regions. Furthermore, the peak

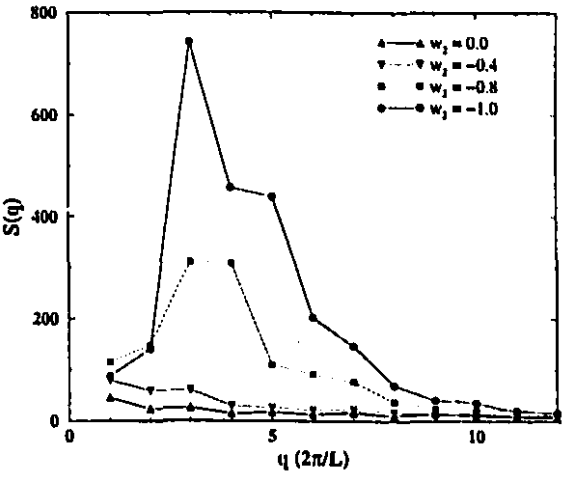

Figure 5.5: Circularly averaged structure factors for the lateral density. The onset of structure accompanying the micro-phase separation is seen as a peak at a non-zero value of q develops. The structure factors for the configurations of fig. (5.1) and fig. (5.2) are shown, as well as two intermediate configurations. The lines are guides to the eye only. Other system parameters are $L = 128$, $K = 655$, $N = 64$ and $w_3 = 0.5$.

height $S(q_{peak})$, which measures the scattering intensity in a scattering experiment, depends on the values of w_2; in particular, the greater the value of $|w_2|$, the larger the peak height [1].

The average distance between clusters, obtained from the peak position of the structure factor, is in all cases almost twice the end-to-end distance of a two dimensional random walk in a Θ-solvent. This result agrees with the scaling analysis of Tang *et. al.* [71] and is consistent with the linear stability analysis of Yeung *et. al.* [80], who suggested that the instability occurs on a finite wavelength on the order of the radius of gyration for a polymer in a Θ-solvent. Furthermore, we observe that this is a robust result; *i.e.*, the average distance between the polymer clusters is seen to be independent of the parameters w_2 and w_3 over a wide range, though the cluster size itself does change with these parameters.

To understand this result, we examined the average end-to-end distance $R_{(x,y,z)}$ of the polymers in the x, y, and z directions, respectively. As w_2 was made increasingly negative, R_z decreased, indicating the collapse of the polymers in increasingly

[1] The system was equilibrated at the fixed value of w_3 and $w_2 = 0$, after which w_2 was gradually decreased to the desired value.

poor solvent conditions. On the other hand, R_x and R_y remained almost constant with a value close to that of a two-dimensional random walk. Thus, in this dense polymer regime, the average end-to-end distance of the polymers in the (x, y) plane does not depend strongly on solvent quality. Since the end-to-end distance measures the approximate size of a polymer, it is reasonable to expect the distance between clusters to be of this order when phase separation sets in, and therefore is also independent of solvent quality. As phase separation continues, the clusters become more concentrated, but the average distance between clusters remains unaffected.

Another interesting question is whether or not the lateral instability in the density profile can be restricted to the tip region of the polymer layer. This possibility was suggested from the analysis of Yeung *et. al.* [80] when w_2 takes values near the onset of the instability for large grafting densities. We therefore varied the grafting density and the value of w_2, in order to find such a situation by calculating the structure factor $S(q)$ in plane sections parallel to the grafting surface. However, we have not yet unambiguously observed an instability restricted to the tip region of the brush, presumably due to the finite length N of each polymer.

Finally, a "phase-diagram" is estimated by varying the system parameters and searching for the limits of stability of the homogeneous phase. This is carried out by fixing w_3 and decreasing w_2 until the micro-phase separated regime is definitely reached. This can be compared with a stability diagram obtained using the random phase approximation [1]. The stability of the uniform lateral density profile is determined by investigating the circularly averaged structure factor, $S(q)$. When $S(q)$ exhibits a peak at finite q, the system is in the micro-phase separated region where a uniform lateral density profile is unstable. When such a peak is absent, uniform lateral density profiles are stable. The points in fig. (5.6) are determined from separate simulations at the indicated values of (w_2, w_3). Fig. (5.6) shows that our simulation

[1] In reference [80], the stability is determined as a function of the two independent parameters

$$\beta = \frac{w_2^4 b^2}{3\sigma^2 w_3^3} \tag{5.10}$$

$$\gamma = N\frac{3w_3^2\sigma^2}{w_2^2 b^2}. \tag{5.11}$$

Therefore, the phase diagram is presented in terms of these variables, with $b^2 = 3$.

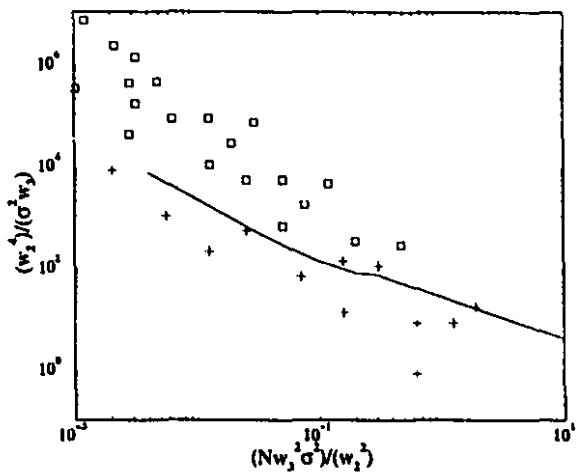

Figure 5.6: Simulation results as a function of the two independent parameters $\beta = w_2^4/(\sigma^2 w_3^3)$ and $\gamma = N w_3^2 \sigma^2 / w_2^2$. The line shown is the stability limit obtained with the random-phase approximation [80]. Micro-phase separated configurations in the unstable regime are represented by open squares. Configurations with a uniform lateral density profile are represented by crosses.

results are consistent with the random phase approximation prediction [80].

6

Binary Brush Phase Separation

The equilibrium structure of a grafted polymer layer composed of two distinct species of homopolymers, the "binary brush", is investigated in various solvent conditions using the coarse grained local density method of section 3.1.2. If the two species are sufficiently immiscible, lateral binary micro-phase separation occurs over a wide range of solvent conditions. Due to the presence of solvent, there is a stage where the brush expands in a laterally homogeneous manner as immiscibility increases. In this stage, laterally averaged quantities are well described by a single solvent related parameter: a modified excluded volume parameter. This is followed by lateral micro-phase separation in which the brush volume remains relatively constant. In Θ-solvent, this phase separation sets in at a degree of immiscibility consistent with a mean field prediction for melt layers. The onset of phase separation occurs at a greater value of immiscibility as solvent quality increases. Furthermore, reducing solvent quality results in a stronger crossover between mixed and phase separated configurations. Under poor solvent conditions, interesting structural variations result from the combination of phase separation from solvent as well as phase separation of the two species. The limit of stability of the homogeneous phase is determined using the random phase approximation, and the results compared to simulation results.

6.1 Introduction

The first studies of polymer brushes were focussed on the "classic" brush introduced in chapter 4; *i.e.*, a monodisperse, homogeneous polymer brush grafted to an infinite, flat plane. In practice, these idealized conditions are never realized, nor necessarily desired. In some instances, one can control the properties of a grafted monolayer by grafting different types of surfactants on the surface [34]. Furthermore, polymer

brushes may possess some degree of heterogeneity, even if not by design. In either case, it is desirable to know the effect of heterogeneity on the properties of the brush. We therefore consider a very simple example of heterogeneity: the two component polymer brush, or **binary brush.** The binary brush is composed of two different

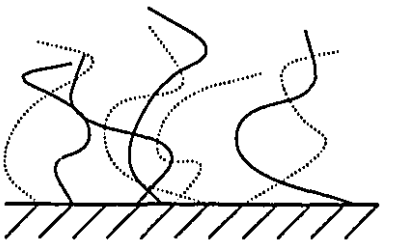

Figure 6.1: The binary polymer brush.

types of homopolymers, identical in every respect except for possibly some mutual interaction between the two binary types, say A and B. Both types are randomly grafted at a plane surface. The mutual interaction between the types is parameterized by w_{ab}.

Marko and Witten [50, 51] predicted instabilities in a symmetric binary brush composed of immiscible chains under melt conditions, and used self-consistent field (SCF) theory to examine the equilibrium properties. They studied two possible ordered phases for sufficiently high immiscibility: a "rippled" phase described in terms of a "density wave" in composition directed along the surface, equivalent to lateral micro-phase separation, and a "layered" phase rich in one component at the bottom of the brush and in the second component at the top of the brush. Marko and Witten showed that lateral micro-phase separation occurs for a value of immiscibility, or w_{ab}, 2.27 times greater than the corresponding value for bulk phase separation in simple blends, while the layered phase would be observed at four times the bulk value. Thus, the lateral instability preempts the layering transition, and is expected to be the one observed. Marko and Witten corroborated the occurrence of micro-phase transitions in binary brushes by studying real space correlations [52].

Brown *et.al.* [9] performed large scale Monte Carlo calculations with the polymers represented by self-avoiding walks on a simple cubic lattice in a symmetric binary brush for near melt conditions; *i.e.*, grafting densities of 0.3 and 0.5 on a surface of area 64×64, with $N = 100$. They observed micro-phase separation after quenching the

system to conditions of strong immiscibility. This was an impressive computational undertaking, requiring "about one *Sparcstation-year*" [9] to perform two quenches. Another simulation by Brown for the same model using simulated annealing confirmed this result [10]. Analytical work for binary brushes under melt conditions has since been extended to the strong demixing limit [25], whereby a self consistent model of the strongly phase separated brush containing phase separated regions and mixed regions was characterized. Lai [43] performed bond-fluctuation Monte Carlo simulations of a binary brush in a good solvent at a lower grafting density of approximately 0.1 on surfaces of area 32 and 64. N was primarily 20 and 40, with some runs having N up to 80. In this case, the equilibrium structures were investigated as a function of immiscibility and varying relative fraction of the binary types. For the symmetric case of equal fractions, the laterally separated phase was again observed. For asymmetric mixtures, layering was observed, with the minority phase segregating to the top of the brush, away from the grafting surface.

In this chapter, we study the two component brush under various solvent conditions. Using the coarse grained local density technique of section 3.1.2, we are able to investigate large systems, yielding configurations showing unmistakable lateral micro-phase separation. With this algorithm, we are able to go beyond previous work, providing more quantitative details than before. We are further able to consider the effect of varying solvent quality on micro-phase separation. We see, in marked contrast to the incompressible melt layer, that the presence of solvent allows for a stage of laterally homogeneous volume expansion in the brush as immiscibility increases, well before the onset of micro-phase separation. Moreover, solvent quality is seen to modulate the lateral micro-phase separation process itself, even though the binary species are indistinguishable with respect to solvent interactions. Our results for the onset of micro-phase separation in a Θ-solvent agree with a mean field prediction for a melt; however, in good solvent, onset of micro-phase separation is delayed. Furthermore, we see evidence that decreasing solvent quality produces a much sharper crossover between mixed configurations and laterally micro-phase separated configurations. We present a preliminary qualitative examination of the binary brush in poor solvent conditions. Finally, we determine the limit of stability

of the homogeneous phase using the random phase approximation and find it to be consistent with results of our simulations. This chapter has been adapted from our previously published article [69].

6.2 Method

As in section 3.1.2 and chapter 5, we describe a system of K polymers, each with N monomers with the Edwards Hamiltonian

$$H\left\{\mathbf{R}_k(n)\right\} = \frac{3}{2b^2}\sum_{k=1}^{K}\int_0^N dn\left(\frac{\partial \mathbf{R}_k(n)}{\partial n}\right)^2 + H_I\left\{\mathbf{R}_k(n)\right\}. \tag{6.1}$$

Again the first term in eqn. (6.1) represents the probability distribution of a Gaussian chain. The interaction Hamiltonian H_I for a binary brush containing two types of monomers, A and B, is given by

$$H_I(\mathbf{r}) = \frac{w_2}{2}\phi^2(\mathbf{r}) + \frac{w_3}{3}\phi^3(\mathbf{r}) + \frac{w_{ab}}{2}\phi_a(\mathbf{r})\,\phi_b(\mathbf{r}). \tag{6.2}$$

Here $\phi_{a,b}(\mathbf{r})$ is the concentration of monomers at the point $\mathbf{r}$, defined by

$$\phi_{a,b}(\mathbf{r}) = \sum_k \int dn\,\delta\left(\mathbf{r} - \mathbf{R}_k^{a,b}(n)\right), \tag{6.3}$$

where the superscripts and subscripts a, b refer to monomers of type A or B, respectively. Furthermore, $\phi(\mathbf{r})$ is the total monomer density, equal to $\phi_a(\mathbf{r}) + \phi_b(\mathbf{r})$. For future reference, we define the monomer density difference at the point $\mathbf{r}$ as $\Phi(\mathbf{r}) = \phi_a(\mathbf{r}) - \phi_b(\mathbf{r})$.

The coefficient w_{ab} is the immiscibility coefficient. For negative w_{ab}, there is an effective attraction between monomers of different types while for positive w_{ab}, the two types of monomer become immiscible. Consequently, within the model described above, $w_{ab} = 0$ describes a monodisperse, homogeneous polymer brush, since polymers of type A and B cannot be distinguished. The excluded volume parameter, w_2, determines the interaction of monomers with the solvent, which we take to be the same for monomers of both types. We reiterate that for positive values of w_2, good solvent conditions prevail, while negative w_2 describes poor solvent conditions. The parameter w_3 is taken to be positive or zero: it is not relevant in good solvent conditions and is set to zero for w_2 positive, and for poor solvent conditions, when w_2 is negative, w_3 is assigned a finite, positive value.

In this study, we consider linear homopolymers with N monomers per polymer. K polymers are randomly and irreversibly grafted by one end to an impenetrable plane with surface density $\sigma = K/L^2$, where L^2 is the area of the plane in the simulation volume. Half of the K polymers are chosen (randomly) to consist entirely of monomers of type A, with the remainder consisting of monomers of type B. The grafting plane is the (x, y) plane plane situated at $z = 0$ and periodic boundary conditions are imposed in the directions tangential to this plane. Monomers are confined to the positive half-space $z \geq 0$, and the top of the simulation box is placed at a large enough value of z to be effectively at infinity. In particular, polymers are grafted at a surface density of $\sigma = 0.1$, on a square plane of area either 128×128, or 64×64. Each polymer contains $N = 64$ monomers and the box size for coarse graining has linear dimensions of 2. The unit of length is chosen such that $b^2 = 3$.

6.3 Results

Two sample configurations of the binary brush, obtained from our simulations, are shown in fig. (6.2) and fig. (6.3). They correspond to different values of the immiscibility parameter, w_{ab}, and two views are presented for each configuration. The upper diagram is the view from above, looking perpendicularly down towards the grafting plane, while the lower diagram in each case is the "edge on" perspective, viewed parallel to the grafting plane, Black lines represent polymers of type A, while grey lines represent polymers of type B.

Fig. (6.2) is a typical configuration in the absence of immiscibility; *i.e.*, $w_{ab} = 0$. In this case both the total monomer density and the distribution of monomers of type A and B should be homogeneous. Indeed, in both views, monomers of types A and B appear evenly distributed. Fig. (6.3) is a typical configuration for w_{ab} large. Strong immiscibility is expected in this case and the view from above clearly shows lateral phase segregation, resulting in micro-phase separated domains rich in either A or B type monomers. Note that the side view gives no indication of layering as monomers of different type do not visibly segregate in the vertical direction. As will be discussed in more detail later, the average domain width is approximately a quarter of the lattice size, which corresponds to twice the lateral end-to-end distance of a

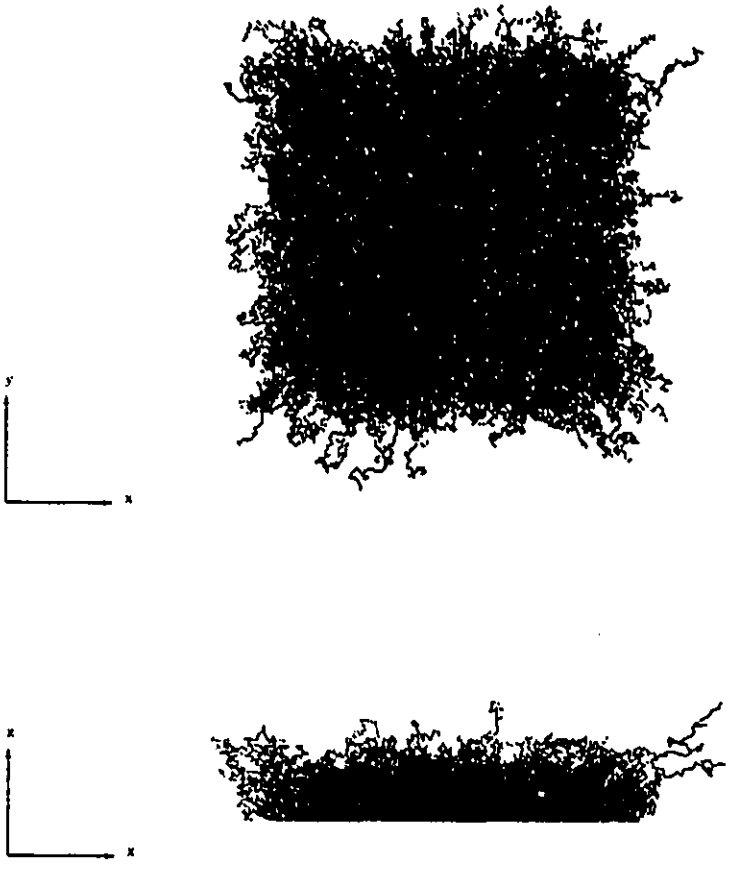

Figure 6.2: Sample configurations of the two component polymer brush, for $w_2 = 0.5$, $w_{ab} = 0.0$ (no immiscibility). The top figure is the view down along the z axis towards the top of the brush, while the the bottom figure is an edge view, parallel to the grafting plane, The system size $L = 128$ and the grafting density $\sigma = 0.1$.

polymer in a Θ-solvent.

These results are qualitatively similar to those reported in previous work [9, 43], from which the following consistent picture emerges. For small values of w_{ab}, entropic effects dominate, favouring the laterally homogeneous state. However, for sufficiently large immiscibility, energetic effects dominate the entropic effects, causing the polymers to phase separate into A rich and B rich domains. If the grafting points were free to move, the phase separation would continue until macro-phase separation into single domains of A and B separated by one interface occurred. However, due to the irreversible end grafting of each polymer onto the grafting surface, macro-phase

Figure 6.3: Sample configurations of the two component polymer brush, for $w_2 = 0.5$, $w_{ab} = 1.5$ (strong immiscibility) for the same system shown in fig. (6.2). There is marked phase separation evident in both views. The edge view indicates that phase separation is lateral, with no evidence of "layering". The system size $L = 128$ and the grafting density $\sigma = 0.1$.

separation cannot take place and the equilibrium structure consists of local domains of single polymer species. Since the polymers fluctuate laterally over a distance of approximately twice the polymer end–to–end distance, it is plausible that the domains should have this size. If the lateral density is sufficiently high (as is expected in a brush), excluded volume interactions will be screened laterally and the end–to–end distance will be that expected for a Θ-solvent. This argument for the selection of domain size where lateral patterns are formed in polymer brushes is quite general and has been observed in such cases as lateral micro-phase separation in poor solvent [68, 80, 71], binary brush melts [9, 51], and binary brushes at lower density as

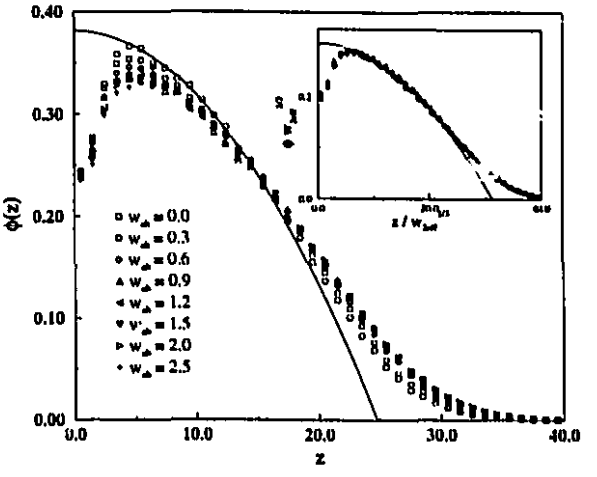

Figure 6.4: Total monomer density profiles for different values of w_{ab}, with solvent quality fixed at $w_2 = 0.5$. The line corresponds to an analytical prediction from SCF theory. The case of $w_{ab} = 0$ is indicated by open circles. The inset shows the profiles for different w_{ab} scaled with an effective good solvent parameter, w_{2eff}. The system size $L = 128$ and the grafting density $\sigma = 0.1$.

seen in reference [43] and in this chapter.

In order to make contact with previous theoretical results for end-grafted polymer brushes, we next examine monomer density distributions as a function of z, the perpendicular distance away from the grafting surface. The monomer density profile is defined by eqn. (4.5) in chapter 4. The definition is completely analogous for the monomer density difference, $\Phi(z)$. Density profiles for the total monomer density are shown in fig. (6.4) for various degrees of immiscibility. Small but systematic changes are evident as w_{ab} is increased. The particular case of $w_{ab} = 0$ corresponds to a binary brush with no differential interactions between A and B type polymers, and is therefore equivalent to a homogeneous brush. In this case, there is an analytical prediction for the density profile, as was seen in chapter 4. The solid line in fig. (6.4) gives the SCF result of eqn. (4.6). The resulting agreement with the simulation data is the same as discussed in chapter 4. That is, there is reasonable agreement except for the depletion zone near the wall and the smooth tail at the top edge of the brush. We note that there are no free parameters to adjust when comparing the data with the expected profile. This highlights one of the advantages of the current simulation method as stated at the beginning of the chapter, that parameters of the simulation

can be formulated directly in terms of polymer field theory.

As w_{ab} is increased from zero, there is a small but distinct tendency for the profile to "flatten out", suggesting that the polymers stretch away from the surface as the repulsion between A and B polymer types increases. Because a more favourable polymer interaction with the solvent would have qualitatively the same effect, we reinterpret the enhanced immiscibility as an increase in solvent quality. An increase in the value of w_{ab} thus modifies w_2, creating an effective value, $w_{2eff} > w_2$. Note that eqn. (4.6) becomes independent of w_2 given the change of variables $\phi \rightarrow w_2^{1/3}\phi$ and $z \rightarrow z/w_2^{1/3}$. We assume this as a good solvent scaling form. Thus, if the data can be described in terms of varying solvent quality, we expect that a rescaling of the profile data using $\phi \rightarrow w_{2eff}^{1/3}\phi$ and $z \rightarrow z/w_{2eff}^{1/3}$ should result in a data collapse onto a universal curve for appropriate values of w_{2eff}. The results are shown in the inset in fig. (6.4) and we do indeed find a convincing data collapse for all values of w_{ab}.

This rescaling does not follow directly from previous work since eqn. (4.6) was derived assuming a laterally featureless brush; in fact, the analysis of Marko and Witten [51] was restricted to the weak segregation limit so that the classical trajectories $z(n)$, where n gives the position of a monomer on a polymer chain, would not be affected by segregation effects. However, there are clear indications from fig. (6.3) and the discussion below that phase separation has occurred over the range in which we fit w_{2eff}, giving rise to clear lateral micro-phase structure. Nonetheless, the brush appears to remain laterally homogeneous *on average*, even after the onset of micro-phase separation, as seen in the profile for the density difference, Φ, shown in fig. (6.5) for the phase separated configuration of fig. (6.3). The total density profile, ϕ, is also shown in this figure to provide scale. The figure shows that there is negligible variation in the Φ profile, its value being close to zero, indicating no significant monomer excess of either type for any value of z. This may help explain why laterally averaged quantities, such as the density profile, are well described by a single parameter, in this case the modified excluded volume parameter. In addition, the lack of variation in the Φ profile shows that there is no vertical phase segregation, supporting previous findings that micro-phase separation is completely lateral.

The fitted values of w_{2eff} are shown in fig. (6.6) as a function of w_{ab}. The increase

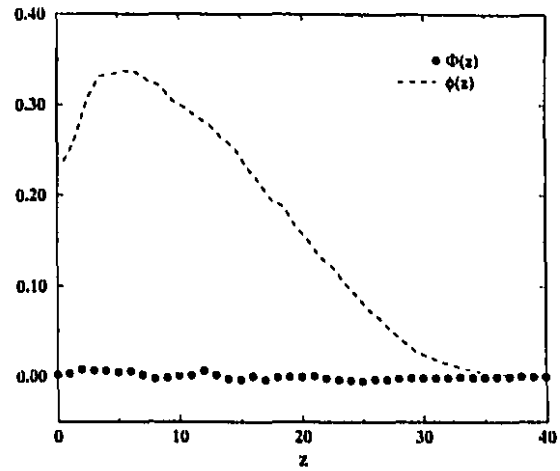

Figure 6.5: Profile of the monomer density difference for $w_{ab} = 1.5$, $w_2 = 0.5$, corresponding to the configuration in fig. (6.3). The total density profile is also shown to provide scale. For all z, the density difference is negligible compared to the density in the layer. The small variation shows little vertical segregation. The system size $L = 128$ and the grafting density $\sigma = 0.1$.

of effective solvent quality with increasing immiscibility can be clearly seen for small values of w_{ab}. For larger values, however, w_{2eff} becomes independent of w_{ab}. In order to explain why w_{2eff} saturates, we propose that the process of micro-phase separation advances in two stages. As immiscibility is increased, we suppose that there is a range of w_{ab} before the onset of micro-phase separation where the energy added to the brush is compensated for by an overall lowering of the brush density achieved by stretching the polymers away from the surface. For w_{ab} greater than a particular value, micro-phase separation sets in and any further increase of immiscibility energy will to a certain extent be compensated by the lateral rearrangement of the monomers. Since this is a lateral ordering process, it does not necessarily require brush expansion and therefore no further increase should be seen in w_{2eff}. As a more direct probe of the brush expansion, we measured the value of z averaged over all monomers in the system as an indication of brush height. Results are given in fig. (6.7). As a function of w_{ab}, we see that there is indeed a stage where the height increases, implying a volume expansion. This is followed by a stage where the rate of expansion is markedly decreased, suggesting saturation. For $w_2 = 0.5$, the saturation begins at the same value of w_{ab} where w_{2eff} begins to saturate in fig. (6.6).

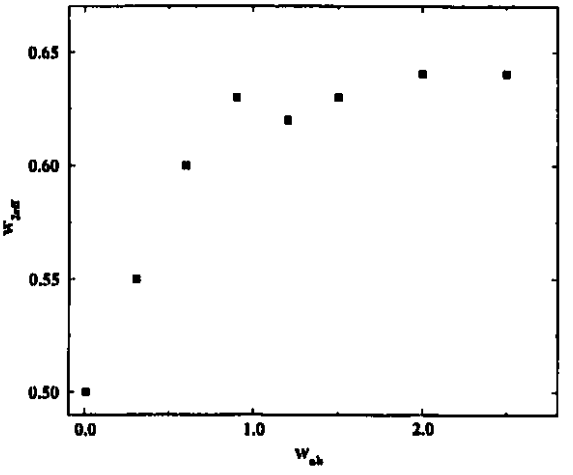

Figure 6.6: The effective excluded parameter w_{2eff} determined from the scaling of the total monomer density profile (fig. (6.4)) as a function of w_{ab}. w_{2eff} appears to begin saturating at $w_{ab} \simeq 1.0$. The system size $L = 128$ and the grafting density $\sigma = 0.1$.

For a more detailed study of the lateral structure, we calculate the structure factor of the plane projected monomer density difference,

$$S(q_x, q_y) = \frac{1}{N_o} \left\langle |\hat{\Phi}_{pp}(q_x, q_y)|^2 \right\rangle \tag{6.4}$$

where the plane projected density difference, Φ_{pp}, is defined

$$\Phi_{pp} \equiv \int dz\, \Phi(x, y, z), \tag{6.5}$$

analogous to the discussion in the previous chapter leading to eqn. (5.6).

In fig. (6.8), we show structure factor results circularly averaged for different values of w_{ab} for a constant value of w_2 corresponding to good solvent. Each structure factor is the result of averaging over five equilibrium configurations [1]. The appearance of a peak in the structure factor at a non zero value of q suggests that a new length scale emerges as w_{ab} increases (when the two species become sufficiently immiscible) and becomes more prominent as w_{ab} is increased. This clearly corresponds to structure that develops as micro-phase separation sets in. The value of q associated with the peak in the structure factor thus corresponds to the length scale determined by

[1] We cannot rule out the possibility of very long time scale motions, which could be present when domains begin to form.

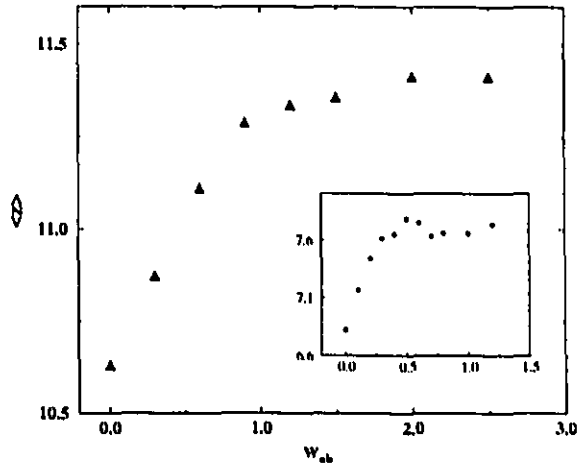

Figure 6.7: Average monomer z value, as a measure of the brush height, plotted as a function of w_{ab} with triangles for $w_2 = 0.5$ and $L = 128$. The dependence of the average z on w_{ab} is qualitatively similar to that of w_{2eff} in fig. (6.6). The same plot is shown with circles for $w_2 = 0.0$, $L = 64$ in the inset.

this local structure. As in the previous chapter, we expect the peak to correspond the average separation between domains. This is indeed likely as the periodic spacing between the microdomains seen in fig. (6.3) is consistent with the peak position of the structure factor observed in fig. (6.8). The average domain spacing is approximately twice the end-to-end distance, projected in the (x, y) plane, of a polymer in a Θ-solvent. As mentioned above, this domain size is consistent with results from previous simulations [9, 43]. Note, moreover, that the peak position stays at $q = 4$ for all higher values of w_{ab}. This implies that, unlike phase separation in a binary alloy, almost no coarsening occurs. In fact, the domains seem to appear at a fixed wavelength, which remains constant regardless of the degree of immiscibility. Similar results were obtained in a previous study [9] where the peak in the structure factor remained constant as one configuration was quenched. Even so, we cannot resolve small changes in the peak position due to the limit of resolution imposed by the finite system size. We remark that structure factors for the total monomer density gave no indication of structure in the total monomer density.

As an indicator for the progress of micro-phase separation, we use the value of the structure factor at the q value corresponding to the local order formed in the

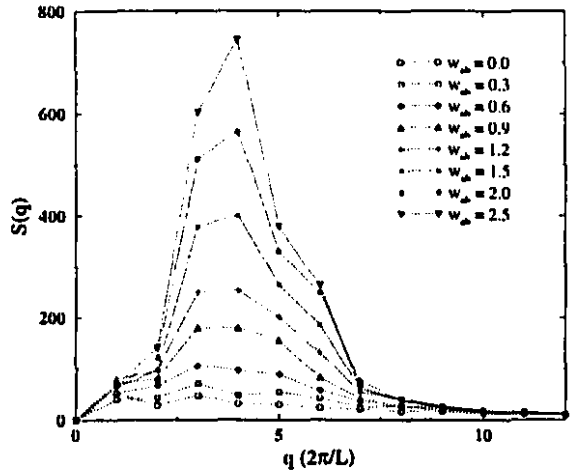

Figure 6.8: Structure factors of the laterally projected monomer density difference, for different values of w_{ab}. The results shown here are circularly averaged. A peak appears in the structure factor at $q = 4$, corresponding to the average domain separation in the micro-phase separated state. The system size $L = 128$ and the grafting density $\sigma = 0.1$. The solvent quality is fixed at $w_2 = 0.5$.

phase separated regime (*i.e.* the peak value of $S(q)$). This is plotted in fig. (6.9) for two cases: a large system with $w_2 = 0.5$, and a smaller system with $w_2 = 0$. For $w_2 = 0.5$, the peak height grows smoothly, suggesting a gradual crossover to micro-phase separated states. For $w_2 = 0$ the crossover is much sharper, even though the system size is smaller. In a previous work [43], the absolute value of the density difference was studied over a wide range of w_{ab} for $N = 20$ and $N = 40$. The authors found no sharpening of the crossover for the case of larger N and thus suggested that there was no true phase transition in the thermodynamic limit. However, they did not vary solvent quality, which, as we have seen, plays an important role. At present, we do not have results necessary for a detailed finite-size scaling analysis of the crossover. Ideally, we would like to study the behaviour of the crossover by systematically increasing the area of the grafting plane, keeping the grafting density, σ, fixed. An example of this is shown in the inset to fig. (6.9). The solvent quality is fixed at $w_2 = 0.5$, and results are shown for two system sizes, $L = 128$ and $L = 64$. When normalized by L^2, there is little system size dependence, giving no evidence for a phase transition. Unfortunately, a proper finite size scaling analysis of the transition would require a prohibitively large computational effort, so we cannot

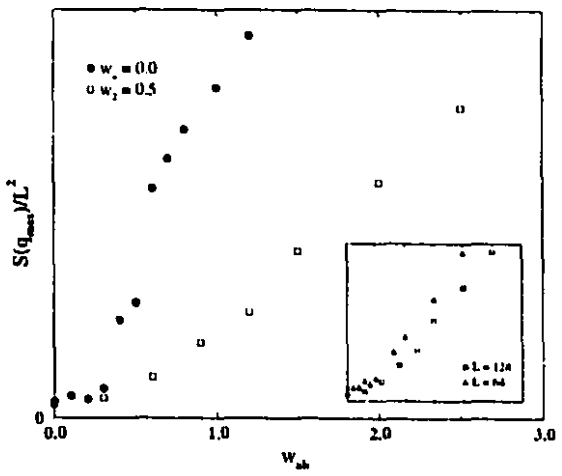

Figure 6.9: The value of $S(q)$ for q corresponding to the order formed in the micro-phase separated state, $S(q_{max})$, as an indicator of micro-phase separation. The filled circles correspond to the case $L = 64$ and $w_2 = 0$. The open squares correspond to the structure factors shown in fig. (6.8). Note that the onset of order is much sharper in the case of $w_2 = 0$. All values of $S(q_{max})$ are normalized by L^2. The inset shows a comparison for two system sizes, $L = 64$ and $L = 128$, for fixed solvent quality $w_2 = 0.5$. Note there is relatively little system size dependence.

properly address the question of the existence of a thermodynamic phase transition at this time. Since the solvent quality affects the crossover, this analysis would be especially interesting in Θ-solvent or marginally poor solvent conditions.

As stated in the Introduction to this chapter, Marko and Witten [51] showed that lateral micro-phase separation under melt conditions occurs when the immiscibility, or w_{ab}, is 2.27 times greater than the bulk phase separation value. Although our simulations were performed for a brush in solvent, a comparison with this prediction is still useful, particularly for the case $w_2 = 0$. A simple mean field calculation [1] shows that bulk phase separation occurs when $w_{ab} = 4h/N^2\sigma$, where h is the height of the brush. From our data, we can estimate h using $h = 2\langle z \rangle$, where $< z >$ is the z value averaged over all monomers. For the case of $w_2 = 0$, fig. (6.9) and fig. (6.7) indicate that micro-phase separation occurs when $w_{ab} \simeq 0.4$ and $< z > \simeq 7.7$, yielding 2.7 for the ratio between micro-phase separation in a Θ-solvent and bulk phase separation. This value is reasonably close to the predicted value for the melt. On the other hand when a good solvent is present such as for $w_2 = 0.5$, fig. (6.9) and fig. (6.7) show that

[1] This can be shown from a simple model, assuming laterally segregated domains and a step function profile.

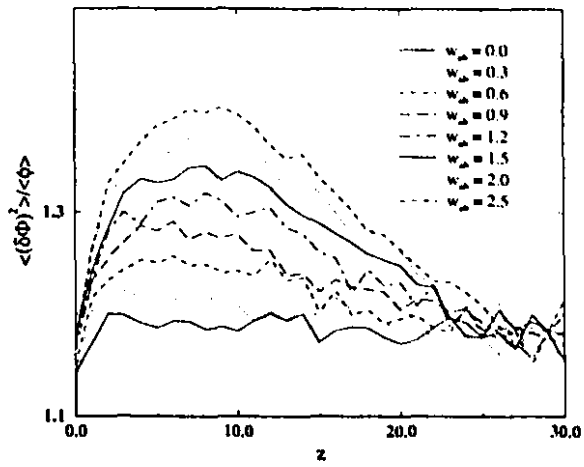

Figure 6.10: Fluctuations of the density difference per monomer, indicating micro-phase separation, shown as a function of z for different values of w_{ab}. Micro-phase separation is strongest where the density profile peaks, and is suppressed at the wall, probably due to grafting. The system size $L = 128$ and the grafting density $\sigma = 0.1$. The solvent quality is fixed at $w_2 = 0.5$.

$w_{ab} \simeq 1.0$ and $< z > \simeq 11.3$ at the instability, giving 4.5 for this ratio. This is further evidence that the nature of the solvent has a marked influence on the occurrence of micro-phase separation.

In fig. (6.10), we show the mean squared density difference fluctuations per monomer as a function of z. Near the grafting plane, the fluctuations in Φ are strongly suppressed due to the fixing of one end of the polymer on that plane. Otherwise, the tendency for micro-phase separation appears proportional to the density. Therefore, micro-phase separation first occurs in the middle of the brush where the density is highest and the brush always remains most strongly separated in this region. This is clear evidence that micro-phase separation does not occur uniformly throughout the brush, and remains nonuniform for all values of w_{ab}. For the melt case, a "composition oscillation" as a function of z was indeed predicted [51], although we see clear qualitative differences. The peak of the density difference profile for the "composition oscillation" was predicted to be very close to the top of the brush in the melt case. We find that, in the presence of solvent, the peak corresponds to the maximum of the total monomer density profile, and decreases monotonically toward the top of the brush.

We next explore micro-phase separation in poor solvent conditions ($w_2 < 0$). As is known from previous work [80, 43, 30, 71, 68], a homogeneous end-grafted polymer brush will undergo a lateral micro-phase separation of monomers from the surrounding solvent at a sufficiently negative value of w_2, resulting in the formation of microdomains of monomer rich regions and monomer poor regions. In the case of an end-grafted binary brush, two types of micro-phase separation are possible: micro-phase separation of monomers from the solvent regardless of type, and binary micro-phase separation due to the immiscibility of the two polymers types. The competition between these two types of micro-phase separation is expected to produce interesting phase behaviour and we have investigated some of the possibilities in a qualitative fashion. In our simulations, both types of micro-phase separation were observed but with very different equilibrium structures depending on the order in which the micro-phase separations were produced.

In fig. (6.11) we show two cases. If the solvent is first made increasingly poor with no immiscibility, micro-phase separation of monomers regardless of type from the solvent is induced. Thus, clusters of solvent separated monomers appear with the expected average cluster spacing, with types A and B mixed evenly inside all clusters. As immiscibility is introduced in this solvent separated state, the types A and B phase separate completely within each cluster. Immiscibility can also be introduced in good solvent, then increased until the two types micro-phase separate at fixed w_2. Now, as the solvent quality is made poor, the monomers indeed separate from the solvent, but in this case, the previously formed binary phase separated domains determine the nature of the clusters formed as monomers phase separate from the solvent. The result is the appearance of larger solvent separated clusters of pure A type or pure B type. Similar structure have been considered in work on grafted AB diblock copolymers, grafted to the surface at the junction of each diblock copolymer [5].

Finally, we can estimate the limits of stability of the laterally homogeneous phase using Green function methods combined with the random phase approximation. As discussed in chapter 3, a mean field phase transition is expected when the lowest eigenvalue of $\mathbf{A}^{-1}$ becomes negative, where $\mathbf{A}$ is the correlation function calculated in the random phase approximation. The details of this calculation for the binary

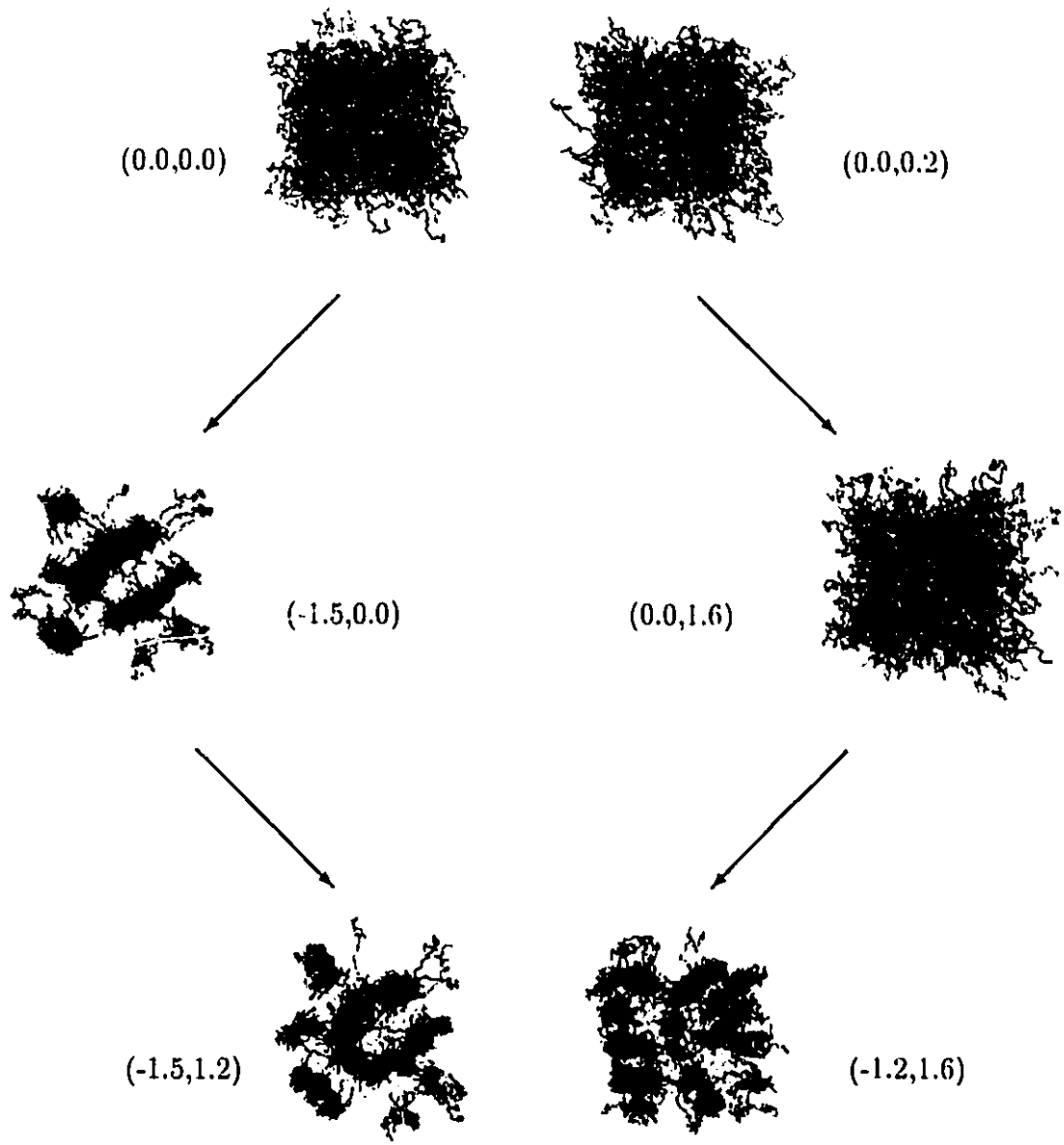

Figure 6.11: Samples of configurations for the binary brush in poor solvent. Two different patterns of annealing are shown. They are, using the notation (w_2, w_{ab}): (sequence left) $(0,0) \rightarrow (-1.5,0) \rightarrow (-1.5,1.2)$, and (sequence right) $(0,0.2) \rightarrow (0,1.6) \rightarrow (-1.2,1.6)$. Intermediate configurations are not shown. The system size $L = 64$, the grafting density $\sigma = 0.1$, and $w_3 = 0.4$ for both sequences.

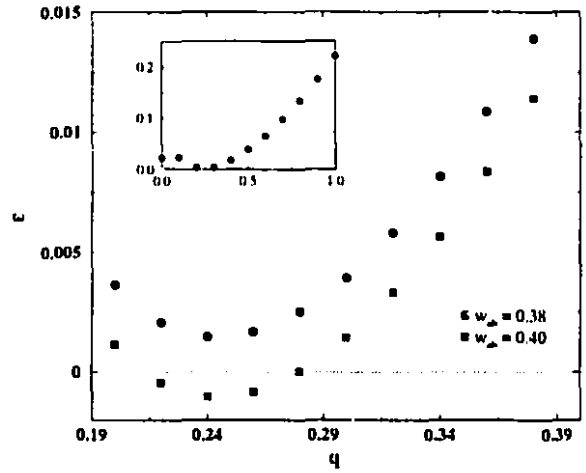

Figure 6.12: Lowest eigenvalue of $\mathbf{A}^{-1}$ shown as a function of q, where q is shown in the same units as fig. (6.8). The inset shows the case for $w_2 = 0.38$ over a larger scale. Note the instability occurs between $w_2 = 0.38$ and $w_2 = 0.40$, since the lowest eigenvalue becomes negative between these values. The value of q at the point where the lowest eigenvalue becomes zero is the wavelength of the instability in the lateral direction.

brush can be found in section A.4, which implements the techniques introduced in section 3.3 and section 3.4. In fig. (6.12), the lowest eigenvalue of $\mathbf{A}^{-1}(z, z'; q)$ is shown as a function of q for a given value of w_2 and w_{ab}. The point (w_2^*, w_{ab}^*) where the lowest eigenvalue becomes negative is the limit of stability of the homogeneous phase; *i.e.*, where binary phase separation occurs. The wave number q^* for the first negative eigenvalue gives the wavelength of the instability in the direction parallel to the grafting plane. From fig. (6.12), the "critical" wave number $q^* = 0.24 \pm 0.02$, and is the same for all (w_2^*, w_{ab}^*) within the precision of our calculations [1]. This value for q^* is consistent with the results of our simulations. From fig. (6.8), we find from simulation that $q^* = 0.22 \pm 0.02$.

The degree of immiscibility, w_{ab}, at the mean field limit of stability was calculated over a range of w_2. The results determine a "phase boundary" in the (w_2, w_{ab}) plane, between homogeneous configurations and laterally micro-phase separated configurations. The results are shown in fig. (6.13). We can compare our simulations with this stability diagram. The simulation results shown in fig. (6.9) were used to characterize configurations for given values of (w_2, w_{ab}) as stable or microphase-separated.

[1] The uncertainty quoted for q^* is from the precision to which we calculate this number.

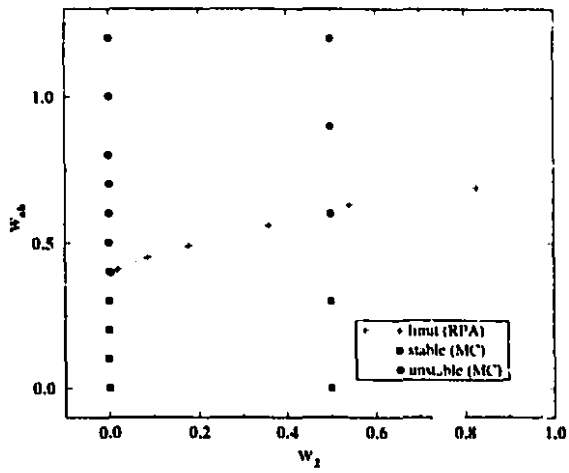

Figure 6.13: Stability diagram, showing the limit of stability of the homogeneous phase, calculated in the random phase approximation. The plus (+) signs are the limits of stability, and therefore demarcate the phase boundary. The line is a guide to the eye only. Based on the results shown in fig. (6.9), the configurations from the previous Monte Carlo simulations are tentatively identified as stable (squares) and unstable, or phase separated (circles).

The crossover point on fig. (6.9) was tentatively identified, and the results shown as points on fig. (6.13). As can be seen, the Monte Carlo results are consistent with the stability limit calculated with the random phase approximation. These results are still preliminary, but the agreement is encouraging.

7

CONCLUSION

Using a Monte Carlo technique based on an Edwards Hamiltonian, we have convincingly demonstrated laterally inhomogeneous micro-phase separation in grafted polymer layers in poor solvent conditions. This was marked by the emergence of a peak in the structure factor at a wave number corresponding to the average distance between micro-domains, which is approximately twice the end vector distance of the random walk parallel to the grafting plane. Furthermore, the peak position was found to be approximately independent of the interaction parameters w_2 and w_3 over a wide range, consistent with previous theoretical considerations [80, 71]. Our estimate of the onset of the lateral density instability from the behaviour of the structure factor agreed with a prediction using the random phase approximation.

We have also observed micro-phase separation in a binary brush due to immiscibility interactions under various solvent conditions. We found that the brush response to increasing immiscibility proceeds in two stages: an overall expansion stage, and a micro-phase separation stage. In the expansion stage where the immiscibility coefficient w_{ab} is relatively small, the brush relaxes by expanding in a laterally uniform fashion away from the grafting plane. The role of w_{ab} is largely to "renormalize" the excluded volume parameter w_2, and polymers of different type mix very well laterally. The total density profile in the direction perpendicular to the grafting plane (the z-direction) is the same as that of a homogeneous polymer brush if the "renormalized" w_2-parameter is used. At larger values of w_{ab}, it is energetically more advantageous for the two polymer species to undergo micro-phase separation, and clear micro-phase separation in the lateral direction was indeed observed. This separation is strongly affected by the solvent quality: good solvent conditions delay the onset of separation, and the crossover is sharper in poorer solvent conditions. We also found

clear evidence of z dependence in the micro-phase separation, in that the demixing of the two types of monomers is non-uniform along the z direction. We have also investigated, in a qualitative manner, the phase behaviour of the binary brush in poor solvent conditions. We found different conformations depending on the detailed path for micro-phase separation. In particular, pure domains of the two different polymer types or mixed domains were observed depending on whether w_2 or w_{ab} was changed first. Finally, using a self consistent field analysis, we constructed a "phase-diagram" showing the limits of stability of the homogeneous phase. This was consistent with the results of our simulations.

These studies convincingly demonstrate the effectiveness of the algorithm developed in this thesis, far surpassing other simulation techniques currently being applied to the polymer brush. This opens up many interesting possibilities for future research. In the binary brush study, we assumed that the solvent interaction for both types was identical. In general, this is certainly not the case, and differential interactions could be easily studied with the above method. Besides questions of phase separation, there are important effects that could be studied that would involve only minor modification to the algorithms presented in this thesis. For example, the assumption of a plane grafting surface could be relaxed and the case of more realistic curvature could be studied, for which there are analytical results in the literature [6]. The stabilizing forces between realistic colloidal particles could then be determined through simulation [20]. Another interesting possibility is to use this Monte Carlo technique self consistently to determine the properties of ionomeric colloids [62, 63], which exhibit many interesting phenomena and have important applications, such as colloid control in aqueous environments (waste-water treatment, oil recovery, *etc.*) [64].

Indeed, there are many outstanding questions on the equilibrium properties of polymer brushes to be addressed. The ideas and techniques introduced or reviewed in this thesis should be central to developing a deeper understanding of these important systems.

APPENDICES

A.1 Langevin functional derivatives

In this appendix, the various terms of $\partial H/\partial x_\beta^k$ are derived for the Langevin equation eqn. (3.31).

A.1.1 Gaussian chain functional derivative

Recall that

$$H_G = \frac{3}{2b^2}\int dn \left(\frac{\partial \mathbf{R}(n)}{\partial n}\right)^2. \tag{A.1}$$

We want the functional derivative $\delta H_G/\delta \mathbf{R}(n')$,

$$\begin{aligned}
\frac{\delta H_G}{\delta \mathbf{R}(n')} &= \frac{\delta}{\delta \mathbf{R}(n')}\left[\frac{3}{2b^2}\int dn \left(\frac{\partial \mathbf{R}(n)}{\partial n}\right)^2\right] \\
&= \frac{3}{2b^2}\int dn\, 2\left(\frac{\partial \mathbf{R}}{\partial n}\right)\frac{\delta}{\delta \mathbf{R}(n')}\frac{\partial \mathbf{R}}{\partial n} \\
&= \frac{3}{b^2}\int dn \frac{\partial \mathbf{R}}{\partial n}\frac{\partial}{\partial n}\frac{\delta \mathbf{R}(n)}{\delta \mathbf{R}(n')} \\
&= \frac{3}{b^2}\int dn \frac{\partial \mathbf{R}}{\partial n}\frac{\partial}{\partial n}\delta(n-n') \\
&= -\frac{3}{b^2}\int dn \frac{\partial^2 \mathbf{R}(n)}{\partial n^2}\delta(n-n') \\
&= -\frac{3}{b^2}\frac{\partial^2 \mathbf{R}(n')}{\partial n'^2},
\end{aligned}$$

using an integration by parts. Thus,

$$\frac{\delta H_G}{\delta \mathbf{R}(n')} = -\frac{3}{b^2}\nabla_n^2 \mathbf{R}(n'). \tag{A.2}$$

A.1.2 The discrete Gaussian derivative

Recall the discrete form for H_G.

$$H_G = \frac{3}{2b^2}\sum_{j=2}^{N}\left((\mathbf{R}_j - \mathbf{R}_{j-1})^2\right)$$

$$= \frac{3}{2b^2}\sum_{j=2}^{N}\left(x_\alpha^j x_\alpha^j - 2x_\alpha^j x_\alpha^{j-1} + x_\alpha^{j-1}x_\alpha^{j-1}\right),$$

where x_α^j is the αth component of the jth monomers. There is an implicit sum over repeated component indices, whereas the sum over monomers is explicit.

We want the partial derivative of H_G with respect to x_β^k,

$$\frac{\delta H_G}{\delta x_\beta^k} = \frac{3}{2b^2}\sum_{j=2}^{N}\frac{\partial}{\partial x_\beta^k}\left(x_\alpha^j x_\alpha^j - 2x_\alpha^j x_\alpha^{j-1} + x_\alpha^{j-1}x_\alpha^{j-1}\right).$$

We need to calculate,

$$\frac{\partial}{\partial x_\beta^k}\left(x_\alpha^j x_\alpha^j\right) = 2x_\alpha^j\frac{\partial x_\alpha^j}{\partial x_\beta^k}$$

$$= 2x_\alpha^j\delta_{j,k}\delta_{\alpha,\beta}$$

$$= 2x_\beta^j\delta_{j,k}$$

and

$$\frac{\partial}{\partial x_\beta^k}\left(-2x_\alpha^j x_\alpha^{j-1}\right) = -2\left(x_\alpha^j\frac{\partial x_\alpha^{j-1}}{\partial x_\beta^k} + x_\alpha^{j-1}\frac{\partial x_\alpha^j}{\partial x_\beta^k}\right)$$

$$= -2\left(x_\alpha^j\delta_{\alpha,\beta}\delta_{j-1,k} + x_\alpha^{j-1}\delta_{\alpha,\beta}\delta j,k\right)$$

$$= -2\left(x_\beta^j\delta_{j-1,k} + x_\beta^{j-1}\delta j,k\right)$$

and finally

$$\frac{\partial}{\partial x_\beta^k}\left(x_\alpha^{j-1}x_\alpha^{j-1}\right) = 2x_\alpha^j\frac{\partial x_\alpha^{j-1}}{\partial x_\beta^k}$$

$$= 2x_\beta^{j-1}\delta_{j-1,k}.$$

Therefore,

$$\frac{\delta H_G}{\delta x_\beta^k} = \frac{3}{b^2}\sum_{j=2}^{N}\left(x_\beta^j\delta_{j,k} - x_\beta^j\delta_{j-1,k} - x_\beta^{j-1}\delta_{j,k} + x_\beta^{j-1}\delta_{j-1,k}\right) \qquad (A.3)$$

Since k can take any value integral between 1 and N,

$$-\frac{\delta H_G}{\delta x_\beta^k}\left(\frac{b^2}{3}\right) = \begin{cases} x_\beta^{k+1} - 2x_\beta^k + x_\beta^{k-1}, & k \neq 0, N \\ x_\beta^1 - x_\beta^0, & k = 0 \\ x_\beta^{N-1} - x_\beta^N, & k = N \end{cases} \tag{A.4}$$

Not surprisingly, this result is identical to what would be obtained from a **finite difference** approximation to the continuous result, eqn. (A.2), being careful to account for the chain ends.

A.1.3 The discrete interaction derivative

Recall from the Edwards Monte Carlo discussion, that the interaction Hamiltonian H_I can be written, for discrete monomers and a Gaussian approximation to the delta function,

$$H_I = \frac{w_2}{2}\left(\frac{3}{4\pi\sigma^2}\right)^{\frac{3}{2}} \sum_{m,n} \exp\left(-\frac{3}{4\sigma^2}\left(\mathbf{R}_n - \mathbf{R}_m\right)^2\right). \tag{A.5}$$

We want to calculate the partial derivative $\partial H_I/\partial x_\beta^k$. Proceeding as in last section,

$$\frac{\partial H_I}{\partial x_\beta^k} = -\frac{3}{4\sigma^2}\frac{w_2}{2}\left(\frac{3}{4\pi\sigma^2}\right)^{\frac{3}{2}} \sum_{n,m} \exp\left(-\frac{3}{4\sigma^2}\left(\mathbf{R}_n - \mathbf{R}_m\right)^2\right) \frac{\partial}{\partial x_\beta^k}\left(\mathbf{R}_n - \mathbf{R}_m\right)^2.$$

Again, implicitly summing over repeated component indices,

$$\begin{aligned} \frac{\partial}{\partial x_\beta^k}\left(\mathbf{R}_n - \mathbf{R}_m\right)^2 &= \frac{\partial}{\partial x_\beta^k}\left(x_\alpha^n x_\alpha^n - 2x_\alpha^n x_\alpha^m + x_\alpha^m x_\alpha^m\right) \\ &= 2\left(x_\alpha^n \frac{\partial x_\alpha^n}{\partial x_\beta^k} - x_\alpha^n \frac{\partial x_\alpha^m}{\partial x_\beta^k} - x_\alpha^m \frac{\partial x_\alpha^n}{\partial x_\beta^k} + x_\alpha^m \frac{\partial x_\alpha^m}{\partial x_\beta^k}\right) \\ &= 2\left(x_\beta^n \delta_{n,k} - x_\beta^n \delta_{m,k} - x_\beta^m \delta_{n,k} + x_\beta^m \delta_{m,k}\right) \end{aligned}$$

Therefore,

$$\frac{\partial H_I}{\partial x_\beta^k} = -\frac{3w_2}{4\sigma^2}\left(\frac{3}{4\pi\sigma^2}\right)^{\frac{3}{2}} \sum_{n,m} e\left(\mathbf{R}_n, \mathbf{R}_m\right)\left(x_\beta^n \delta_{n,k} - x_\beta^n \delta_{m,k} - x_\beta^m \delta_{n,k} + x_\beta^m \delta_{m,k}\right) \tag{A.6}$$

where

$$e\left(\mathbf{R}_n, \mathbf{R}_m\right) = \exp\left(-\frac{3}{4\sigma^2}\left(\mathbf{R}_n - \mathbf{R}_m\right)^2\right). \tag{A.7}$$

Noting that $e(\mathbf{R}_n, \mathbf{R}_m) = e(\mathbf{R}_n, \mathbf{R}_n)$,

$$\sum_{n,m} e(\mathbf{R}_n, \mathbf{R}_m) \left(x_\beta^n \delta_{n,k} - x_\beta^n \delta_{m,k} - x_\beta^m \delta_{n,k} + x_\beta^m \delta_{m,k} \right)$$

$$= 2 \left(\sum_m e(\mathbf{R}_k, \mathbf{R}_m) x_\beta^k - \sum_m e(\mathbf{R}_k, \mathbf{R}_m) x_\beta^m \right).$$

Finally,

$$\frac{\partial H_I}{\partial x_\beta^k} = -\frac{3w_2}{2\sigma^2} \left(\frac{3}{4\pi\sigma^2} \right)^{\frac{3}{2}} \sum_m \left(x_\beta^k - x_\beta^m \right) \exp\left(-\frac{3}{4\sigma^2} (\mathbf{R}_n - \mathbf{R}_m)^2 \right) \qquad (A.8)$$

A.2 Mean field brush solution

The self consistent mean field solution was discussed in a general way in section 3.3. In this appendix, the particulars of determining the Green function for polymers grafted to an impenetrable interface will be discussed. For explicitness, the polymers are considered to be grafted to a plane at $z = 0$, and to be excluded from the half space $z < 0$. [1] This method has been used widely and with much success. For some selected examples, see references [78, 58]

Recall from section 3.3.2 that the Green function obeys [2]

$$\left(\partial_n - \frac{b^2}{6} \partial_{\mathbf{r}}^2 + V(z) \right) G(\mathbf{r}, \mathbf{r}'; n) = \delta(\mathbf{r} - \mathbf{r}') \delta(n). \qquad (A.9)$$

where $G(\mathbf{r}, \mathbf{r}'; 0) = 0$ for $n < 0$. In the following, $b^2 = 3$, as is customary in the rest of the thesis. It can be shown [80] that G is separable,

$$G(\mathbf{r}, \mathbf{r}'; n) = G_o(\mathbf{x}, \mathbf{x}'; n) F(z, z'; n), \qquad (A.10)$$

where $\mathbf{x} = (x, y)$. In consequence [80],

$$\left(\partial_n - \frac{1}{2} \partial_{\mathbf{x}}^2 \right) G_o(\mathbf{x}, \mathbf{x}'; n) = \delta(\mathbf{x} - \mathbf{x}') \delta(n)$$

$$\left(\partial_n - \frac{1}{2} \partial_z^2 + V(z) \right) F(z, z'; n) = \delta(z - z') \delta(n), \qquad (A.11)$$

[1] As in section 3.4, this section follows reference [80]. I have also benefitted greatly from notes provided by C. Yeung and A. Balazs.

[2] In this appendix, we will use the notation

$$\partial_x = \frac{\partial}{\partial x}$$

$$\partial_x^2 = \frac{\partial^2}{\partial x^2}, \text{ etc.}$$

where $\partial_{\mathbf{x}}^2 = \partial_x^2 + \partial_y^2$. We recognize $G_o(\mathbf{x}, \mathbf{x}'; n)$ as the propagator for free diffusion [1],

$$G_o(\mathbf{x}, \mathbf{x}'; n) = \frac{1}{2\pi N} \exp\left(-\frac{|\mathbf{x} - \mathbf{x}'|^2}{2N}\right). \tag{A.12}$$

The one dimensional Green function $F(z, z'; n)$ can be solved for numerically as discussed in section 3.3.2, using the adsorbing boundary condition $F(z, z'; n) = 0$ for $z, z' = 0$ [21].

As in section 3.3.2, a self consistent solution is obtained by setting $V(z) = w_2\langle\phi(z)\rangle_o$ using the resulting Green function to solve for $\langle\phi(z)\rangle_o$, then iterating until convergence is attained. Note, however, that eqn. (A.11) yields the Green function for one polymer in a self consistent field. The brush concentration is obtained simply by multiplying the one polymer density by the grafting density σ,

$$\phi(z) = \frac{\sigma \int dz' \int_0^N dn\, F(z, 0; n)\, F(z', z; N - n)}{\int dz'\, F(z', 0; N)}. \tag{A.13}$$

Thus, one determines the Green function for one polymer in a self consistently determined field of all polymers in the brush.

A.3 Mean field brush correlation function

A general calculation of the correlation function in the mean field approximation was presented in section 3.4.1. In this appendix, the details of this calculation for the polymer brush is discussed. As in the previous section, much of this section's discussion deals with treating the $\mathbf{x}$ direction analytically and separately from the z direction.

As in section 3.4.1, we need to calculate the mean field correlation function $\mathbf{A}_o$

$$\mathbf{A}_o(\mathbf{r}, \mathbf{r}') \equiv \langle\phi(\mathbf{r})\,\phi(\mathbf{r}')\rangle_o - \langle\phi(\mathbf{r})\rangle_o\langle\phi(\mathbf{r}')\rangle_o, \tag{A.14}$$

where $\langle\rangle_o$ is the mean field average, calculated with the mean field Green function. Note that the concentration can be written

$$\phi(\mathbf{r}) = \sum_i \phi_i(\mathbf{r}), \tag{A.15}$$

[1] See, for example, reference [11], section 7.7.

where ϕ_i is the concentration due to the ith chain at $\mathbf{r}$. Thus,

$$\mathbf{A}_o(\mathbf{r},\mathbf{r}') = \sum_{i,j}\left\{ \langle\phi_i(\mathbf{r})\,\phi_j(\mathbf{r}')\rangle_o - \langle\phi_i(\mathbf{r})\rangle_o\langle\phi_j(\mathbf{r}')\rangle_o \right\} \tag{A.16}$$

In the mean field approximation, the chains are independent. Therefore, for $i \neq j$,

$$\langle\phi_i(\mathbf{r})\,\phi_j(\mathbf{r}')\rangle_o = \langle\phi_i(\mathbf{r})\rangle_o\langle\phi_j(\mathbf{r}')\rangle_o, \tag{A.17}$$

and eqn. (A.16) becomes

$$\begin{aligned}\mathbf{A}_o(\mathbf{r},\mathbf{r}') &= \sum_i\left\{ \langle\phi_i(\mathbf{r})\,\phi_i(\mathbf{r}')\rangle_o - \langle\phi_i(\mathbf{r})\rangle_o\langle\phi_i(\mathbf{r}')\rangle_o \right\} \\ &= A_I - A_{II}.\end{aligned}$$

Similar to eqn. (3.78) for the average in terms of the Green function, the first term on the right hand side becomes

$$\begin{aligned}A_I = \sum_i \frac{1}{\mathcal{Z}}\int d\mathbf{r}_N \int_0^N dn \int_0^n dn' \\ \left\{ G(\mathbf{r}_N,\mathbf{r};N-n)\,G(\mathbf{r},\mathbf{r}';n-n')\,G\left(\mathbf{r}',\mathbf{x}_o^i;n'\right) + \right. \\ \left. G(\mathbf{r}_N,\mathbf{r}';N-n)\,G(\mathbf{r}',\mathbf{r};n-n')\,G\left(\mathbf{r},\mathbf{x}_o^i;n'\right) \right\},\end{aligned}$$

where

$$\mathcal{Z} = \int d\mathbf{r}_N\, G(\mathbf{r}_N,\mathbf{r}_0;N) \tag{A.18}$$

and $\mathbf{x}_o^i = (x_i, y_i, 0)$, the grafting point of the ith chain. Replacing the sum by an integral over the grafting surface,

$$\sum_i = \sigma\int d\mathbf{x}_o\,, \tag{A.19}$$

we find

$$\begin{aligned}A_I = \frac{\sigma}{\mathcal{Z}}\int \mathbf{x}_o \int d\mathbf{r}_N \int_0^N dn \int_0^n dn' \\ \left\{ G(\mathbf{r}_N,\mathbf{r};N-n)\,G(\mathbf{r},\mathbf{r}';n-n')\,G(\mathbf{r}',\mathbf{x}_o;n') + \right. \\ \left. G(\mathbf{r}_N,\mathbf{r}';N-n)\,G(\mathbf{r}',\mathbf{r};n-n')\,G(\mathbf{r},\mathbf{x}_o;n') \right\}.\end{aligned}$$

The Green function is separated as in the previous section;

$$A_I = \frac{\sigma}{\mathcal{Z}} \int \mathbf{x}_o \int d\mathbf{x}_N \, dz_N \int_0^N dn \int_0^n dn' \Big\{ G_o(\mathbf{x}_N, \mathbf{x}; N-n) \, F(z_N, z; N-n) \times$$
$$G_o(\mathbf{x}, \mathbf{x}'; n-n') \, F(z, z'; n-n') \, G_o(\mathbf{x}', \mathbf{x}_o; n') \, F(z', 0; n') +$$
$$G_o(\mathbf{x}_N, \mathbf{x}'; N-n) \, F(z_N, z'; N-n) \, G_o(\mathbf{x}', \mathbf{x}; n-n') \, F(z', z; n-n') \times$$
$$G_o(\mathbf{x}, \mathbf{x}_o; n') \, F(z, 0; n') \Big\}.$$

From eqn. (A.12), we see that $G_o(\mathbf{x}, \mathbf{x}'; N)$ is normalized. Performing the integrals over $\mathbf{x}_N$ and $\mathbf{x}_o$ therefore gives

$$A_I = \frac{\sigma}{\mathcal{Z}} \int dz_N \int_0^N dn \int^n dn' \, G_o(\mathbf{x}, \mathbf{x}'; n-n') \times$$
$$\Big\{ F(z_N, z; N-n) \, F(z, z'; n-n') \, F(z', 0; n') +$$
$$F(z_N, z'; N-n) \, F(z', z; n-n') \, F(z, 0; n') \Big\}, \qquad \text{(A.20)}$$

using the fact that $G_o(\mathbf{x}', \mathbf{x}; n-n') = G_o(\mathbf{x}, \mathbf{x}'; n-n')$. Similar considerations show that

$$A_{II} = \frac{\sigma}{\mathcal{Z}^2} \int_0^N dn \, dn' \int dz_N \, dz'_N \Big\{ G_o(\mathbf{x}, \mathbf{x}'; n+n') \times$$
$$F(z_N, z; N-n) \, F(z, 0; n) \, F(z'_N, z'; N-n') \, F(z', 0; n') \Big\}. \qquad \text{(A.21)}$$

These equations, eqn. (A.20) and eqn. (A.21), give the mean field correlation function for a polymer brush, in terms of the one dimensional Green function $F(z, z'; N)$, whose determination was discussed in the previous appendix. Diagonalization of the correlation function is also simpler in this form; the correlation $\mathbf{A}_o$ is seen to be a function $\mathbf{A}_o(\mathbf{x} - \mathbf{x}', z, z')$. Translational invariance in the x direction means that the eigenmodes are the Fourier modes in this direction. $\mathbf{A}_o$ can be easily Fourier transformed analytically, so for every q of interest, only the matrix $(\mathbf{A}_o)_q(z, z')$ needs be diagonalized numerically.

A.4 Mean field stability of binary brush

The interaction Hamiltonian for the binary brush in good solvent is given by eqn. (6.2) with w_3 set to zero,

$$H_I = \int dr \left(\frac{w_2}{2} \phi^2 (\mathrm{r}) + \frac{w_{ab}}{2} \phi_a (\mathrm{r}) \phi_b (\mathrm{r}) \right), \tag{A.22}$$

where $\phi = \phi_a + \phi_b$. The mean field approximation to eqn. (A.22) can be derived with the definitions

$$\phi (\mathrm{r}) = \langle \phi (\mathrm{r}) \rangle + \delta \phi (\mathrm{r})$$

$$\phi_a (\mathrm{r}) = \langle \phi_a (\mathrm{r}) \rangle + \delta \phi_a (\mathrm{r})$$

$$\phi_b (\mathrm{r}) = \langle \phi_b (\mathrm{r}) \rangle + \delta \phi_b (\mathrm{r})$$

where the average $\langle\rangle$ denotes the equilibrium average. Substituting these expressions into eqn. (A.22) and ignoring terms of second order in the concentration fluctuations gives

$$\frac{w_2}{2} \int dr \phi^2 (\mathrm{r}) \approx \frac{w_2}{2} \int dr \left(\langle \phi (\mathrm{r}) \rangle^2 + 2 \langle \phi (\mathrm{r}) \rangle \delta \phi (\mathrm{r}) \right)$$

$$\frac{w_{ab}}{2} \int dr \phi_a (\mathrm{r}) \phi_b (\mathrm{r}) \approx \frac{w_{ab}}{2} \int dr \left(\langle \phi_a (\mathrm{r}) \rangle \langle \phi_b (\mathrm{r}) \rangle + \langle \phi_a (\mathrm{r}) \rangle \delta \phi_b (\mathrm{r}) + \langle \phi_b (\mathrm{r}) \rangle \delta \phi_a (\mathrm{r}) \right).$$

Since the average concentration $\langle \phi_x \rangle$ is a constant with respect to functional integration, the terms involving only averages can be set to zero without loss of generality. The concentrations can be defined microscopically;

$$\phi_x = \sum_{i \in X} \int dn \delta (\mathrm{r} - \mathbf{R}_x (n)),$$

where the sum $\sum_{i \in X}$ is a sum over all polymers of type X. Consequently,

$$\frac{w_2}{2} \int dr \phi^2 (\mathrm{r}) \approx \sum_i \int dr w_2 \langle \phi (\mathbf{R}_i (n)) \rangle$$

$$\frac{w_{ab}}{2} \int dr \phi_a (\mathrm{r}) \phi_b (\mathrm{r}) \approx \frac{w_{ab}}{2} \int dr \left(\sum_{i \in B} \langle \phi_a (\mathbf{R}_i (n)) \rangle + \sum_{i \in A} \langle \phi_b (\mathbf{R}_i (n)) \rangle \right),$$

where $\sum_i = \sum_{i \in A} + \sum_{i \in B}$. Using the Gaussian chain energy contribution

$$H_G = \frac{3}{2b^2} \sum_i \int dn \left(\frac{\partial \mathbf{R}_i (n)}{\partial n} \right)^2,$$

the Edwards Hamiltonian in the mean field approximation becomes

$$H_o = \sum_{i\in A}\int dn\left(\frac{3}{2b^2}\left(\frac{\partial \mathbf{R}_i(n)}{\partial n}\right)^2 + w_2\langle\phi(\mathbf{R}_i(n))\rangle + \frac{w_{ab}}{2}\langle\phi_b(\mathbf{R}_i(n))\rangle\right) + \sum_{i\in B}\int dn\left(\frac{3}{2b^2}\left(\frac{\partial \mathbf{R}_i(n)}{\partial n}\right)^2 + w_2\langle\phi(\mathbf{R}_i(n))\rangle + \frac{w_{ab}}{2}\langle\phi_a(\mathbf{R}_i(n))\rangle\right) \quad \text{(A.23)}$$

Thus, in the mean field approximation, all chains are independent, only interacting through the self consistently determined mean fields $\langle\phi\rangle$, $\langle\phi_a\rangle$ and $\langle\phi_b\rangle$. In the fully symmetric case, where the number of A type polymer equals the number of B type polymers, $\langle\phi_a\rangle = \langle\phi_b\rangle = \langle\phi\rangle/2$, and the mean field Hamiltonian becomes

$$H_o = \sum_i \int dn\left(\frac{3}{2b^2}\left(\frac{\partial \mathbf{R}_i(n)}{\partial n}\right)^2 + \left(w_2 + \frac{w_{ab}}{4}\right)\langle\phi(\mathbf{R}_i(n))\rangle\right). \quad \text{(A.24)}$$

Equilibrium averages for this system can be calculated using Green function methods, as discussed in section 3.3.2 and section A.2.

If the concentration fluctuations are retained to all orders, then the full Hamiltonian is written

$$H = H_o + H_\delta, \quad \text{(A.25)}$$

where H_o is given by eqn. (A.24), and

$$H_\delta = \int d\mathbf{r}\left[\frac{w_2}{2}(\delta\phi(\mathbf{r}))^2 + \frac{w_{ab}}{2}\delta\phi_a(\mathbf{r})\,\delta\phi_b(\mathbf{r})\right]. \quad \text{(A.26)}$$

In order to be sensitive to binary phase separation, it behooves us to rewrite eqn. (A.26) in terms of the total density and the density difference

$$\phi(\mathbf{r}) = \phi_a(\mathbf{r}) + \phi_b(\mathbf{r})$$

$$\Phi(\mathbf{r}) = \phi_a(\mathbf{r}) - \phi_b(\mathbf{r}).$$

In terms of these new variables, eqn. (A.26) becomes

$$H_\delta = \int d\mathbf{r}\left[\left(\frac{w_2}{2} + \frac{w_{ab}}{8}\right)(\delta\phi(\mathbf{r}))^2 - \frac{w_{ab}}{8}(\delta\Phi(\mathbf{r}))^2\right]. \quad \text{(A.27)}$$

As an approximation, assume that there are no fluctuations in the total density; *i.e.*, $\delta\phi = 0$. Therefore, fluctuations are assumed to be purely *compositional*. In this case, the fluctuation Hamiltonian is

$$H_\delta = -\int d\mathbf{r} \frac{w_{ab}}{8} \left(\delta\Phi\left(\mathbf{r}\right)\right)^2 . \tag{A.28}$$

Following section 3.3.2, the correlation function in the random phase approximation is written

$$\mathbf{A}\left(\mathbf{r},\mathbf{r}'\right)^{-1} = \mathbf{A}_o\left(\mathbf{r},\mathbf{r}'\right)^{-1} - \frac{w_{ab}}{4}\delta\left(\mathbf{r}-\mathbf{r}'\right), \tag{A.29}$$

where the correlation function is the correlation of fluctuations in the density difference

$$\mathbf{A}\left(\mathbf{r},\mathbf{r}'\right) = \left\langle \delta\Phi\left(\mathbf{r}\right)\delta\Phi\left(\mathbf{r}'\right)\right\rangle . \tag{A.30}$$

The mean field correlation $\mathbf{A}_o$ is calculated with respect to the mean field Hamiltonian H_o, eqn. (A.24). The details of this calculation are discussed in section A.3. The mean field solution is unstable when the lowest eigenvector of $\mathbf{A}$ becomes negative. Due to translation invariance in the plane parallel to the grafting plane, the eigenvectors are the Fourier modes; thus,

$$\int dz' \int d\mathbf{x}' \mathbf{A}_o\left(\mathbf{r},\mathbf{r}'\right) \exp\left(i\left(\mathbf{q}\cdot\mathbf{x}'\right)\right) = \delta\left(\mathbf{q}+\mathbf{q}'\right)\mathbf{A}_o\left(z,z';\mathbf{q}\right) \tag{A.31}$$

Here, $\mathbf{r} = (\mathbf{x}, z)$ and $\mathbf{q}$ is a vector in the (x, y) plane. The Fourier transform can be performed analytically with respect to $\mathbf{x}$. Then, for each value of $\mathbf{q}$, one can numerically diagonalize $\mathbf{A}_o\left(z,z';\mathbf{q}\right)$ to obtain the eigenvalues. Eqn. (A.29) can then be used to determine the eigenvalues of $\mathbf{A}$.

BIBLIOGRAPHY

[1] S. Alexander. Adsorption of chain molecules with a polar head a scaling description. *J. Physique*, 38:983, 1977.

[2] S. Alexander. Polymer adsorption on small spheres. a scaling approach. *J. Physique*, 38:977, 1977.

[3] R. E. Allan, editor. *Oxford Dictionary of Current English.* Oxford University Press, New York, 7 edition, 1984.

[4] P. Auroy, L. Auvray, and L. Léger. Characterization of the brush regime for grafted polymer layers at the solid-liquid interface. *Phys. Rev. Lett.*, 66:719, 1991.

[5] Anna Balazs and Ekaterina Zhulina. private communication. manuscript in preparation, 1996.

[6] R. C. Ball, J. F. Marko, S. T. Milner, and T. A. Witten. Polymers grafted to a convex surface. *Macromolecules*, 24:693, 1991.

[7] R. Baranowski and M. D. Whitmore. Theory of the structure of adsorbed block copolymers: Detailed comparison with experiment. *J. Chem. Phys.*, 103:2343, 1995.

[8] K. Binder. *Monte Carlo Methods in Statistical Physics.* Springer-Verlag, Berlin, 1979.

[9] G. Brown, A. Chakrabarti, and J. F. Marko. Microphase separation of a dense two-component grafted-polymer layer. *Europhys. Lett.*, 25:239, 1994.

[10] Gregory Brown. *Surface directed phase separation in polymer brushes.* PhD thesis, Kansas State University, 1995.

[11] Frederick W. Byron and Robert W. Fuller. *Mathematics of classical and quantum physics.* Dover, New York, 1970.

[12] Amitabha Chakrabarti and Raul Toral. Density profile of terminally anchored polymer chains: A monte carlo study. *Macromolecules*, 23:2016, 1990.

[13] Amitabha Chakrabarti and Raul Toral. Static and dynamic properties of two-dimensional polymer melts. *J. Phys. France*, 51:915, 1990.

[14] Hue Sun Chan and Ken A. Dill. Intrachain loops in polymers: Effects of excluded volume. *J. Chem. Phys.*, 90:492, 1989.

[15] Hue Sun Chan and Ken A. Dill. Polymer principles in protein structure and stability. *Ann. Rev. Biophys. Biophys. Chem.*, 20:447, 1991.

[16] J. P. Cotton. Polymer excluded volume exponent ν: An experimental verification of the n vector model for $n = 0$. *J. Physique Lett.*, 41:L-231, 1980.

[17] P. G. de Gennes. *Scaling Concepts in Polymer Physics.* Cornell University Press, Ithaca, 1979.

[18] P. G. de Gennes. Conformations of polymers attached to an interface. *Macromolecules*, 13:1069, 1980.

[19] P. G. de Gennes. Polymers at an interface; a simplified view. *Adv. Colloid Interace Sci.*, 27:189, 1987.

[20] Ronald Dickman and Daniel C. Hong. New simulation method for grafted polymeric brushes. *J. Chem. Phys.*, 95:4650, 1991.

[21] Edmund A. DiMarzio. Proper accounting of conformations of a polymer near a surface. *J. Chem. Phys.*, 42:2101, 1965.

[22] M. Doi and S. F. Edwards. *The Theory of Polymer Dynamics.* Oxford University Press, New York, 1986.

[23] A. K. Dolan and S. F. Edwards. Theory of the stabilization of colloids by adsorbed polymer. *Proc. R. Soc. Lond. A*, 337:509, 1974.

[24] A. K. Dolan and S. F. Edwards. The effect of excluded volume on polymer dispersant action. *Proc. R. Soc. Lond. A*, 343:427, 1975.

[25] Hui Dong. Phase separation of grafted polymers under strong demixing interaction. *J. Phys. II France*, 3:999, 1993.

[26] S. F. Edwards. The statistical mechanics of polymers with excluded volume. *Proc. Phys. Soc.*, 85:613, 1965.

[27] Hans Frauenfelder, Stephen G. Sligar, and Peter G. Wolynes. The energy landscapes and motions of proteins. *Science*, 254:1598, 1991.

[28] Karl F. Freed. *Renormalization group theory of macromolecules.* John Wiley and Sons, New York, 1987.

[29] Nigel Goldenfeld. *Lecture on phase transitions and the renormalization group*, volume 85 of *Frontiers in Physics.* Addison-Wesley, Don Mills, 1992.

[30] Gary S. Grest and Michael Murat. Structure of grafted polymeric brushes in solvents of varying quality: A molecular dynamics study. *Macromolecules*, 26:3108, 1993.

[31] Gary S. Grest and Michael Murat. Computer simulations of tethered chains. unpublished, 1995.

[32] Alexander Yu. Grosberg and Alexei R. Khokhlov. *Statistical Physics of Macromolecules.* American Institute of Physics, New York, 1994.

[33] J. C. Le Guillou and J. Zinn-Justin. Accurate critical exponents from field theory. *J. Phys. France*, 50:1365, 1989.

[34] A. Halperin. Polymeric surfactants: Phase behaviour of binary mixture monolayers. *Europhys. Lett.*, 4:439, 1987.

[35] A. Halperin. Collapse of grafted chains in poor solvents. *J. Phys. France*, 49:547, 1988.

[36] Kanglin Huang and Anna C. Balazs. A two-dimensional self-consistent-field model for grafted chains: Determining the properties of grafted homopolymers in poor solvents. *Macromolecules*, 26:4736, 1993.

[37] Y. Kantor and M. Kardar. Polymers with rondom self-interactions. *Europhys. Lett.*, 14:421, 1991.

[38] Yacov Kantor, Mehran Kardar, and David R. Nelson. Statistical mechanics of tethered surfaces. *Phys. Rev. Lett.*, 57:791, 1986.

[39] A. Karim, J. F. Douglas, J. F. Ankner, and L. J. Fetters. Neutron reflectivity study of the density profile of a model end-grafted polymer brush: Influence of solvent quality. *Phys. Rev. Lett.*, 73:3407, 1994.

[40] A. Karim, J. F. Douglas, S. K. Satija, L. J. Fetters, D. H. Reneker, and M. D. Foster. Self-organization of polymer brush layers in a poor solvent. *J. Phys. II France*, 5:1441, 1995.

[41] M. S. Kent, L. T. Lee, B. J. Factor, R. Rondelez, and G. S. Smith. Tethered chains in good solvent conditions: An experimental study involving langmuir diblock copolymer monolayers. *J. Chem. Phys.*, 103:2320, 1995.

[42] Martin D. Lacasse. *Exact Dynamics of Small Ising Systems.* PhD thesis, McGill University, 1995.

[43] Pik-Yin Lai. Binary mixture of grafted polymer chains: A monte carlo simulation. *J. Chem. Phys.*, 100:3351, 1994.

[44] Pik-Yin Lai and Kurt Binder. Structure and dynamics of grafted polymer layers: A monte carlo simulation. *J. Chem. Phys.*, 95:9288, 1991.

[45] Pik-Yin Lai and Kurt Binder. Structure and dynamics of polymer brushes near the θ point: A monte carlo simulation. *J. Chem. Phys.*, 97:586, 1992.

[46] Pik-Yin Lai and E. B. Zhulina. Monte carlo test of the self-consistent field theory of a polymer brush. *J. Phys. II France*, 2:547, 1992.

[47] M. Laradji, H. Guo, and M. J. Zuckermann. An off-lattice monte carlo simulation of polymer brushes in good solvents. *Phys. Rev. E.*, 49:3199, 1994.

[48] Albert L. Lehninger. *Principles of Biochemisty.* Worth Publishers, Inc., New York, 1982.

[49] N. Madras, A. Orlitsky, and L. A. Shepp. Monte carlo generation of self-avoiding walks with fixed endpoints and fixed length. *J. Stat. Phys.*, 58:159, 1990.

[50] J. F. Marko and T. A. Witten. Phase separation in a grafted polymer layer. *Mat. Res. Soc. Extended Abstract*, 25:155, 1990.

[51] J. F. Marko and T. A. Witten. Phase separation in a grafted polymer layer. *Phys. Rev. Lett.*, 66(11):1541, March 1991.

[52] J. F. Marko and T. A. Witten. Correlations in grafted polymer layers. *Macromolecules*, 25:296, 1992.

[53] D. Martin, P. Wilson, J. Liao, and M Jones. Chain-end defects in extended-chain polymer solids. *MRS Bulletin*, 20(9):47, September 1995.

[54] S. T. Milner. Polymer brushes. *Science*, 251:905, 1991.

[55] S. T. Milner, T. A. Witten, and M. E. Cates. Theory of the grafted polymer brush. *Macromolecules*, 21:2610, 1988.

[56] Scott T. Milner. Strong-stretching and scheutjens-fleer descriptions of grafted polymer brushes. *J. Chem. Soc. Faraday Trans.*, 86:1349, 1990.

[57] Michael Murat and Gary S. Grest. Interaction between grafted polymeric brushes: A molecular dynamics study. *Phys. Rev. Lett.*, 63:1074, 1989.

[58] M. Muthukumar and Jyh-Shyong Ho. Self-consistent field theory of surfaces with terminally attached chains. *Macromolecules*, 22:965, 1989.

[59] Donald H. Napper. *Polymeric Stabilization of Colloidal Dispersions.* Academic Press, San Diego, 1983.

[60] R. Parry, H. Bassow, P. Merrill, and R. Tellefsen. *Chemistry: Experimental Foundations.* Prentice-Hall, Inc., New Jersey, 3 edition, 1982.

[61] M. Plischke and D. H. Boal. Absence of a crumpling transition in strongly self-avoiding tethered membranes. *Phys. Rev. A*, 38:4943, 1988.

[62] David Ronis. Statistical mechanics of ionomeric colloids. 2. ionomer conformational equilibria. *Macromolecules*, 26:2016, 1993.

[63] David Ronis. Statistical mechanics of ionomeric colloids: Interparticle correlations and conformational equilibria in suspensions of polymer coated colloids. *Phys. Rev. E*, 49:5438, 1994.

[64] R. S. Ross and P. Pincus. The polyelectrolyte brush: Poor solvent. *Macromolecules*, 25:2177, 1991.

[65] R. S. Ross and P. Pincus. Bundles: End-grafted polymer layers in poor solvent. *Europhys. Lett.*, 19:79, 1992.

[66] D. F. K. Shim and M. E. Cates. Finite extensibility and density saturation effects in the polymer brush. *J. Phys. France*, 50:3535, 1989.

[67] Denise Siqueira, Karsten Koehler, and Manfred Stamm. Structures at the surface of dry thin films of grafted copolymers. *Langmuir*, 11:3092, 1995.

[68] K. G. Soga, Hong Guo, and M. J. Zuckermann. Polymer brushes in a poor solvent. *Europhys. Lett.*, 29:531, 1995.

[69] K. G. Soga, M. J. Zuckermann, and Hong Guo. Binary polymer brush in a solvent. *Macromolecules*, 1996.

[70] Hai Tang. Laterally inhomogeneous melt polymer brushes. 1. perturbation analysis and general predictions. *Macromolecules*, 28:6258, 1995.

[71] Hai Tang and Igal Szleifer. Phase behavior of grafted polymers in poor solvents. *Europhys. Lett.*, 28:19, 1994.

[72] Brad L. Thiel and Christopher Viney. A non-periodic lattice model for crystals in *nephila clavipes* major ampullate silk. *MRS Bulletin*, 20(9):52, September 1995.

[73] Toon and Ellis. *Foundations of Chemistry.* Holt Rinehart and Winston Inc., New York, 1973.

[74] L. R. G. Treloar. *Introduction to polymer science.* Springer-Verlag, New York, 1970.

[75] F. T. Wall and J. J. Erpenbeck. New method for the statistical computation of polymer dimensions. *J. Chem. Phys*, 30:634, 1959.

[76] F. T. Wall, Stanley Windwer, and Paul J. Gans. Monte carlo study of coiling-type molecules. i. macromolecular configurations. *J. Chem. Phys*, 38:2220, 1963.

[77] George M. Whitesides. Self-assembling materials. *Scientific American*, 273(3):146, September 1995.

[78] M. D. Whitmore and J. Noolandi. Theory of adsorbed block copolymers. *Macromolecules*, 23:3321, 1990.

[79] D. R. M. Williams. *J. Phys. II*, 3:1313, 1993.

[80] Chuck Yeung, Anna C. Balazs, and David Jasnow. Lateral instabilities in a grafted layer in poor solvent. *Macromolecules*, 26:1914, 1993.

[81] W. Zhao, H. H. Rafailovich, and J. Sokolov. Lateral structure of a grafted polymer layer in a poor solvent. *Macromolecules*, 27:2933, 1994.

[82] Jiayi Zhu, Adi Eisenberg, and R. Bruce Lennox. Interfacial behavior of block polyelectrolytes. 1. novel surface micelle formation. *J. Am. Chem. Soc.*, 113:5583, 1991.

[83] Jiayi Zhu, R. Bruce Lennox, and Adi Eisenberg. Interfacial behavior of block polyelectrolytes. 2. aggregation numbers of surface micelles. *Langmuir*, 7:1579, 1991.

[S4] E. B. Zhulina, T. M. Birshstein, V. A. Pryamitsyn, and L. I. Klushin. Inhomogeneous structure of collapsed polymer brushes under deformation. *Macromolecules*, 28:8612, 1995.

[S5] E. B. Zhulina, O. V. Borisov, V. A. Pryamitsyn, and T. M. Birshstein. Coil-globule type transitions in polymers. 1. collapse of layers of grafted polymer chains. *Macromolecules*, 24:140, 1991.

[S6] Ekaterina B. Zhulina, Oleg V. Borisov, and Victor A. Priamitsyn. Theory of steric stabilization of colloid dispersions by grafted polymers. *J. Colloid Interace Sci.*, 137:495, 1990.